DISS. ETH NO. 27478

QUANTITATIVE IMAGING OF STARCH GRANULE DEVELOPMENT IN LEAVES

A thesis submitted to attain the degree of
DOCTOR OF SCIENCES of ETH ZURICH (Dr sc. ETH Zurich)

presented by

LEO ARTHUR BURGY

M. sc., Universität Bern

born on 05.01.1993 citizen of

GURMELS FR

accepted on the recommendation of

Prof. Samuel C. Zeeman,

Prof. Anders Meibom and

Prof. Martin Pilhofer

2021

To my parents

Acknowledgments

This project would not have been possible without the support of a number of people. I especially thank Prof. Samuel Zeeman for putting his trust in me and allowing me to become independent in my research; Simona Eicke for her invaluable help with experimental work and for her close collaboration; Dr Kuan-Jen Lu, for integrating me quickly in the lab and the topic; my colleagues of the Institute of Molecular Plant Biology and more specifically of the Plant Biochemistry for their support and their resilience after some of my unsuccessful iterations; Prof. Martin Pilhofer, who helped me set up the cryo-EM analyses and his helpful insights; Prof. Anders Meibom, who sparked with the idea of applying the NanoSIMS to investigate the development of starch granules, put the NanoSIMS resources at my disposal and always showed great interest in the project; Dr Stephane Escrig for his support and invaluable help in setting up a robust workflow; Dr Louise Jensen who helped me devise the serial sectioning method and shared her electron microscopy expertise. I also thank my family and my friends, who helped me deal with my doubts throughout this endeavour and always encouraged me.

Summary

Starch is the main storage carbohydrate in plants. In leaves, chloroplasts synthesise starch throughout the day to buffer diurnal changes in light energy availability, degrading it at night to support metabolism. Starch consists of the glucose polymers: amylopectin and amylose. Amylopectin is a highly branched polymer able to adopt a crystalline form, while amylose a mostly linear polymer deposited within the amylopectin matrix. Each chloroplast produces several insoluble lenticular granules, each a few micrometres in diameter. Our knowledge of starch synthesis has benefited from extensive genetic and biochemical studies and numerous proteins are now known to be involved. However, the way the proteins interact and coordinate with each other remains largely unknown. Further, few studies have considered the spatial organisation of these proteins within the chloroplasts.

Recently, a number of proteins involved in starch granule initiation have been described. In the absence of one or more of these proteins, chloroplasts contained fewer, enlarged granules, and the speculative models describing the molecular mechanisms underpinning initiation have been proposed. However, no one has described exactly how starch granules are initiated: most biochemical procedures used to investigate starch tend to analyse bulk starch rather than to consider the formation of individual granules. Innovative microscopy approaches providing both spatial and temporal resolution are crucial to investigate the mechanisms of granule initiation and development in vivo. To that aim, I coupled electron microscopy with isotope labelling and secondary ion mass spectrometry and with 3-dimensional tomographic reconstruction. By applying these tools to *Arabidopsis thaliana* genetic resources, I captured the pattern of granule initiation, and subsequent expansion patterns that determine starch granule morphology within the chloroplast.

First, I reveal that new granules form early in the day via the coalescence of multiple initials and that they owe their final lenticular shape to the anisotropic growth, with high rate at their equator and low rates at their poles. Second, I showed that plants deficient in SS4 have uniform patterns of starch accumulation, resulting in round-shaped starch granules, and that the N-terminus of SS4 is critical for the anisotropic growth pattern. Third, I showed that plants deficient in GBSS, the enzyme responsible for the amylose synthesis, display lower rates of synthesis in their cores, confirming the hypothesis that amylose is synthesised within the amylopectin matrix. Finally, I investigated recently discovered starch granule initiation mutants and showed that these can be defined as either unable to properly initiate parallel

granules or capable of proper initiation, but that these events are incorrectly localised within the chloroplast.

In conclusion, high-resolution imaging is essential to define the very first steps of starch biosynthesis and, using serial block face scanning microscopy, I extracted information about the form and number of starch granule initials with an unprecedented precision, which revealed the rich dynamic of the starch granule development. As the use of fixed tissue precludes real-time imaging, I used isotopic labelling to cache temporal information about the use of assimilated carbon for granule growth, subsequently revealed by NanoSIMS imaging. Applying these methods has provided new insight into the roles on new non-enzymatic proteins that control the number of starch granules, probably by scaffolding other initiation factors at specific locations in the chloroplast. I hope that these breakthroughs in understanding starch biosynthesis will help guide applied research to improving starch crops and will inspire the combined use of these techniques to resolve compelling biological questions in other fields.

Résumé

L'amidon est le principal glucide de stockage des plantes. Dans les feuilles, les chloroplastes synthétisent l'amidon tout au long de la journée pour tamponner les changements diurnes de la disponibilité de l'énergie lumineuse, le dégradant la nuit pour soutenir le métabolisme. L'amidon est constitué de polymères de glucose, l'amylopectine et l'amylose. L'amylopectine est un polymère très ramifié capable d'adopter une forme cristalline, tandis que l'amylose est un polymère essentiellement linéaire déposé dans la matrice d'amylopectine. Chaque chloroplaste produit plusieurs granules lenticulaires insolubles, chacun de quelques micromètres de diamètre. Notre connaissance de la synthèse de l'amidon a bénéficié d'études génétiques et biochimiques approfondies et l'on sait maintenant que de nombreuses protéines sont impliquées. Cependant, la manière dont les protéines interagissent et se coordonnent entre elles reste largement inconnue. En outre, peu d'études ont pris en compte l'organisation spatiale de ces protéines dans les chloroplastes.

Récemment, un certain nombre de protéines impliquées dans l'initiation des granules d'amidon a été décrit. En l'absence d'une ou plusieurs de ces protéines, les chloroplastes contiennent moins de granules agrandis et plusieurs modèles spéculatifs décrivant les mécanismes moléculaires qui sous-tendent l'initiation ont été proposés. Cependant, personne n'a décrit exactement comment les granules d'amidon sont initiés : la plupart des procédures biochimiques utilisées pour étudier l'amidon tendent à analyser l'amidon en vrac plutôt qu'à considérer la formation de granules individuels. Des approches microscopiques innovantes offrant une résolution à la fois spatiale et temporelle sont essentielles pour étudier les mécanismes de l'initiation et du développement des granules in vivo. À cette fin, j'ai couplé la microscopie électronique avec le marquage isotopique et la spectrométrie de masse des ions secondaires et avec la reconstruction tomographique tridimensionnelle. En appliquant ces outils aux ressources génétiques d'*Arabidopsis thaliana*, j'ai capturé le schéma d'initiation des granules et les schémas d'expansion ultérieurs qui déterminent la morphologie des granules d'amidon au sein du chloroplaste.

Tout d'abord, je révèle que les nouveaux granules se forment tôt dans la journée par la coalescence de multiples initiales et qu'ils doivent leur forme lenticulaire finale à la croissance anisotrope, avec un taux élevé à l'équateur et un taux faible aux pôles. Deuxièmement, j'ai montré que les plantes déficientes en SS4 ont des modèles uniformes d'accumulation d'amidon, ce qui donne des granules d'amidon de forme ronde, et que

l'extrémité N de SS4 est essentielle pour le modèle de croissance anisotrope. Troisièmement, j'ai montré que les plantes déficientes en GBSS, l'enzyme responsable de la synthèse de l'amylose, présentent des taux de synthèse plus faibles dans leurs noyaux, confirmant l'hypothèse selon laquelle l'amylose est synthétisée dans la matrice de l'amylopectine. Enfin, j'ai étudié des mutants d'initiation de granules d'amidon récemment découverts et j'ai montré qu'ils peuvent être définis comme incapables d'initier correctement des granules parallèles ou capables d'une initiation correcte, mais que ces événements sont incorrectement localisés dans le chloroplaste.

En conclusion, l'imagerie à haute résolution est essentielle pour définir les toutes premières étapes de la biosynthèse de l'amidon et, à l'aide de la microscopie à balayage de blocs en série, j'ai extrait des informations sur la forme et le nombre d'initiales des granules d'amidon avec une précision sans précédent, ce qui a révélé la riche dynamique du développement des granules d'amidon. Comme l'utilisation de tissu fixe empêche l'imagerie en temps réel, j'ai utilisé le marquage isotopique pour préserver les informations temporelles relatives à l'utilisation du carbone assimilé pour la croissance des granules, révélées ensuite par l'imagerie NanoSIMS. L'application de ces méthodes a permis de mieux comprendre le rôle des nouvelles protéines non enzymatiques qui contrôlent le nombre de granules d'amidon, probablement en utilisant d'autres facteurs d'initiation à des endroits spécifiques du chloroplaste. J'espère que ces percées dans la compréhension de la biosynthèse de l'amidon aideront à orienter la recherche appliquée vers l'amélioration des cultures d'amidon et inspireront l'utilisation combinée de ces techniques pour résoudre des questions biologiques pressantes dans d'autres domaines.

Contents

Introduction

All living organisms require a continued supply of free energy for mechanical work, active transport of molecules/ions and synthesis of molecules from simple precursors. The free energy that helps them maintain a state far from equilibrium is derived from the environment (sunlight or organic/inorganic chemical compounds) (Berg et al., 2002). The discontinuous availability of the energy source is a key factor in the evolution of energy management. The assimilation of energy into the biosphere occurs when sunlight is trapped through phototransduction whereby the absorption of a photon is coupled with the generation of an electrochemical potential through a biological membrane. The potential thus generated is used to reduce nicotinamide adenine dinucleotide phosphate ($NADP^+$) into NAPDH and to phosphorylate adenosine diphosphate (ADP) into ATP. In plants, phototransduction is realised through the photosynthesis and takes place across the thylakoid membrane of chloroplasts.

The acquisition of energy through phototransduction allows the formation of ATP (chemical energy) and NADPH (reducing power). These are harnessed to fix carbon dioxide (CO_2) through the Calvin-Benson cycle (CBC). The CBC consists of three phases: (1) the fixation of CO_2 on the CO_2 acceptor, ribulose 1,5-bisphosphate (RuBP); (2) the reduction of 3-phosphoglycerate (3-PGA) to triose-phosphates (triose-P), i.e., glyceraldehyde 3-phosphate (GAP) and its isomer dihydroxyacetone phosphate (DHAP); (3) the regeneration of the CO_2 acceptor, ribulose 1,5-bisphosphate. Five out of six of the triose-P are kept for the regeneration of RuBP, rendering the CBC autocatalytic while the remaining one leaves the cycle to participate in the synthesis of other metabolites.

The triose-P not recycled in the CBC are either converted into glucose and stored as transient starch or exported to the cytosol. In leaves, the concentrations of triose-P and inorganic orthophosphate (P_i) play an essential role in regulating the fluxes between the chloroplast and the cytosol. The ratio between these two fluxes depends on the species; some invest more into starch while other investing less. Further, the partitioning is variable within species depending on the environmental conditions such as temperature or the length of the day. In the stroma, the triose-P can be combined into hexose-phosphates and further participate in

starch synthesis or exported to cytosol in exchange for P_i. This allows large amounts of fixed carbon to be stored in a compact, osmotically inert form.

During the day, when the production of sugar-phosphates from photosynthesis exceeds the requirements for plant growth, glucose is extracted from the stroma through its polymerization and branching into insoluble starch granules. Triose-P can be combined into fructose 6-phosphate (F6P), which can be isomerised into glucose 6-phosphate (G6P) by phosphoglucose isomerase (PGI) and converted into glucose 1-phosphate (G1P) by phosphoglucomutase (PGM). These interconvertible hexose-phosphates collectively form the hexose pool (Figure 0.1). However, the conversion of ATP and G1P into ADP-glucose (ADP-Glc) by ADP-glucose pyrophosphorylase (AGPase) is essentially irreversible as the concomitantly released inorganic pyrophosphate is rapidly hydrolysed to P_i. This represents the first committed step for starch biosynthesis, and it is therefore not surprising that the AGPase is highly regulated. Plants defective in PGI, PGM or AGPase contain very little starch, illustrating that this pathway delivers the major flux into starch (Caspar et al., 1985, Lin et al. 1988, Tsai et al., 2009). Growth of such starchless mutant plants in a day-night regime causes a significant reduction in growth, particularly if the days are short, highlighting the importance of starch in stabilising the energy budget at night. However, when exposed to very long days or continuous light, these plants grow comparably to their wild-type counterparts (Smith and Stitt, 2007; Fernandez et al., 2017).

In the cytosol, most triose-P are combined into hexose-phosphates and used to synthesise sucrose via the sequential activity of the sucrose phosphate synthase and the sucrose phosphate phosphatase from F6P and UDP-Glucose (Figure 0.1). The latter reaction is essentially irreversible due to the hydrolysis of P_i from sucrose-6-phosphate. Sucrose can be transported to sink tissues via the phloem. Its degradation, mediated by invertases and sucrose synthases, provides the cell with hexoses for energy production and with carbon skeleton for the biosynthesis amino acids and structural carbohydrates (Ruan, 2012; Stein, 2019). The degradation of sucrose prevents the formation of an equilibrium between the sink and the source, maintaining the source-to-sink flow.

The synthesis of sucrose is tightly integrated with both CO_2 fixation and starch synthesis (Koch, 2004; Barratt et al., 2009). The export of stromal triose-P requires the import of cytosolic P_i via triose-P/phosphate translocator (Riesmeier et al., 1993; Hausler et al., 1998; Schneider et al., 2002). In the cytosol, triose-P can be converted to Fructose 1,6-bisphosphate

(F16BP), which can in turn be converted to F6P by the FBPase. The FBPase activity is regulated by the concentration of the signal metabolite Fructose 2,6-bisphosphate (F26BP) (McCormick et al., 2015; Kruger et al., 1995; Okar et al., 1999). F26BP is both produced and degraded by the bifunctional enzyme F2KP, which acts both as a 6-phosphofructo-2-kinase and a fructose-2,6-bisphosphatase (Figure 0.1). The F2KP is allosterically regulated by P_i, P P_i, triose-P, PEP, pyruvate, GA2P, GA3P, DHAP and F6P (Larondelle et al., 1986; Markham et al., 2002).

When the rate of photosynthesis increases, this favours the export of stromal triose-P to the cytosol in exchange for P_i. An increase of triose-P in the cytosol lowers the F26BP, by inhibiting the kinase activity of F2KP. This allows and increased flux to sucrose through the activation of FBPase, and the utilisation of the exported triose-P. Thus, sucrose production is adjusting to the supply in triose-P from the photosynthesis. When the sucrose synthesis is higher than the exporting capacity of the leaf, the conversion of F6P to sucrose-phosphate by the sucrose-phosphate synthase is inhibited, increasing the concentration of F6P. Consequently, the phosphatase activity of F2KP rises F26BP, which inhibits the FBPase activity, limiting the sucrose synthesis rate. The cytosolic concentration of P_i decreases and the triose-P increase, limiting further export from the chloroplast. The increasing triose-P/ P_i ratio in the stroma promotes the starch synthesis shifting the balance from sucrose to starch production (see Nielsen et al., 2004 for a comprehensive review).

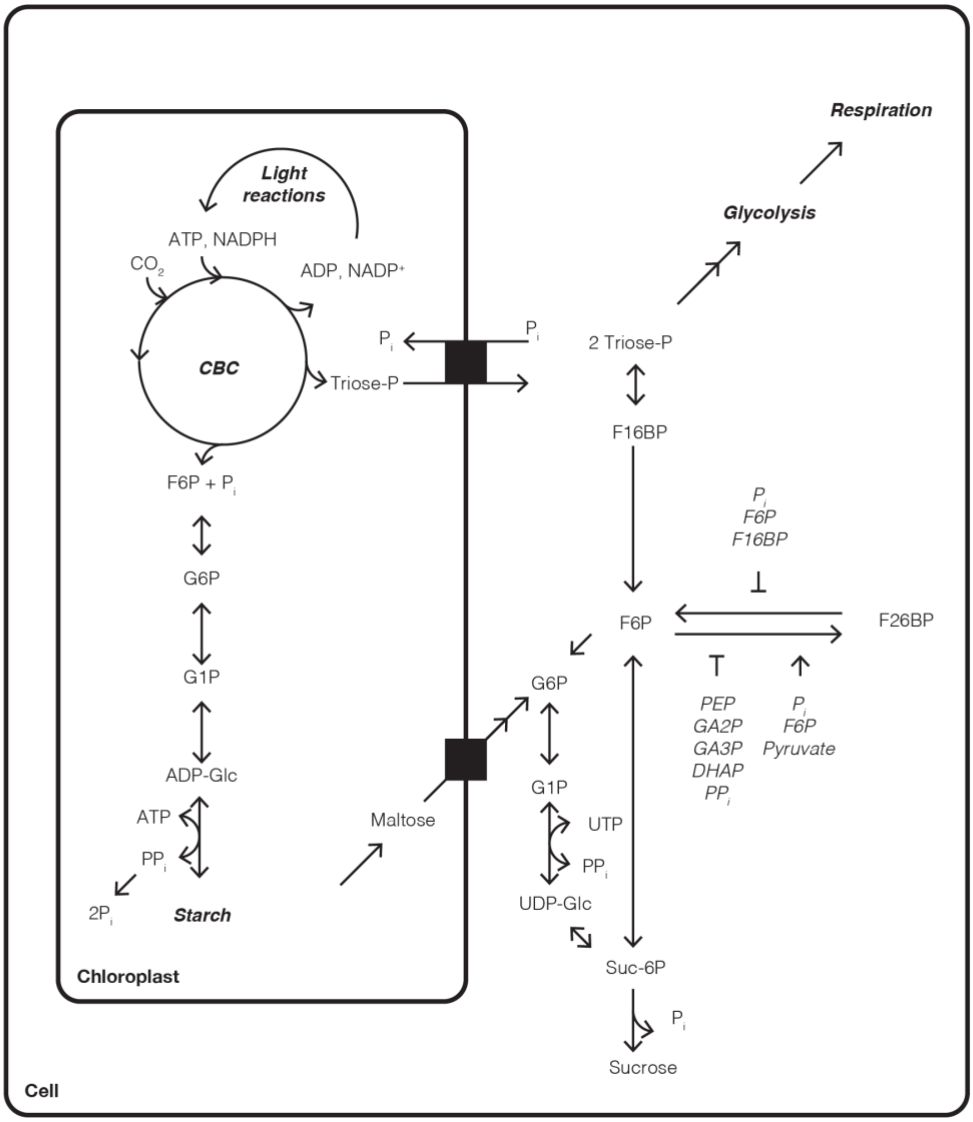

Figure 0.1. Carbon metabolism in Arabidopsis leaves. The reducing power and the energy rich ATP produced by the light reaction of photosynthesis are harnessed to fix the CO_2 via the Calvin Benson cycle. A fraction of the triose-P leaves the Calvin-Benson cycle (CBC) to be exported to the cytosol or to be converted into hexose-P. Starch synthesis starts with starch synthases that catalyse the condensation of ADP-Glc onto pre-existing glucans. The partitioning between starch- and sucrose synthesis is explained in the text.

Starch composition

Starch is made of two glucans: amylopectin and amylose. Glucosyl units are linked through α-1,4-bonds to form chains, that are branched through α-1,6-bonds. While amylopectin has a high density of branching points (4-5% of the bonds are branch points), amylose contains far fewer branches (ca. 0.1% of the bonds are branch points) (Bergthaller et al., 2007). Here, I review the role of the starch synthases (SSs), the branching enzymes (SBEs), and the debranching enzymes (DBEs) in creating the starch polymers.

Biosynthesis of amylopectin

The matrix of starch is composed of amylopectin, the branched polymer consisting of linear glucose chains, branched together into a gigantic molecule with a racemic or tree-like structure. The conformation of the branches allows neighbouring, parallel branches to form double helices that pack into layers, leading to concentric semi-crystalline lamellae, between which are amorphous lamellae which harbour most of the branch points (Figure 0.1) (Sterling, 1962; Oostergetel et al., 1989; Blanshard et al., 1984). The first step of starch synthesis is the formation of ADP-Glc—the glucosyl donor for starch synthesis in plants—using G1P and ATP, catalysed by AGPase (Espada, 1962; Ballicora et al., 2004). This reaction also releases pyrophosphate, which is cleaved to P_i by plastidial pyrophosphatase. This removal of pyrophosphate makes the production of ADP-Glc essentially irreversible (Stitt et Zeeman, 2012). AGPase is the ultimate step in the production of ADP-Glc and the enzyme has the pivotal function to control the flux of assimilated carbon into starch. Not surprisingly, AGPase is finely regulated via different mechanisms that act over different timescales. For rapid regulation, AGPase activity is controlled through allosteric activation by 3-PGA and inhibition by P_i (Heldt et al., 1977). The AGPase enzyme is also redox activated, being more active and more sensitive to allosteric regulation when in its reduced state (Tiessen et al., 2002; Mugford et al., 2014). As a consequence, the formation of ADP-Glc is promoted during the day when light-activated thioredoxins reduce AGPase and when 3-PGA is produced via the Calvin-Benson cycle (Fu1998; Ballicora et al., 2000; Michalska et al., 2009). AGPase activity thereby adjusts automatically to match the need for starch synthesis: when photosynthesis is low, less 3-PGA is available, AGPase activity is reduced, while when photosynthesis is high, and the redox environment is more reduced, AGPase activity is increased, diverting more glucose for starch synthesis (Michalska et al., 2009; Kolbe2005; Thormaehlen et al., 2013).

Starch synthases

Starch synthases (EC 2.4.1.21) belong to the glucosyltransferase (GT) family 5 (CAzY: Lombard et al., 2014) and typically possess a conserved C-terminal catalytic domain and a variable N-terminal extension. SSs transfer the glycosyl moiety of ADP-Glc to the non-reducing end of a pre-existing glucan (Ball, 2003; Pfister et Zeeman, 2016). The catalytic site of SS is located between the two glycosyltransferase domains; GT-5, that binds to the acceptor glucan and GT-1, that binds to the sugar nucleotide glucosyl donor (Buschiazzo et al., 2004; Leterrier et al., 2008). At least six soluble SSs (SS1–6) exist in the stroma and one is almost exclusively bound to the starch granule (Delvalle et al., 2005; Zhang et al., 2008; Roldan et al., 2007; Abt et al., 2020; Helle et al., 2018). The SSs mostly differ by the structure of their N-terminal, some of which contain predicted structures including coiled-coil motifs (GBSS, SS3–5) or carbohydrate binding modules (CBMs; SS3), with which they can interact with other proteins and glucans, respectively (Hennen-Bierwagen et al., 2008; Hennen-Bierwagen et al., 2009; Gamez-Arjona et al., 2014). The functions of SSs have been deduced from the modifications observed in the chain length profile of amylopectin in their respective knock-out mutants, i.e., the decreased abundance of certain lengths have been used to infer that these chains were normally elongated by the missing SS. However, since the absence of one isoform modifies the nature of the substrate for the other isoforms, it can be difficult to unambiguously define the role of each, individually. Furthermore, several as-yet unknown factors could influence starch biosynthesis. A recent alternative approach to study the SSs alongside other proteins involved in starch biosynthesis was to express them in yeast cells, in which glycogen biosynthesis has been first deactivated (Pfister et al., 2016). This allows the role of each SS in determining glucan structure to be investigated in the presence of different combinations of the other starch biosynthetic enzymes.

The SS1 isoform acts on short chains (DP6–7) derived from the SBE reactions (see below), elongating them by a few glucosyl units (to DP8–10) (Delvalle et al., 2005; Szydlowski et al., 2011). The expression of SS1 in yeast confirmed several conclusions about the function of SS1: cells expressing only SS1 produced more soluble glucans and increased the proportion of short chains (DP6–10), while there were fewer intermediate chains (DP11–25) (Pfister et al., 2016). The produced glucans displayed lower crystallinity; this is likely due to the inability of the short chains to form higher-order structures (see above). Interestingly, SS1 is able to elongate the substrate maltoheptaose up to DP15 in vitro and can produce a range of chain lengths in presence of SBE (Brust et al., 2013). The limited spectrum of chain

elongation observed in the wild type could be explained by the overlap in preference with other starch synthases (Zhang et al., 2008).

Plants lacking SS2 often display starch granules with an altered morphology, more amylose and a lower crystallinity (Zhang et al., 2008). The chain length distribution of ss2 mutants show a lower proportion of DP18 and a higher proportion around DP8, suggesting that SS2 elongates chains of DP8 to DP13–20. The starch phenotype of ss2 mutants might also be partly the result of disturbed protein-protein interactions, which in cereals are known to occur between SS2 and SS1 and SBEs (Liu et al., 2012). However, SS2 activity in elongating the short chains can be clearly established (Szydlowski et al., 2011). Indeed, mutation of SS2 in Arabidopsis results in small amounts of phytoglycogen and enhances the accumulation of phytoglycogen in isa mutants of both rice and Arabidopsis (Fujita et al., 2012; Pfister et al., 2014).

The function of SS3 is less well defined compared with that of SS1 and SS2. However, its role in elongating long, cluster-spanning chains has been proposed in several species. The long N-terminus of SS3—the longest amongst the SSs—contains three CBMs for carbohydrate binding and predicted coiled coils motifs that may be involved in protein-protein interactions (Zhang et al., 2005). The proportion of short chains decreases in ss3 mutants although this change is small in magnitude compared to the lack of SS1 or SS2 (Zhang et al., 2005). In Arabidopsis, SS3 does not influence the number of granules in chloroplasts, but it seems to assist SS4, as their simultaneous deficiency cause the chloroplasts to be devoid of starch granules (Szydlowski et al., 2009; Seung et al., 2016, see below).

The isoform SS4 has, in contrast to the other SSs, little detectable impact on the amylopectin structure but in Arabidopsis it is essential for normal starch granule initiation and morphology (Roldán et al., 2007; Szydlowski et al., 2009; Crumpton-Taylor et al., 2013; Lu et al., 2018). The C-terminal catalytic domain of SS4 promotes the granule formation and interacts with the glucan-binding protein Protein Targeting to Starch 2 (PTST2, see below), which is proposed to provide it with suitable glucans (Seung et al., 2017). This may be vital during the granule initiation to prevent the enzymatic degradation of the starch granule primers by α- and iso-amylases (Seung et al., 2016). The N-terminus of SS4 contains predicted coiled coils motifs, and this part of the protein is required to interact with MFP1, which directs it to specific regions within the chloroplast (Seung et al., 2018). The N-

terminus also influences the morphology of the granule, although it is unclear how this is brought about. Plants deficient in SS4 also display reduction in their overall starch turnover, a slow starch accumulation rate during the day and a slow degradation rate at night (Szydlowski et al., 2009). Starch levels are higher at dawn compared to wild-type plants, but lower than wild-type levels at dusk. Chloroplasts contain fewer granules (80% chloroplast sections are starchless) but the granules that are present are spherical and enlarged (Roldan et al., 2007; Crumpton-Taylor et al., 2013; Lu et al., 2018). This decreases the surface area available to biosynthetic or degrading enzymes per unit starch volume, which has been proposed as an explanation of the lower starch turnover (Roldán et al., 2007; Crumpton-Taylor et al., 2013). The concentration of ADP-Glc in *ss4* mutant is particularly high, suggesting that the other SSs cannot use it when SS4 is absent (Crumpton-Taylor et al., 2013; Ragel et al., 2013). In the absence of α-amylase AMY3, the *amy3ss4* mutant contains a higher starch concentration than in wild type and chloroplasts contained more starch granules (Seung et al., 2016). Together with the activity of isoamylase as a negative regulator of starch granule initiation (Burton et al., 2002; Bustos et al., 2004), this suggests that SS4 and its associated PTST proteins could protect nascent starch primers against premature degrading activities. Further, the presence of SS4 in a heterologous yeast system consistently promotes the fraction of insoluble glucans (Pfister et al., 2016).

SS5 is an unusual isoform, which has only recently received attention. It is widely conserved among plants and its function seems to reflect that of its closest relative, SS4. Like SS4, SS5 also influences the number of starch granules; chloroplasts of *ss5* mutants contain fewer large irregular, flattened starch granules. The starch concentration, by contrast, resembles that of the wild type, and amylopectin structure is unaffected (Abt et al., 2020). SS5 shares with SS4 a putative surface binding site for glucans (Nielsen et al., 2018), but in contrast to the other SSs, SS5 is almost certainly not an active glycosyltransferase since it lacks the GT1 subdomain. It contains coiled coil motifs, used to form multimers and for interactions with the proposed structural/scaffolding protein MRC (for Myosin-Related Chloroplast protein), through which it has been proposed to exert its function (Seung et al., 2018; Vandromme2018) in influencing the number of granules. A seventh putative isoform, SS6, has been recently described in potato tubers (Helles et al., 2018). Although catalytically inactive, its specific expression during the formation of the tuber suggests a yet to be investigated role in starch biosynthesis.

Branching enzymes

SBEs (EC 2.4.1.18) belong to the same family of enzymes as α-amylases (CAZy: glycoside hydrolase family 13 (GH13)), but rather than acting as hydrolases, they catalyse the branching of an α-1-4-linked glucan via the formation of α-1-6-bonds. Like α-amylases, SBEs initially break and α-1-4 linkages, making a transient enzyme-glucan intermediate, then transfer the cleaved part to the C6 position of a glucose unit from the same or another glucan chain. Thus, an α-1,6-branch is formed via a glucanotransferase reaction. In addition to a central catalytic α-amylase-like domain, SBEs contain an N-terminal carbohydrate binding module family 48 (CBM48), and a C-terminal part (Abad et al., 2002). Based on their amino acid sequence, SBEs are separated into class I and class II. In some cases, e.g., SBE2 in maize, there are more than one gene copy encoding each SBE class, which often have distinct, tissue-specific expression patterns (Rahman et al., 2001). In Arabidopsis, there are two class-II SBEs (BE2 and BE3) both of which are expressed in leaves and seem to be redundant to some extent (Dumez et al., 2006). There is no class-I SBE in Arabidopsis.

Although most of the cluster structure of amylopectin derives from the placement of branches by SBEs, the actual distribution of branch points is difficult to obtain due to the analytical limitations. Rather, SBEs are generally described by the length of the glucans they transfer in vitro rather than their placement. Accordingly, class-I SBEs tend to be more active on amylose and to transfer longer chains than class-II SBEs, which seems to be more active on amylopectin (Guan et al., 1993). Based on in vitro evidence on rice, class-I BEs are proposed to participate in the construction of new clusters by branching dextrins from an existing cluster to a newly synthesised (by SS3), unbranched glucan. Then, class-II BEs add internal branches on the moved branches, which are further elongated by SS1 and SS2 (Nakamura et al., 2010). The deficiency of class-II SBE activity results in amylopectin with fewer branches and longer chains, and with increased levels of amylose, known as the ae phenotype, which produces less digestible starch.

Debranching enzymes

Plant debranching enzymes (DBEs; CAZy: glycoside hydrolase family 13) also belong to the α-amylases family and release linear chains by hydrolysing α-1,6-linkages from an existing branched glucan. In plants, there are two DBE types: isoamylases (ISA1-3; E.C. 3.2.1.68) and limit-dextrinase (LDA; E.C. 3.2.1.41). Like the SBEs, both DBE types possess an N-terminal starch-binding domain and an α-amylase-like domain (Janecek et al., 2014). In Arabidopsis, ISA1 and ISA2 proteins associate to form a single isoamylase enzyme that is active during

the synthesis of amylopectin, with ISA1 being a catalytic subunit and ISA2 being non-catalytic (Streb et al., 2014). In mutants lacking this ISA, most of the starch is replaced by phytoglycogen, a water-soluble polysaccharide resembling glycogen in many ways (Zeeman et al., 1998; Wattebled et al., 2005; Sundberg et al., 2013). It is therefore thought that ISA ensures that only appropriate glucans are elongated by SSs by removing "misplaced" glucans, thus enabling the subsequent crystallisation of the parallel chains. In agreement with this hypothesis, when all the DBEs are removed from Arabidopsis, starch is completely replaced by phytoglycogen (Streb et al., 2008). However, the strict requirement of ISA for crystallisation is questioned by the fact that starch is still produced when the α-amylase 3 is further removed. In the light of these pieces of evidence, it seems more likely that debranching merely enhances crystallisation rather than enables it. In contrast, the other DBEs, ISA3 and LDA, appear to debranch starch during its degradation. Consequently, *isa3* and *lda* mutants display a starch excess phenotype (Streb et al., 2012).

Biosynthesis of amylose

Amylose is the minor component of starch, accounting for 10% to 30% of starch by weight. Its degree of polymerisation (DP) is around a few thousand units (Perez et Bertoft, 2018). Each amylose molecule contains between 5-20 branches and it is a minor contributor to starch granule architecture, compared with amylopectin (Wang et al., 2019). Within the amylopectin matrix, amylose is thought to occur in a largely amorphous state and when extracted, it readily precipitates, likely by forming helical structures. Amylose content increases with the maturation of the granules, supporting the hypothesis that amylose synthesis occurs within the existing amylopectin matrix (Denyer et al., 1996; Tatge et al., 1999). This may allow to pack more glucose per volume, filling the looser, amorphous regions of the extant granule. Starches devoid of amylose are valued because after cooking, the resultant pastes tend to be stickier and more transparent —both properties being of interest for food and industrial applications. In contrast, starches with high amylose content are interesting from a health viewpoint as they pass the stomach and the small intestine incompletely digested and can feed the microbiota of the large intestine (Englyst et al., 1992; Hu et al., 2004).

Amylose is exclusively synthesised by Granule Bound Starch Synthase (GBSS) within the amylopectin matrix of the granule (Denyer et al., 1999; Cuesta et al., 2016). *in vitro* evidence suggests that GBSS processively elongates the same glucan, unlike other soluble SSs, which act distributively, releasing its glucan product immediately after they have transferred one

glycosyl unit (Edwards et al., 1999; Denyer et al., 1999). The primers of amylose synthesis are probably small glucans (up to DP7) that diffuse through the granule matrix or chains from the trimming process of amylopectin (Denyer et al., 2001).

GBSS has the shortest amino-acid sequence of all starch synthases and does not have any CBM on its N-terminal (Seung, 2020). This raises the open question as to how GBSS binds to starch. However, it has recently been elucidated how GBSS is targeted to the starch granule in Arabidopsis. This occurs via a coiled-coil mediated interaction with Protein Targeting to Starch 1 (PTST1), a plastidial protein that also contains a CBM48 domain with which it binds to starch to deliver GBSS (Seung et al., 2015; Lohmeier et al., 2008). This interaction is not strictly required for amylose synthesis, but it enhances the process; cassava deficient in PTST1 had storage roots with only half of the amylose content (Bull et al., 2018).

Architecture of the starch granule

The starch granule owes many of its properties to the arrangement of the glucan chains of amylopectin. The reported degree of polymerisation is higher than that of amylose molecules, ranging from 0.5–1.5 x 10^4 units depending on the analytical method and the botanical source (Takeda et al., 1987, Takeda et al., 1989, Takeda et al., 2003). Amylopectin exhibits crystalline patterns that can be deduced from x-ray scattering of powdered starches (Buleon et al., 1998). These crystalline structures are radially oriented as shown by the Maltese motif emerging from starch granules shed with polarised light (Perez et al., 2009). This arrangement is intrinsic to the topology of the branching points, which are heterogeneously positioned throughout the amylopectin molecule. Local concentrations of branching points generate arrays of parallel chains that twist two by two to form double helices. Collectively, these dense bundles form crystalline layers that alternate with amorphous layers containing the branch points. At a higher scale, these semi-crystalline regions form concentric rings (200–300 nm thick) that alternate with amorphous regions where the glucans are assumed to be less well organised. The concentric layers look like growth rings, yet it is uncertain whether they reflect periodical growth, as some studies have revealed that starch granules still exhibit growth rings even when produced in constant conditions (e.g., continuous light or in in-vitro culture in the dark with exogenous sugars) (Buttrose et al., 1962; Zeeman et al., 2002; Pilling and Smith, 2003).

To analyse the constituting branches in amylopectin, its branches are specifically hydrolysed at α-D-(1–6)-linkages via isoamylases or pullulanase. The branches are then separated by an appropriate chromatographic or an electrophoretic technique. The resulting chain length distribution contains different populations, hence the term “polymodal distribution”. Amylopectin consists of external chains (long of 19 to 28 residues), that have no branching point, internal chains (29 to 31) and the chains with the free reducing end (25 to 27) that bear external branches (approx. every 6th residue) (Fig 0.2) (Hizukuri, 1986; Jane et al., 1999; Bertoft et al., 2008). The specific arrangement of the clusters within the semicrystalline matrix is still debated and no direct experimental evidence has yet favoured one specific model. In the cluster model, proposed independently from two authors (Nikuni, 1969; French, 1972), the clusters result from branching points that are regularly interspaced along the internal chains spanning several clusters. In contrast, in the building block backbone model, the clusters are linked together, and their chains lie tangentially to the inter-block chains.

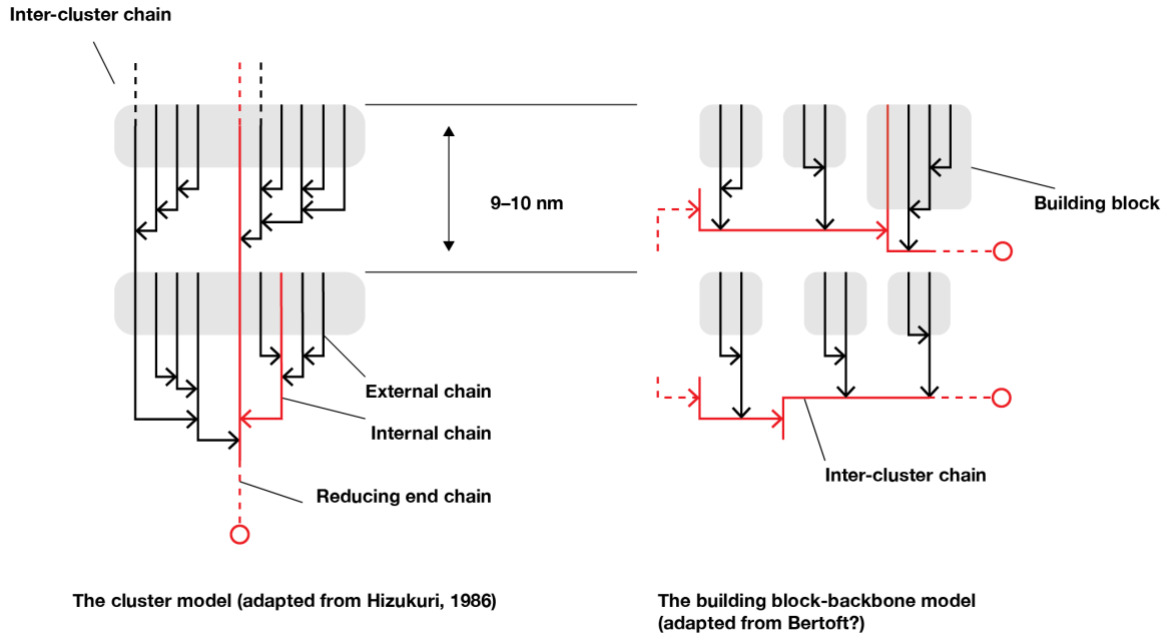

Figure 0.2. Structures proposed for amylopectin. In the cluster model, the molecules of amylopectin are expanding radially, and their clusters are also oriented perpendicular to the granule surface. The only chain with a free reducing end is labelled with a round tail. Internal chains are branched onto other internal chains and harbour themselves other chains, unlike external chains. The light grey boxes represent regions where parallel branches form double helices. In the building block-backbone model, the clusters are spreading outward from the tangential internal chains that runs tangentially with respect to the granule surface.

Starch granule development

If the process of starch biosynthesis is nowadays well understood, the same cannot be said of the dynamics of individual starch granules. The lack of data results from the difficulty of observing individual granules repeatedly in their native environment. Attempts to describe the granule dynamics have thus been limited to measuring the starch concentration across a time series and acquiring snapshots at certain time points (e.g., at dawn and at dusk in leaves). The initiation of granules has been evaluated by counting the number of granules present in chloroplast sections. Using 3D-images of Arabidopsis chloroplasts, the number of granules was evaluated to 5–15 granules (Crumpton-Taylor et al., 2012). In that study, the number of granules did not change massively as a function of the starch amount and the presence of residual starch granules at dawn led to the suggestion that mature chloroplasts are unlikely to re-initiate their whole pool of granules every day, but rather re-accumulate starch onto the same granules. In storage organs, the number of starch granules in each amyloplast, varies greatly, ranging from one to several tens. It is worth noting that in storage organs, starch content and granule numbers follow a different dynamic compared with transitory starch in leaves, since storage starch is not periodically degraded. Furthermore, amyloplasts are not thought to contain membranes comparable to the thylakoids, which in chloroplasts serve to compartmentalise the starch granules into different parts of the plastid stroma. Nonetheless, amyloplasts of rice endosperm contain septa-like structures that appear to separate the compound starch granules; they may participate in the process of amyloplast fission (Yun et al., 2010).

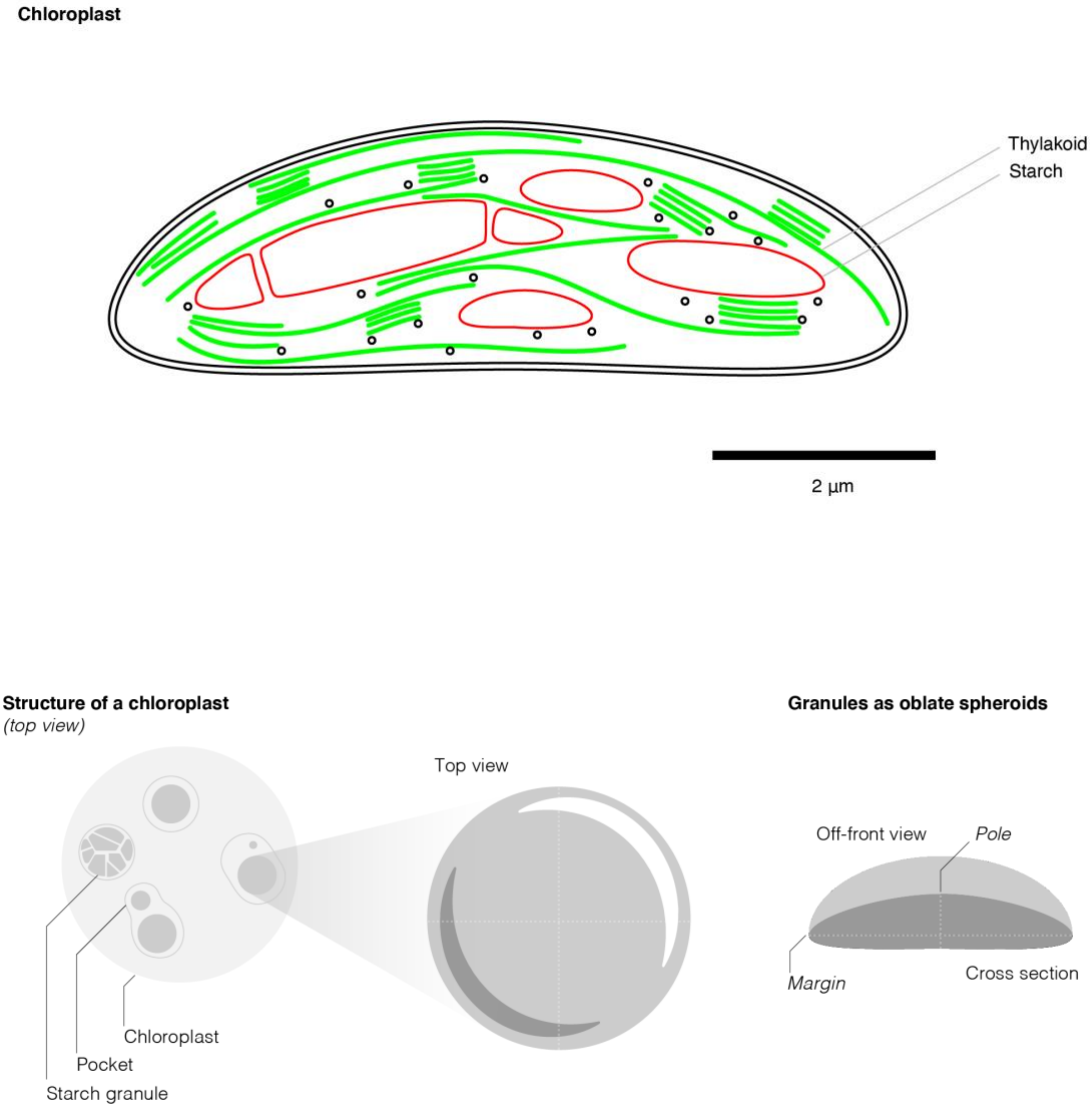

Figure 0.3. Chloroplast structure. Chloroplasts are found in various cell type of the green parts, mostly mesophyll cells. Photosynthesis takes place in the thylakoid membranes (green). About 40% of the photosynthetically fixed CO_2 is stored into starch granules (red). The number of visible granules in a typical 2D microscopy sections is an underestimate of the total number of granules. Granule sections appear elongated but should be considered as flattened spheres. Sometimes multiple granules are not separated by thylakoid membranes and thus occur within the same "stromal pocket".

In absence of any external constraint, a uniform accumulation of starch all surfaces of a nascent starch granule should leads to the growth of a spherical structure. While some starch granules indeed appear spherical, extracted storage starch granules display a variety of shapes depending on the botanical source. For example, some are polyhedral, thought to result from granules growing adjacent to other inside the envelope of the amyloplast, resulting in compound granules. In contrast, all transient starch granules observed to date are flattened to

various degree along their polar axis (Seung et al., 2018). Conceivably, the accumulation of starch could be limited by the pressure exerted by the thylakoid membranes, which are parallel to the equatorial plane of the chloroplast. However, as some mutants show nearly spherical granules, this explanation does not seem likely. Alternatively, the granules could be initiated in a planar rather than punctate fashion. Unfortunately, few biochemical factors affecting granule growth have yet been characterised and the process of granule initiation itself is not well described. However, there is growing evidence that SS4 is essential for the lenticular shape of Arabidopsis leaf starch granules, as when it is removed, chloroplasts display very rounded starch granules (Lu et al., 2018).

The initiation of starch granules

The mechanism of initiation of glycogen, the analogue of starch in animal and fungi, is known; its simplicity, involving only two interacting enzymes, contrasts with the rich picture emerging for starch granule initiation. For the record, the initiation of glycogen particles (often referred to as granules, even though they are soluble) is triggered by the self-glycosylating protein glycogenin (GN). This enzyme dimerises and, using UDP-Glc as a substrate, glycosylates a tyrosine residue and then extends the glucan primer to a length of 10–20 residues. Finally, the glucan primer is elongated by glycogen synthases (GS) (Krisman et al., 1975; Lomako et al., 1988; Pitcher et al., 1988). However, although the role of GN is widely accepted, its activity seems not to be necessarily essential for glycogen synthesis. Mutants of yeast lacking GN failed to produce glycogen but this could be reverted by mutations affecting other areas of carbohydrate metabolism (Torija et al., 2005). Furthermore, it appears that bacteria lack GN, despite being able to synthesise glycogen (see Wilson et al., 2010). For example, in *Agrobacterium tumefaciens*, it was shown that GS itself could act as a priming enzyme (Ugalde et al., 2003), although surprisingly little is known about the priming of glycogen in prokaryotes. Some attempted to find a hypothetical "amylogenin" i.e., the analogue of the glycogenin, in plants (Singh et al., 1995; Chatterjee et al., 2005). Further investigations though revealed that this protein is indeed involved in the biosynthesis of cell wall (Rennie et al., 2012). Thus, so far, there is no evidence of a simple self-glycosylating protein that would be responsible for the initiation of starch granules.

Considerable progress has been made in understanding the initiation of starch granules in recent years. The priming of a granule thought to start with a malto-oligosaccharides (MOS), whose length may be diverse, ranging from the shortest – the disaccharide maltose to glucans with a length of 10 or more. Leloir postulated that the glucan elongation happens via the

condensation of ADP-Glc onto a pre-existing glucan (Leloir et al., 1961). Some have questioned this mechanism and proposed that glucans could be elongated on their reducing end (Mukerjea and Robyt, 2013). However, direct evidence revealed that at least SS1 and SS2 catalyse the transfer of ADP-Glc at the non-reducing end of the glucans and not at their reducing end (Larson et al., 2016; Xie et al., 2018). There is still uncertainty over how MOS are synthesised de-novo. Early reports describe the de-novo production of maltose (Linden et al., 1984), while other studies have suggested that starch synthases are able to initiate glucans in a primer-independent fashion (Kreis et al., 1980; Szydlowski et al., 2009).

Once starch metabolism has been initiated, its biosynthesis or degradation would become an appreciable source of such MOS. For example, MOS may come from the trimming activity of debranching enzymes (ISA1/2), which are believed to remove mis-placed branches during amylopectin maturation. The hypothesis of ISA isoforms as generators of glucan primers for further granule initiation is appealing but its strength has been lowered by the presence of many small granules in mutants lacking ISA1/2 (Burton et al., 2002; Fujita et al., 2003; Bustos et al., 2004; Delatte et al., 2005; Kubo et al., 2010). Indeed, this has led to suggestions that ISA may serve to inhibit granule initiation (Kawagoe et al., 2005; Burton et al., 2002). Nevertheless, numerous reports provide circumstantial evidence for the importance of enzymes that can generate MOS in controlling starch granule initiation (Satoh2008; Hwang et al., 2016; Malinova et al., 2017; Seung et al., 2016)

During the last decade, a number of newly identified proteins have been shown to be involved in starch granule initiation and growth in Arabidopsis leaves. These proteins either influence the number of granules that form or alter their shape, or both. The first factor identified was the starch synthase SS4 (Roldan et al., 2007). In the *ss4* mutant, the starch content is higher at dawn and lower at dusk compared to wild-type plants. Strikingly, chloroplasts contain zero, one, and occasionally more enlarged, rounded granules (Roldan et al., 2007, Malinova et al., 2017) a stark reduction from the usual 5–7 granules reported for the wild type. It was been proposed that the spherical granules in *ss4* could result from the combination of the decreased granule number combined with a reduction in night-time starch degradation (Malinova et al., 2017). The majority of the *ss4* chloroplast sections had no starch granule (Lu et al., 2018) and furthermore, the mutant accumulates large amounts of ADP-Glc, probably because in the absence of starch granule initiation, this substrate cannot be used. This correlated with impaired photosynthetic performance, chlorosis and reduced plant growth (Ragel et al., 2013). This is presumably increased ADP-Glc sequesters

adenylates and decreases free P_i, which in turn inhibits photophosphorylation and causes photo-inhibition.

The SS4 protein contains a C-terminal catalytic domain and, unlike the other SS, it has an extension at its N-terminus with four regions containing predicted coiled-coil motifs. The C-terminal contains the glycosyltransferase (GT) domain and is catalytically active. When expressed in the *ss4* mutant this domain alone is sufficient to restore granule initiation by elongating glucans in the early steps of granule development (Lu et al., 2018). However, the granules retained their unusual, rounded shape, characteristic of the *ss4* mutant. The coiled-coil motifs at the N-terminus of SS4 may facilitate interactions with other proteins (Raynaud et al., 2016) and the presence of this part of the protein is required to localise it to specific regions within the chloroplast. In doing so, it appears to influence the direction of the starch granule growth, resulting in wild-type-like, flattened starch granules. This was the case even when the N-terminus was appended to another protein such as the GS from A. tumefaciens (Lu et al., 2018).

After the discovery of the role of SS4 in granule initiation, new players were actively searched, based on the presence of putative coiled coil motifs (which could interact with those of SS4) or using assays to detect protein-protein interactions. Among the discovered interaction partners was, PTST2, a chloroplast-targeted protein containing a CARBOHYDRATE-BINDING MODULE 48 (CBM48) and predicted coiled-coil motifs (Seung et al., 2018). PTST2 was shown to bind to certain MOS via its CBM48 – specifically β-cyclodextrin and maltodecaose. This led to the suggestion that PTST2 may provide SS4 (which lacks a comparable CBM domain) with substrates that already have the propensity to form helical structures and are this suitable for elaboration into a starch granule initial. Interestingly, the association of SS4 with PTST2 appears not to be via coiled-coil interactions with eth N-terminus of SS4, since PTST2 could interact with the C-terminal domain alone. Plants mutated in PTST2 also have a starch-granule-initiation phenotype with some similarities and some differences to that of *ss4*. The amount of starch in of *ptst2* mutants is slightly higher than in the wild type, both at dawn and dusk. Most *ptst2* chloroplast sections contained far fewer starch granules than the wild type although while larger, these granules were still flattened (as in the wild type), rather than rounded (as in *ss4*). Thus, the starch granule phenotype in *ptst2* is less severe than *ss4*, and most chloroplasts contained at least one granule (Seung et al., 2017). The *ptst2* mutants still accumulated 30 times more ADP-Glc than the wild type, but the was only one third of that accumulated in the *ss4* mutant.

Remarkably, in transgenic lines over-expressing PTST2, chloroplasts showed a marked stimulation in granule initiation, with the number increased by an order of magnitude.

Arabidopsis also contains PTST3—a protein which is, in many respects, similar to PTST2, although it has not been studied to the same degree. Like PTST2, PTST3 is a chloroplast-targeted protein containing a CBM48 and predicted coiled-coil motifs, and it was found to associate with its homolog, PTST2 using immunoprecipitation experiments. However, these analyses did not reveal a direct interaction with SS4 (Seung et al., 2017). Mutation of PTST3 once again, leads to a reduction in granule number, but the phenotype is milder compared to *ptst2*. Plants mutated in both PTST2 and PTST3 displayed even fewer granules, and the severity of the phenotype approached that of the *ss4* mutant.

After the discovery of the function of PTST2 and SS4 in granule initiation, immunoprecipitation and yeast-2-hybrid approaches identified additional new players. Immunoprecipitation of PTST2 revealed that besides SS4, two proteins harbouring long coiled-coils containing domains, but no known enzymatic activity could be retrieved: MAR-BINDING FILAMENT PROTEIN (MFP1) and MYOSIN-RESEMBLING CHLOROPLAST PROTEIN (MRC) (Seung et al., 2018). MFP1 was first reported as a filament like protein that binds with DNA (Meier et al., 1996). It was then suggested to attach chromatin to specific sites of the nuclear matrix and has a predicted N-terminal transmembrane domain (Gindulis et al., 1999). Further, proteolysis analysis revealed that MFP1 was anchored to the thylakoid membrane via its transmembrane N-terminal domain and was suggested to have a stromal C-terminal DNA-binding domain (Jeong et al., 2003). MRC was also identified in yeast-2-hybrid experiments where SS4 was used as a bait protein, and in that case designated as PII, for PROTEIN INVOLVED IN STARCH INITIATION (Vandromme et al., 2019a). The roles of MRC and MFP1 in granule initiation was again confirmed by mutational analyses, with decreased number of granules found in the *mrc* and *mfp1* mutants, even though the reductions were less marked than in *ptst2* and *ss4* mutants.

Chloroplasts of *mfp1* contained fewer, larger flattened granules. Interestingly, unlike the other factors described thus far, MFP1 is not a soluble protein but is found fully associated with the stromal side of the thylakoid membrane (Jeong et al., 2003). Both PTST2 and SS4 have also been reported to be partially localised to the thylakoids, although for SS4, the evidence is inconsistent. In the case of PTST2, there is good evidence to suggest that a fraction of the protein is tethered to the thylakoids by MFP1. Both proteins, when fluorescently tagged,

show an overlapping, patchy distribution within the chloroplast (Seung et al., 2018). In the *mfp1* mutant, the partial thylakoid localisation of PTST2 is lost and it behaves like a soluble protein. Furthermore, the patchy distribution of fluorescently tagged PTST2 vanishes in *mfp1*, and instead it forms 1–2 punctae per chloroplast. These data have contributed to the idea that MFP1 serves to localising other components of the starch-granule-initiation apparatus and thereby determine sites where starch granules will form.

MRC was discovered by searching for interaction partners of PTST2 (via immunoprecipitation) and of SS4 (Seung et al., 2018; Vandromme et al., 2019a). MRC has no CBM and is thus not directly interacting with glucans (Vandromme et al., 2019a). Further, no recognisable protein domain was reported so far but it may well interact with PTST2 and SS4 via its numerous predicted coil-coiled containing domains. It has been proposed to be required for the correct folding of SS4 or, alternatively, to offer primer substrates to SS4, and/or to prevent the degradation of such primers (Vandromme et al., 2019a). Chloroplasts deficient in MRC contain fewer starch granules but were still flattened (Seung et al., 2018; Vandromme et al., 2019a). When MRC was fluorescently tagged, it was distributed in speckles and this distribution was not altered when MFP1 was absent, suggesting that it is not involved in MFP1 localisation (Seung et al., 2018). The distribution pattern of MRC is similar to that of SS5, with which it interacts, suggesting that SS5 influences the number of granules via MRC (Abt et al., 2020). However, since both *mrc* and ss5 granules retain their flattened morphology, they are unlikely involved in defining the shape of the granule. MRC may have a role in bringing SS4 and SS5 into contact with other factors.

The discovery of these new factors involved in starch granule initiation prompts the reconsideration of the extent of the network of protein interactions and the possibility of other, yet unknown proteins that help orchestrate amylopectin synthesis. It is though reassuring that some of the new factors described in Arabidopsis (e.g., PTST2) play roles in starch biosynthesis in other systems like the cereal endosperm (Pen et al., 2014; Saito et al., 2018). In rice, PTST2 homolog (FLO6, for FLOURY ENDOSPERM 6) was identified even before it was studied in Arabidopsis. Like PTST2, FLO6 contains a CBM48 module known to bind to starch (Boraston et al., 2004; Guillen et al., 2010; Janecek et al., 2011) but has no enzymatic activity. Similarly, a longstanding mutant in barley (franubet; Suh2004) was recently attributed to a mutation in the FLO6 ortholog (Saito et al., 2017), and the gene has been very recently studied in wheat (Chia et al., 2020). In rice, FLO6 was found to interact with ISA1 via its N-terminus, suggesting that FLO6 bridges ISA1 to its substrate (Pen et al.,

2014). However, in Arabidopsis chloroplasts, PTST2 was proposed to interact with SS4, and no interaction with ISA1 could be detected (Seung et al., 2017). Rice plants mutated in FLO6 accumulated less starch but contained more proteins and lipids than wild type plants. Rice grains of the *flo6* mutant display a lose filling, giving their white, floury appearance. The regular compound granules normally seen in rice were severely altered: certain amyloplasts were devoid of starch, while others contained either single large granules or numerous minute granules. Isoamylases are important for normal starch synthesis, yet their role in starch granule initiation has remained the subject of speculation. They could accelerate the crystallisation of the starch primer so that it escapes the degradation machinery (Ball et al., 1996; Myers et al., 2000). Alternatively, it was suggested that isoamylases may participate in the degradation of the soluble α-glucans, which accumulates in their absence, and go on to form phytoglycogen (Zeeman et al., 1998).

Analysing granule development

While the biochemistry of starch is nowadays relatively well understood, the cell biology side has not reached the same level of understanding. Indeed, the research on starch has always been fostered by its industrial applications, where it is often sufficient to consider starch as a bulk matter. Yet, the mechanisms of the granule formation and its regulation within the plastid should not be neglected if we want to engineer starches with innovative properties relevant to the many industrial processes that utilise it.

Several methods exist to characterise the size and morphology of starch granules *ex situ*, but these inevitably remove the cellular context by which these characteristics emerge, i.e., extraction erases the "molecular sociology" (Robinson et al., 2007). The naivest approach to examine the morphology of starch granules is to extract them and then examine them via microscopy (typically light microscopy or scanning electron microscopy). Starch granules are robust and stable and can readily be extracted by homogenising plant material. The starch granules can be separated from the rest of the cellular debris using a combination of filtration and centrifugation steps, which can include refinements such as density steps or gradients (e.g., using Percoll) when necessary. These techniques work well when the granule size is known in advance to be homogeneous or unimodal. However, in cases where the size distribution is wide, or multimodal, the granules captured may be biased toward the largest or smallest ones, depending on the purification procedure applied. When the granules need extracting conservatively, purification steps should be minimised. In the case of Arabidopsis starch, leaves are typically ground in an aqueous, detergent-containing medium to disrupt the membrane rich chloroplasts, filtered through nylon meshes to remove cellular debris, and starch collected by high-speed centrifugation.

As an alternative to microscopy, parameters of granule size and morphology can be estimated in solution using other techniques. The size of granules can be evaluated via the Coulter principle, by which the particles to be sized are suspended in an electrolyte solution and passed through a small opening, where the voltage change is recorded between two electrodes. The change in ionic current will be altered when a particle passes through; this change, known as impedance, is used to count the particles. Besides the counting, particle size can be measured since the strength of the signal is proportional to it. This method was initially developed in the 1940s for sizing blood cells but later found many industrial applications. The Coulter counter method has been often used to size the starch granules

(Morrison et al., 1986; Tester et al., 2008; Vandromme et al., 2019a; Vandromme et al., 2019ab).

Alternatively, the granule morphology can be evaluated by their scattering response to an incident laser. One popular method, flow cytometry, compares the light signal the granules generate when passing through an optical system. The calibration is achieved with standard sizing acrylic beads, which have a similar refractive index. This is an efficient method to assess the overall size distribution of starch granules, as the average diameter is readily determined from large numbers of observations. Other morphological parameters such as irregularity or sphericity can be more difficult to capture, however. While the abovementioned techniques have the advantage of analysing many granules, the contextual information is missing. For instance, it is common to see polyhedral granules, such as in rice starch. However, observations of the same granules *in situ* in the rice endosperm shows that these polyhedral granules derive from compound granules produced side-by-side within the same amyloplast. Presumably, in the absence of neighbouring granules and the resulting compaction, round granules would form.

Relevant information from the sub-cellular environment is required to build up a fine understanding of the granule initiation and their subsequent development within the plastid. The normal technique to observe starch granules within a plant cell is through the fixation and embedding of tissue, followed by semi-thin sectioning. Plastid sections and the starch granules within can then be observed using light microscopy. This approach has some limitations. First, fixation and embedding can cause some changes (artefacts) in the appearance of the cellular ultrastructure. Second, plastic semi-thin sections of leaf mesophyll cells reveal the shape and the number of granules within the chloroplast sections but does not allow the smaller granules to be analysed with sufficient resolution, nor the potential interface between the granules and the surrounding structures such as the thylakoid membranes. Third, sections typically capture only part of the chloroplast or starch granule so the plane of section strongly influences the appearance (e.g., a discoid granule can appear circular or as an elongated ellipse, depending on its orientation relative to the section) (Figure 0.2). Light microscopy is therefore limited to the general appearance of the granule, and the number of granule sections.

Confocal laser scanning microscopy

To observe chloroplasts in further detail, two imaging techniques are available: Confocal laser scanning microscopy (CLSM) and electron microscopy (EM). Each aims at overcoming the limited resolving power of light microscopy (LM). CLSM takes a middle point between the real-time imaging possibility of LM and the great resolution of EM (Brakenhoff, 1989). The ideal sample depth ranges from 50 to 100 μm (Pawley, 2006), while a 140-nm resolution can be attained (Brakenhoff, 1980). First evidence of resolution improvement of confocal imaging was applied to LM in the late 1970s (Sheppard et al., 1977). A confocal microscope uses point illumination, by which the light beam is focussed on each point of the volume of interest. Because it does not illuminate the whole sample, the contributions of out-of-focus volume are suppressed, enhancing the contrast. Since the signal comes only from a point in the sample at a time, the main limiting factor is the low the signal-to-noise ratio. The signal can be strengthened by increasing either the pinhole diameter or the acquisition time. So called optical sections are acquired by scanning consecutive planes without further computational costs, simply by moving the stage.

The emission spectra of the numerous auto-fluorescent pigments present in plastids can be used for localisation within the tissue of interest (Egea et al., 2010; Bahaji et al., 2011). Further, CLSM can be leveraged with fluorescent versions of proteins of interest, through which a variety of cellular mechanisms have been investigated (e.g., Mackinder et al., 2017). Different fluorescent dyes can be used to simultaneously identify the patterns of multiple factors. However, the relatively long acquisition time can make the imaging difficult for mobile systems, although these can be immobilised (e.g., with low melting point agarose). CLSM can be challenging when applied to larger systems; if that is the case, tissue explants and protoplasts can be employed.

CLSM has been routinely used to localise proteins involved in starch biosynthesis (Seung et al., 2018; Abt et al., 2020). Investigating starch localisation patterns within chloroplasts can also be carried out, via the labelling of known granule associated like GBSS, i.e., in GBSS-GFP-expressing plants (Szydlowski et al., 2009; Bahahi et al., 2011). It is also possible to study starch via the absence of autofluorescence. Taking advantage of the fact that chloroplasts are auto-fluorescent but not the starch granules, Vandromme and colleagues (2019) characterised the gaps inside the chloroplasts. The results appeared similar to the granule morphologies derived from EM images; however, the method only provides a mean for the general morphology of mature granules. It does not permit the examination of the

smaller granule initials, nor abutting granules, and it does not reveal the precise location of the granules with respect to the thylakoids. Another fluorescence-based method to study starch in guard cells, used a modified propidium iodide staining (Truernit et al., 2008; Fluetsch et al., 2018) on epidermal peels. In this case, the starch granules are stained using the periodic acid – Schiff (PAS) method (Chawla et al., 2017), permitting great resolution using CLSM, by which the starch granules can be visualised and measured (Fluetsch et al., 2018).

Electron microscopy

Electron Microscopy (EM) has been widely used to investigate sub-cellular structures, including the cellular environment in which starch granules are made and also the internal structures of starch itself. As the wavelengths of visible light are too long to interact with small structures of interest (small starch granule initials are ~100 nm in diameter), the replacement of photons by electrons, whose associated wavelengths are much shorter, allows these structures to be imaged. The downside of EM is that the electron beam is very sensitive to the medium it travels in (the air) before it hits the sample and within the sample (medium thickness). Therefore, the chamber containing the optics needs to be under vacuum and the sample is typically still fixed and embedded. Thus, while resolution is improved, some of the problems associated with light microscopy remain. Furthermore, unless using the most advanced microscopes adapted for work with frozen samples, the electron density of the cellular components generally require enhancement.

Besides the heavy sample preparation to withstand the conditions of the microscope chamber, for Transmission Electron Microscopy (TEM), the sample needs to be prepared as ultra-thin sections (a few tens of nanometres thick) so that it can be traversed by electrons. These constraints call for the sample to be stabilised; the structures of the tissue are therefore cross-linked using a fixative solution, in most cases using an aldehyde (formaldehyde, glutaraldehyde), that can cross-link biomolecules through their aldehyde groups. The sample is then dehydrated with ethanol, infiltrated with an epoxy resin and finally plasticised. Contrasting agents are often introduced to delineate the membranes and biomolecules by specifically oxidising alkenyl bonds. The agent must contain an element with a sufficient mass number to be able to diffract the electron beam when imaged, since most of the atoms making up the tissue (H, C, N, O, P, S) are below the atomic number 50 and impact on relatively few of the electron trajectories.

Clearly, the need for fixed samples prevents cellular processes from being imaged in real time, as is sometimes possible using light or confocal microscopy. Furthermore, the need for thin sections for TEM prevents imaging in the z-dimension. Thus, if the high lateral resolution of EM imaging is to be used to visualise the initiation and development of starch granules, it must be combined with complementary techniques, to both increase the z-resolution and to incorporate some sort of temporal resolution.

Tomography

As described above, sample for TEM need to be thinned so that the resulting sections are thin enough to transmit electrons (typically <100 nm). This inevitably reduces the possibility for imaging a depth of field. Nevertheless, several techniques have been developed to image cellular ultrastructure in 3D. When the structures of interest are smaller than 100 nm, such as ribosomes and cellular membranes, it is possible to treat even ultrathin sections as a volume and obtain information in the z-dimension by imaging a tilt series of each section. Using this tilt series allows 3D information to be calculated in silico and z-stacks to be generated. Chemical fixation and the infiltration can be replaced by plunge-freezing the specimen. This, when combined with further sample preparation steps (cryo-sectioning or cryo focussed-ion-beam [FIB] milling), can yield unstained samples in a near-native state in vitrified water, which can be imaged using advanced instruments. At that scale, tomographic images of homogeneous particles can be averaged to increase the signal-noise ratio. This approach offers the greatest resolution but is limited to suitable specimens and the analysis of certain cellular structures. For example, cryo-EM tomography has recently offered important insights into the sub-organellar machinery of Chlamydomonas reinhardtii chloroplasts (Engel et al., 2015; Schaffer et al., 2017; Albert et al., 2019).

Many biological structures are one or more orders of magnitude larger than those imaged by TEM-based tomography. When dealing with larger structures like whole organelles or cells, however, constraints quickly add up. Imaging is nonetheless possible if the sample block surface is incrementally milled or planned and imaged by Scanning Electron Microscopy (SEM) to detect the backscattered electrons. The first method to remove matter from the sample block face involves milling it with an ion beam (FIB-SEM); the technique is routinely used in material sciences and has been successfully applied in life sciences (e.g., Uwizeye et al., 2020). It has the advantage of milling very small increments in the z-dimension (a few nm) but allows only small volumes to be sampled.

Alternatively, the block face can be planed with a microtome, as for the preparation of conventional ultra-thin sections. With care, consecutive sections can be “glued” together side by side and the resulting ribbon can be transferred to a conductive support and imaged sequentially by SEM; the volume is recreated by stacking the slice images. This method has several caveats as reasons for the ribbon to go awry during or after sectioning are numerous. Furthermore, the sequential images need to be aligned which can be difficult when there is local distortion during sectioning and imaging. These problems limit its adoption for routine use. Nevertheless, serial sectioning has a key advantage in that the sections can be kept for further analyses, such as correlative light microscopy or mass spectrometry, as described below. Interestingly, by incorporating a microtome into the stage of the scanning electron microscope, the sample’s block surface can be repeatedly imaged and planed by the microtome, progressively revealing the underlying tissue. The whole imaging-sectioning is automated and does not rely on the formation of an intermediary state (the ribbon), during which the sample can be damaged. This approach brings together the optimal combination of high resolution and a large, sampled volume (up to hundreds of micrometres in the x, and z axes). The above-mentioned methods were successfully applied to study the ultra-structures of chloroplast (Bussi et al., 2019; Pipitone et al., 2020). However, the sample preparation prevents the chloroplasts to be tracked over time; making impossible to directly study the development of starch granules.

In contrast, confocal laser scanning microscopy provides the ability to study in real time the chloroplast but compromises the spatial resolution. Nevertheless, by combining the autofluorescence with 3D structured illumination microscopy (Iwai et al., 2018), it is possible to image chloroplasts beyond the limitations imposed by optical systems (e.g., diffraction barrier), which could potentially be applied to starch biosynthesis. Alternatively, as a new approach to study the dynamic of starch granule development with EM, described herein, one can first perform stable isotope labelling, image the structures of interest with SEM, then retrieve the location of the label with secondary ion mass spectrometry (see below).

Secondary ion mass spectrometry (SIMS)

Answering many questions in metabolism involves resolving the destination and use of specific metabolites. To that end, the use of labelled molecules is a powerful tool but requires a method to recapture and quantify the label after it has entered the biological system. However, as biological systems are typically complex and heterogeneous, the isolation of a single molecular species from within a specific subcellular compartment, without

contamination from the environment or other parts of the system can be challenging. It is therefore necessary to be able to probe the system in situ, at the cellular scale. Biomolecules and in particular, proteins can be tagged with a fluorescent tags or dyes. However, it is often difficult to exclude an effect caused by the tag/dye itself, and for small metabolites this approach is impractical or impossible. In this case, the ideal marker can be simply an element of the molecule with a specific isotopic signature (^{2}H, ^{13}C, ^{15}N, etc). Assimilation and utilisation of this isotopically labelled molecule can then be measured through mass spectrometry, or other means in the case of radioisotopes. Tagging molecules with stable isotope atoms was used by Rudolph Schoenheimer in the early twentieth century to track the proteins in the body. Sadly, at the time, the technique could not be used at the subcellular levels, since imaging was not possible.

In the early 1960s, Raymond Castaing and Georges Slodzian pioneered in mass filtered emission ion microscopy using secondary ions to tackle the problem of elemental localisation (Colliex, 2019), the raison d'etre of many of these endeavours being to advance geochemistry, metallurgy and electronics. Despite the first reports of the use of such methods in life sciences in the 1970s (Galle, 1970), the application suffered from constraints inherent to cells, and it is only in the last two decades that SIMS imaging has emerged as a powerful tool. To be useful in life science SIMS has to overcome several challenges.

Until the 2000, it was not possible to analyse multiple ions simultaneously and their ratio had to be measured one ion at a time (Hindie et al., 1990; Lousier et al., 2000). Repeating the scan for different ions was a noticeable source of error, as the sample position and state was sequentially modified. Hence, the emergence of multiple ion mass spectrometers considerably improved the quality of the signal.

Developed at the Office National d'Études et de Recherches Aérospatiales, the NanoSIMS was naturally aimed at cosmochemistry. It has an experimental mass resolution of 10000, a secondary ion transmission of about 70–80% and a lateral resolution of 33 nm, making it also a valuable microscopic method in life science research. In a NanoSIMS, a probe (the primary beam) is used to scan the surface of a solid sample. The impact of the probe triggers the ejection of atoms, among which some are spontaneously ionised. Those are condensed along the secondary column, the hexapole electron lens and the electrostatic sector and diffracted according to their mass/charge ratio by a magnetic sector. Finally, the abundance of each species is measured by multi-detection units consisting of a deflection plate, a selection slit

and an electron multiplier (Peteranderl et al., 2004). In a NanoSIMS 50L, it is possible to simultaneously record the counts of up to 7 masses (Figure 0.4).

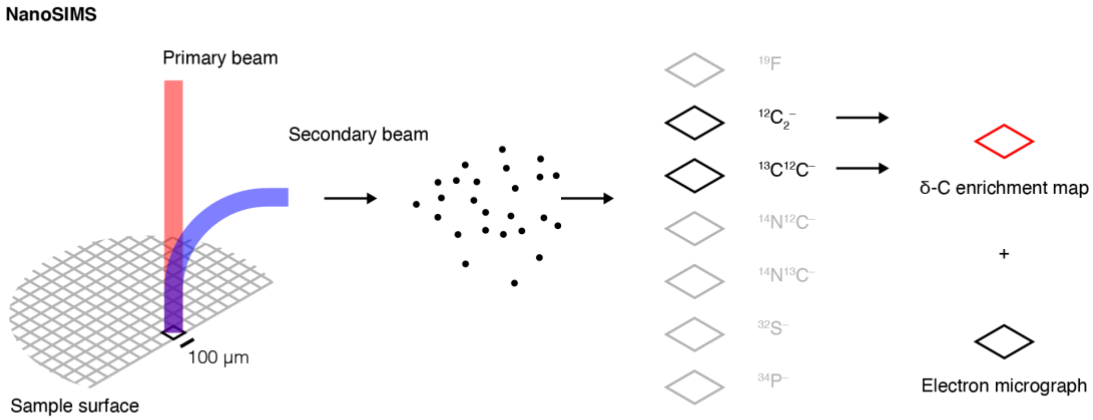

Figure 0.4. Nanoscale secondary ion mass spectrometry (NanoSIMS). The primary beam (e.g., Cs^+) interacts with the sample surface and ejects matter. Some species are spontaneously ionised (secondary ions) and can thus be accelerated through the coupled mass spectrometer. These secondary ions are simultaneously quantified, giving each an ionic image of the sample. By taking the ratio of certain species of interest and by comparing it with the natural abundance, enrichment maps are obtained.

Under standard analytical conditions, the NanoSIMS uses a caesium ions (Cs^+) primary beam with an impact energy of 16 keV and a current of 0.8 pA, reaching a lateral resolution of 100 nm. Depending on the chemical nature of the species of interest, the current needs to be augmented at the expense of the lateral resolution. The acquisition time is about 1 ms per pixel and the raster dimensions are 256 x 256 pixels. For biological applications, most relevant ion species come up negatively charged. Therefore, the primary ion beam is made up of Cs^+. Biologically relevant ion species include the single ions $^1H^-$, $^2D^-$, $^{12}C^-$, $^{13}C^-$, $^{16}O^-$, $^{18}O^-$, $^{19}F^-$, $^{31}P^-$, and $^{32}S^-$ and the cluster ions $^{12}C^1H^-$, $^{13}C1H^-$, $^{12}C^2D^-$, $^{13}C^2D^-$, $^{12}C^{14}N^-$, $^{13}C^{14}N^-$, $^{12}C^{15}N^-$, and $^{13}C^{15}N^-$. Due to the low electron affinity of nitrogen, it doesn't form ions and must be analysed through the cyanide (high electron affinity, 3.82 eV). Detecting the cyanide leads to isobaric interferences (ionic species with extremely similar mass to charge ratios), which are overcome by the high mass resolution of the NanoSIMS.

Most NanoSIMS analyses on biological specimens are performed on fixed tissues that have been previously imaged by microscopic methods (typically EM). The required sample preparation will alter its chemical composition in at least two ways. First, the numerous

washing steps and the dehydration may selectively remove label depending on the tissue, especially when the label is in soluble compounds in the cell cytosol, the plastid stroma, or the vacuole. Second, the resin infiltration inevitably dilutes the ^{13}C signal by the addition of ^{12}C. However, the relative ratio (when normalised to the natural abundance) remains unchanged (Pernice et al., 2014). These alterations can be offset with various approaches. The conventional sample preparation can be replaced with cryo-fixation and freeze-substitution. Although, this does not completely suppress the risk of label re-distribution within the cell. Alternatively, the recent development of cryo-NanoSIMS aims at overcoming the above-mentioned pitfalls (Jensen et al., 2020).

However, for the analysis of starch this disadvantage is turned into an advantage, since starch is insoluble and preserved during fixation, this selective washing indeed increasing the overall contrast. During the data processing, all the planes from each ion species are aligned and accumulated. In a second step, the ratio between ion species of interest is computed pixel-wise. Additionally, the ratio is normalised to the natural abundance and centred at 0. The natural abundance is computed from an unlabelled control sample, embedded alongside the labelled samples, to account for any inherent experimental variability.

The magnitude of the signal greatly varies depending on the nature of the metabolites of interest. Therefore, accumulation of several NanoSIMS planes is generally necessary. In addition, the visual evidence needs to be completed with statistical analysis to quantify the uncertainty. Fortunately, starch is produced rapidly and in large quantities. Its synthesis has been already imaged using NanoSIMS, when investigating inorganic carbon and nitrogen assimilation in the dinoflagellate endosymbionts of corals (Kopp et al., 2015). In the case of leaves, the assimilation of carbon dioxide by photosynthesizing chloroplasts happens even more rapidly (over a time scale of a few minutes) and, in Arabidopsis, up to half of the photoassimilates are directly converted to starch. Consequently, a 15-min pulse of $^{13}CO_2$ is sufficient to reach ^{13}C-enrichments in starch of 10000 permille.

Outlook and aims of this thesis

Techniques used to characterise starch that provide measurements about a large population of granules (e.g., starch concentration per plant, shape and size distributions of extracted starch granules) or give incomplete pictures (e.g., quantification from chloroplast section) give useful overviews, but a full understanding of granule dynamic requires major improvements in spatial and temporal resolution. The properties of starch granules (number, shape) are the result of the concerted effort of a number of factors. Yet, their mechanism cannot be observed with sufficient time-space resolution. Modern ionic imaging/NanoSIMS, properly applied, can remove these limits, enabling us to visualise initiation events and trace starch accumulation.

The spatial resolution will be enhanced by using electron microscopy, with resolution down to a few nanometres, while resolution in depth will be achieved by serial block face scanning electron microscopy (SBF-SEM). The temporal resolution can be enhanced by time-course sampling during the day. However, the data so acquired remain snapshots; the image does not indicate when the visible granules have been initiated, nor how much starch they have accumulated. To remedy that problem, in-vivo starch labelling can be done at specific times by providing photosynthesising plants with a pulse of $^{13}CO_2$-containing air. With NanoSIMS, label information can be retrieved from previously EM-imaged sections containing granules of interest, with enrichment indicating where starch was accumulated during the pulse. When a chase period in $^{12}CO_2$ follows the pulse, it becomes possible to compare the current starch granule morphology and with the now-internal labelled regions synthesised earlier.

In my first chapter, I describe starch granule initiation in previously de-starched chloroplasts. Entire chloroplasts were imaged using SBF-SEM to capture every granule in 3D. A workflow was established to label starch with pulses of $^{13}CO_2$ and probe ^{13}C-enrichment in mesophyll cell chloroplasts containing granule sections with NanoSIMS. Pulses applied at the start of the day revealed that granules initiate in parallel and coalesce, while pulses applied later in the day revealed anisotropic growth along the granule margin. Similar experiments on *ss4* mutants with spherical granules, reveal a loss of anisotropic starch deposition. Finally, experiments on *gbss* mutants deficient in the granule-bound starch synthase responsible of amylose synthesis reveals that its action occurs within the amylopectin matrix.

In my second chapter, I applied these techniques to look at the role of the proteins of starch granule initiation. Given that de-starched wild type chloroplasts are able to start off parallel

initiations in several discrete locations, I examined whether this ability is conserved in mutants with an average lower granule number (*mfp1*, *mrc*, *ptst2*, *ptst3*, *ss4*). Examination of SBF-SEM of chloroplasts at dawn revealed differences in their capacity for initiating multiple granules; the mutants *mrc* and *ss4* have notable reduced cluster size in comparison with *mfp1* and *ptst2* which were able to initiate parallel granules. I therefore propose a hierarchy in their function and speculate that MRC/SS4 control the granule initiation more directly than MFP1/PTST2.

Chapter 1

Starch is formed by coalescence of granule initials and directed anisotropic growth, controlled by the non-enzymatic domain of STARCH SYNTHASE 4.

Submitted to Nature Communications

Léo Bürgy[1], Simona Eicke[1], Christophe Kopp[2], Camilla Jenny[1], Kuan Jen Lu[1], Stephane Escrig[2], Anders Meibom[2,3], Samuel C. Zeeman[1]*

[1] Institute of molecular plant biology, ETH Zurich, 8092 Zurich, Switzerland

[2] Laboratory for biological geochemistry, Ecole Polytechnique Fédérale de Lausanne (EPFL), Lausanne, Switzerland

[3] Centre for Advanced Surface Analysis, University of Lausanne, Lausanne, Switzerland

* Correspondence to: samuel.zeeman@biol.ethz.ch

Author contributions Leo Bürgy conducted most of the experiments. Simona Eicke and Leo Bürgy helped with electron microscopy procedures. Christophe Kopp did the preliminary work on NanoSIMS on starch granules and acquired the images related to *gbss* and starch midday accumulation. Kuan-Jen supervised Camilla Jenny's master thesis, which acquired and analysed the NanoSIMS related to the accumulation patterns when SS4 is knocked out. Anders Meibom and Stephane Escrig provided technical support to acquire NanoSIMS images. Leo Bürgy prepared all the figures and wrote the manuscript together with Samuel C. Zeeman, with input from all authors.

Abstract

Living cells orchestrate enzyme activities to produce myriads of biopolymers but cell-biological understanding of such processes is scarce. Starch, a plant biopolymer forming discrete, semi-crystalline granules within plastids, plays a central role in glucose storage, which is fundamental to life. Combining complementary imaging techniques and Arabidopsis genetics we reveal that, in chloroplasts, multiple starch granules initiate in stromal pockets between thylakoid membranes. These initials coalesce, then grow anisotropically to form lenticular granules. The major starch polymer, amylopectin, is synthesized at the granule surface, while the minor amylose component is deposited internally. The non-enzymatic domain of STARCH SYNTHASE 4, which controls the protein's localization, is required for anisotropic growth. These results present us with a new conceptual framework for understanding the biosynthesis of this key nutrient.

Introduction

The major source of calories for society are plant-derived carbohydrates. The most important of these carbohydrates is starch—a remarkable, insoluble biopolymer (Smith and Zeeman, 2020). Starch forms as discrete, semi-crystalline granules within sub-cellular plastid compartments, i.e., the chloroplasts of green plants and algae and the amyloplasts of non-green heterotrophic tissues, such as seeds, roots and tubers. The main molecular constituents of starch are the glucans amylopectin (70–90%) and amylose (10–30%). Amylopectin is a branched polymer, synthesized by a suite of interdependent enzymes, and underpins the semi-crystalline nature of starch. Amylopectin fine-structure varies between plant species as a function of the relative amounts and complex interplay between the starch biosynthesis enzymes (Perez and Bertoft). Amylose is an essentially linear polymer made by a single enzyme, Granule-Bound Starch Synthase (GBSS; Denyer et al., 2001). Observed variations in the number, size and morphology of starch granules are highly species specific (Jane et al., 1994; Matsushima et al., 2013) and the morphological characteristics of starch in archaeological remains are used as identifiers of crop species used by early civilizations (Piperno et al., 2000; Copeland et al., 2018). However, despite the global importance of starch for past, current and future human civilizations, the genetic and cell-biological basis for the structural and morphological diversity of starch is largely unknown.

In leaves, starch is formed in chloroplasts during the day from photo-assimilated CO_2 and degraded to support metabolism at night, when photosynthesis cannot occur. Arabidopsis chloroplasts were reported to produce 5–7 lenticular starch granules on average (Crumpton-Taylor et al., 2012). The starch biosynthetic enzymes are well known (Pfister and Zeeman, 2016): α-1,4-linked glucan chains are elongated by a set of five starch synthases (SS: E.C. 2.4.1.21). The α-1,6-branches are introduced by two branching enzymes (BE: E.C. 2.4.1.18) and the structure is finally tailored by isoamylase-type debranching enzymes (ISA: E.C. 3.2.1.68) to promote its crystallization into a lamellar structure with a 9- to 10-nm periodicity. The capacity to form insoluble, semi-crystalline starch-like granules was recently engineered into the non-starch synthesizing yeast Saccharomyces cerevisiae through the introduction of the Arabidopsis enzymes. This synthetic biology approach demonstrated that the core components of starch biosynthetic apparatus are indeed identified (Pfister et al., 2016).

The starch synthase isoform STARCH SYNTHASE 4 (SS4) is known to play a key role in starch granule initiation, with *ss4* mutant chloroplasts exhibiting a strongly diminished

number of granules (Roldan et al., 2007; Crumpton-Taylor et al., 2013; Ragel et al., 2013). Furthermore, *ss4* mutant granules are aberrant in morphology, i.e., more spherical than lenticular. The abilities of SS4 to both promote granule initiation and control their growth depend on its C-terminal glucosyltransferase domain and on its non-enzymatic N-terminus, respectively (Lu et al., 2018). However, the molecular mechanisms underpinning SS4 function are not understood. Recent genetic studies have identified additional proteins involved in granule initiation and growth (Seung and Smith, 2019; Abt et al., 2020). These include PROTEIN TARGETING TO STARCH (PTST) family proteins, which are proposed to deliver glucan substrates to SS4 (Seung et al., 2019), SS5, a non-enzymatic homolog of SS4 (Abt et al., 2020), and two coiled-coil domain proteins MAR-BINDING FILAMENT-LIKE PROTEIN 1 (MFP1) and MYOSIN-RELATED CHLOROPLASTIC PROTEIN (MRC) that bind to and help localize PTST2 and/or SS4 (Seung et al., 2018, Vandromme et al., 2019a). The precise molecular functions of these proteins are also unclear due to the lack of knowledge about the actual process of starch granule initiation.

To discover how starch granule initiation occurs and to track subsequent granule development, we employed a suite of complementary microscopic methods. Serial block face scanning electron microscopy (SBF-SEM) allowed us to visualize the initiation processes in 3D and quantify changes in granule numbers. The additional use of carbon isotope labelling and quantitative nano-scale secondary ion mass spectrometry (NanoSIMS), in combination with molecular genetic approaches, enabled us to understand the role of granule initials and follow granule expansion patterns during the day. These findings provide a new level of mechanistic insight into the cell biology of starch biosynthesis.

Results

Starch granule quantification during the day

We used serial block face scanning electron microscopy (SBF-SEM) to image mesophyll cell volumes from leaves of wild-type plants. Leaves sampled at the end of a 12-h day had 7.0 ± 0.7 mg g^{-1} fresh weight (FW) starch (SD, n=4) and their chloroplasts contained 12.8 ± 2.3 (SD, n=8) lenticular granules. Leaves sampled at the end of the night had 0.24 ± 0.03 mg g^{-1} FW (SD, n=4) starch and 4.4 ± 1.0 (SD, n=5) granules per chloroplasts, which appeared as small discs, thinned at the poles (Figure 1.1A). Thus, only 3% of the mass of starch accumulated in the leaf during the day remained at the end of the following night, but the cores of 35% of the granules were preserved. These cores presumably serve as substrates for renewed starch synthesis during the next day, in parallel with the initiation of new starch granules. To visualize starch granule development, we sampled leaf tissue after 15 min, 30 min, and 8 h light. There were no striking changes after 15 or 30 min (Figure 1.1B–C), with granule shape similar to that at the end of the night. After 8 h light, chloroplasts contained more granules with one or occasionally more granules in a given stromal pocket (defined by groups of starch granules not separated by thylakoid membranes; Figure 1.1D). However, granules newly initiated in the light could not be distinguished from pre-existing granules.

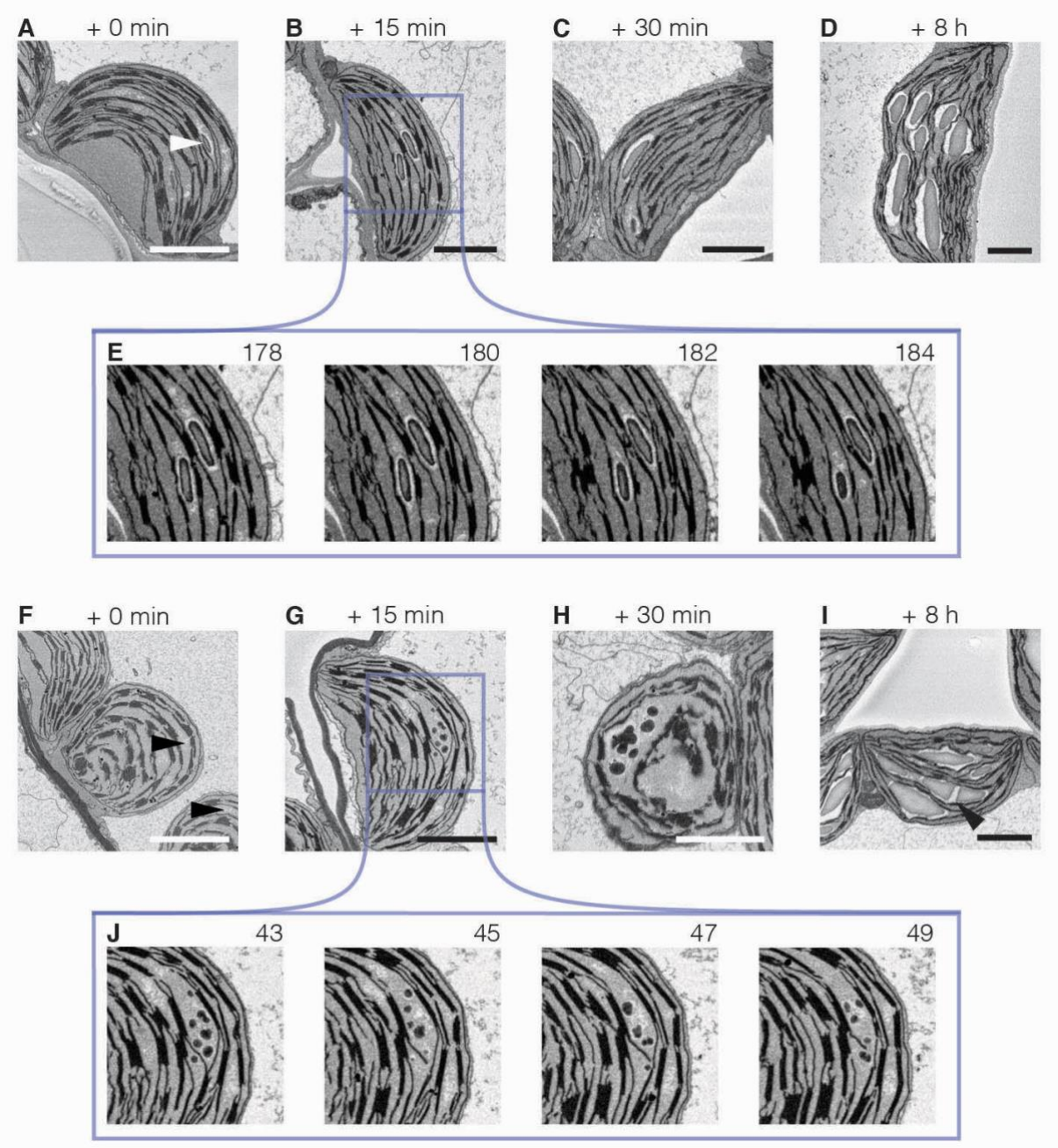

Figure 1.1. See legend on next page.

Figure 1.1: De-starched chloroplasts exhibit parallel initiation of starch granules shortly after dawn. Chloroplast sections from an SBF-SEM stack (with 50-nm Z-resolution, inverted SEM images) sampled from the mesophyll of fully expanded leaves of 35-day old Arabidopsis plants grown in a 12h:12h diel regime. Starch granules appear as dark-grey disks between thylakoid membranes. (**A**–**D**) Representative chloroplast sections from plants harvested (**A**) at the end of a regular 12-h night, with a remaining starch granule (white arrowhead), (**B**) after 15 min light, (**C**) after 30 min light, and (**D**) after 8 h light. (**E**) Series of images (with steps of 100 nm in the Z-axis) from the sample stack in (B). (**F**–**I**), Representative chloroplast sections from plants exposed to a prolonged night and harvested (**F**) at the end of the 4-h night extension, (**G**) after 15 min light, (H) after 30 min light, and (**I**) after 8 h light; The black arrowhead indicates stromal spaces with a floccular appearance. The white arrowhead indicates parallel surfaces of abutting granules. (**J**) Alternating serial sections (with steps of 100 nm in the Z-axis) from the sample stack in (G). Note the numerous starch initials. Scale bars: 2 µm. Further presentations of these data are given in Supplementary Movies S1.1–S1.4.

To observe newly initiated granules, chloroplasts were further de-starched by exposing plants to a 4-h extension of the night. We repeated the SBF-SEM analysis, sampling after the long night and 15 min, 30 min, and 8 h into the day (Figure 1.1F–J). Image stacks were manually segmented to delineate the starch-containing pockets and their respective starch granules at the different time points. The image segmentation yielded the number of starch granules per chloroplast, the number of pockets, and the number of granules per pocket (cluster size) (Figure 1.2). As expected, chloroplasts contained no starch granules after 16-h darkness, but each chloroplast had several regions where the stroma was less electron dense and floccular in appearance (Figure 1.1F, arrowhead; Supplementary Movie S1.4). When exposed to light for 15 min, some of these regions (on average, 5 per chloroplast) contained starch granule initials (Figure 1.1G). Occasionally there was a single granule initial, but usually a cluster was observed (with an average of 4.1 initials, with one pocket exceptionally containing 28 initials: Figure 1.2A–D; Movie S1.4). After 30 min light, the number of pockets was unchanged, but the diameter of the granules had enlarged, many had an irregular appearance, and the average number of granule initials per cluster had decreased to 3.1 (Figure 1.1H; Figure 1.2D; Supplementary Movie S1.2). After 8 h light, chloroplasts contained regular lenticular (oblate spheroid) granules, occupying more pockets than earlier in the day (11 on average). At this time there were more granules per chloroplast than after 30 min (averages of 20 and 16, respectively), but the cluster size had decreased further (on average, 1.9, with typically just one or two; Figure 1.1I; Supplementary Movie S1.3). Interestingly, when there was more than one granule per stromal space, the abutting surfaces were flat, e.g., Figure 1.1I arrowhead. We computed the total surface area and starch volume for each chloroplast and

derived the surface-to-volume ratio. As expected, surface area and volume both increased at the later time points, while the surface area to volume ratio declined (Figure 1.2E).

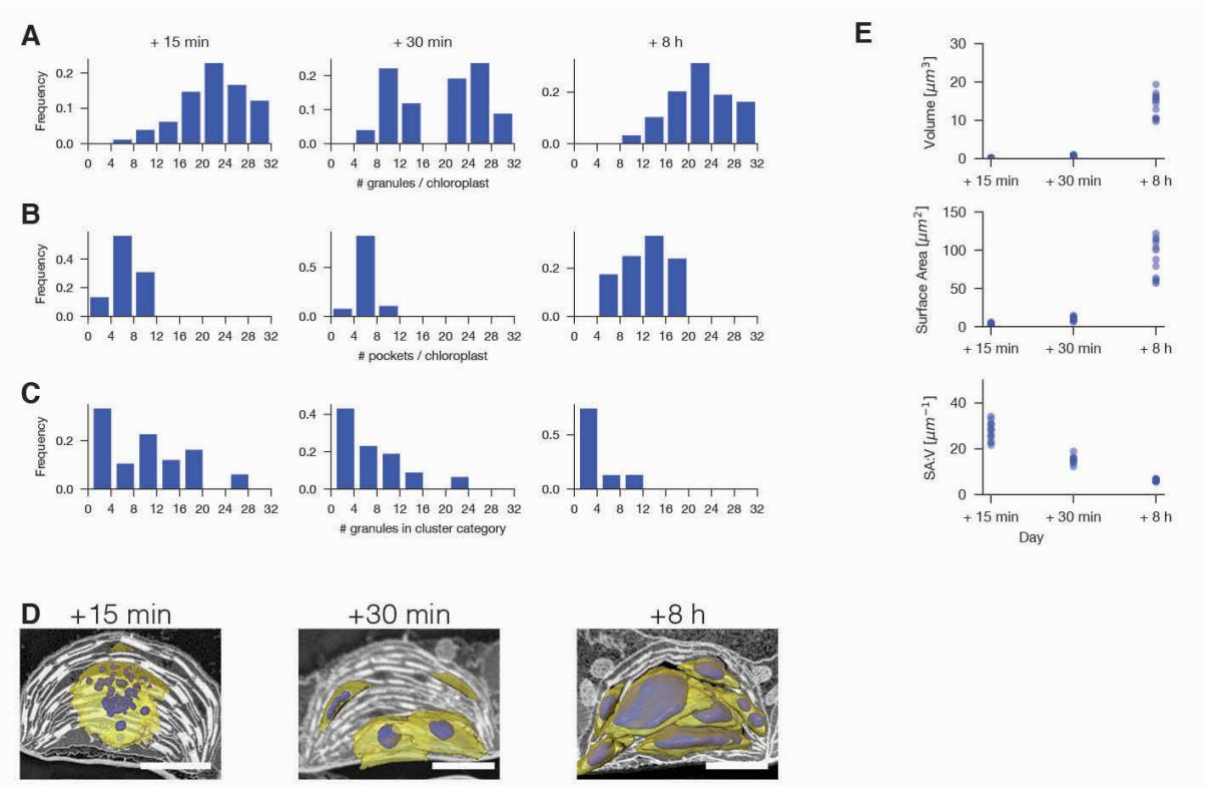

Figure 1.2: Imaging of entire chloroplasts to determine the exact number of starch granules. Tomographic reconstruction from SBF-SEM image stacks of entire chloroplasts from plants sampled after a prolonged night and after 15 min, 30 min and 8 h light. (**A**) The number of granules per chloroplast. (**B**) The number of starch-containing pockets per chloroplast. (**C**) Number of granules in each cluster category. Data in (**A**–**C**) are expressed as frequency distributions (bins of 4), where the height of the bar represents the summed frequencies within each bin. For each time point, two plants from two independent experiments were examined. In total, 20, 18 and 21 chloroplasts were examined for the 15-min, 30-min and 8-h time points, respectively. (**D**) 3D-renderings of representative chloroplasts (non-inverted SEM images) with the pockets (yellow) and their starch granules (violet). (**E**) The total surface area (top), volume (middle) and the surface area-to-volume ratio (SA:V; bottom) for the total starch in each chloroplast.

Coalescence and anisotropic growth of starch granules

The fact that granule number per chloroplast was highest after 15 min light (on average, > 20) and decreased by around 50% after 30 min light without a change in the number of starch-containing pockets suggests that either some starch granule initials are degraded again, or granule initials coalesced as starch synthesis proceeded. The irregular appearance of granules

after 30 min is suggestive of the latter, implying that granules can have multiple initiations. Furthermore, the fact that after 8 h light, the numbers of both starch granules and starch-containing pockets increased suggests that new granules continued to be initiated during the day.

To determine whether starch granule initials do indeed coalesce during the day and understand how they grow, we performed $^{13}CO_2$ stable isotope labelling of illuminated plants, followed by transmission electron microscopy (TEM) and subsequent high-resolution, quantitative isotope mapping of the imaged samples using NanoSIMS (20). After de-starching chloroplasts by extending the night to 16 h, a pulse of $^{13}CO_2$ air was given at the start of the day to label newly formed starch during the first 15 min of photosynthesis. Leaf samples harvested immediately after the pulse, or after a 15-min, 45-min, or 4-h chase in normal air, were chemically fixed and embedded in resin for TEM analysis. During fixation and dehydration, most soluble ^{13}C-labelled compounds are lost from the sample, while ^{13}C-labeled cellular structures, including starch, are preserved. All of the starch initials clustering in pockets were labelled after the pulse of $^{13}CO_2$, showing that they were newly synthesized (Figure 1.3A). After subsequent 15-min and 45-min chases, we observed unambiguous coalescence events where granules forming around labelled starch initials had started to fuse (Figure 1.3B and C). After the 4-h chase, starch granules could be observed with more than one distinct region of ^{13}C -enrichment embedded within them (Figure 1.3D; for further examples, see Figure S1.1). Thus, newly initiated, labelled granules continue to grow and fuse using unlabeled photoassimilates produced during the chase.

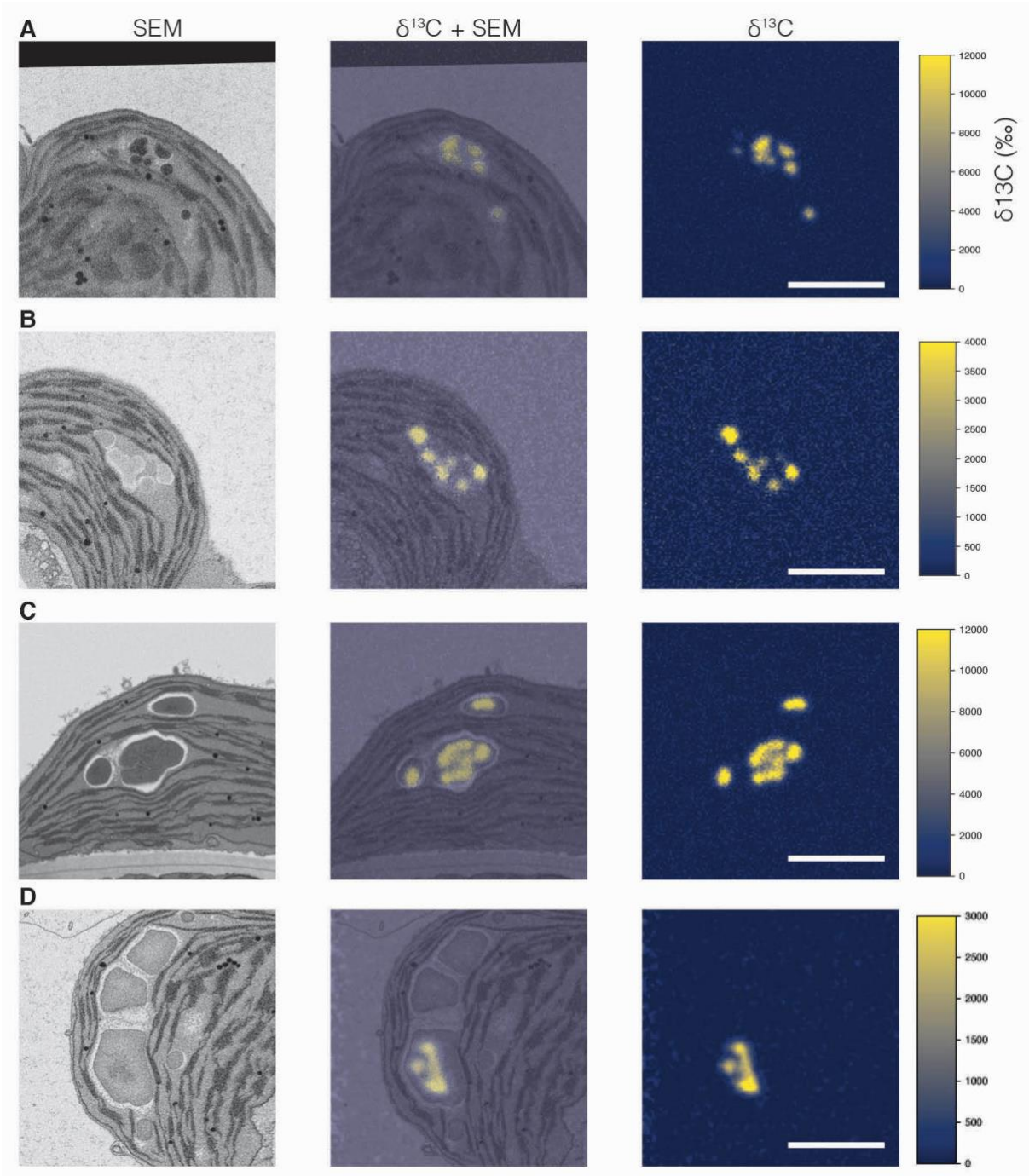

Figure 1.3: Coalescence of starch granule initials tracked with stable isotope labelling, EM and NanoSIMS imaging. Plants subjected to a 4-h night extension were labelled with a pulse of $^{13}CO_2$ for 15 min in the light, then harvested immediately (**A**), or after a chase of 15 min (**B**), 45 min (**C**), or 4 h (**D**) in normal air in the light. In each case samples were fixed and embedded for EM and NanoSIMS imaging. The electron micrograph (right, inverted SEM image) and the enrichment map (left) and their overlay (center) are shown. The ^{13}C-enrichment is reported as per mille. Note the multiple labelled initials in each stromal space, with increasing degree of coalescence during the chase in normal air. Scale bar: 2 µm.

Next, we examined more closely the pattern of granule growth after these initiation and coalescence events. First, plants treated with an extended night (16 h) were allowed to

photosynthesize for 45 min in the light, then labelled for 15 min with $^{13}CO_2$. In leaves sampled immediately afterwards, all granules were labelled, predominantly at the surface with much less enrichment in the existing granule core. The pattern of surface labelling was non-uniform, with much more label incorporated onto the margins of the granules than onto the faces, showing that they were expanding rapidly equatorially, and less so at their poles (Figure 1.4A). This clearly indicates that an expansion pattern is established early in the day and dictates the characteristic lenticular granule shape. In a second experiment, plants treated with a normal 12-h night were labelled with $^{13}CO_2$at midday for 1 h (to achieve sufficient labelling over the increased granule surface area). As for the first experiment, most label was incorporated non-uniformly onto the granule surface, with stronger enrichment along the margins than on the faces (Figure 1.4B; Figure S1.1). Interestingly, where granules abutted, label incorporation was also observed on the flattened surfaces. We quantified the enrichment on the granule surface contour and mapped it to the unit circle, starting at a point furthest from margins, i.e., closest to the barycenter of the granule, to obtain enrichment profiles. Aligning the enrichment profiles revealed that regions of rapid growth coincided with the granule margins and were characterized by several-fold higher ^{13}C-label than the slow-growing granule surfaces (Figure 1.4C). However, not all granules showed rapid growth equally on both margins. Furthermore, rapid growth was less evident on the flattened surfaces of abutting granules. For further examples, see Figure S1.1.

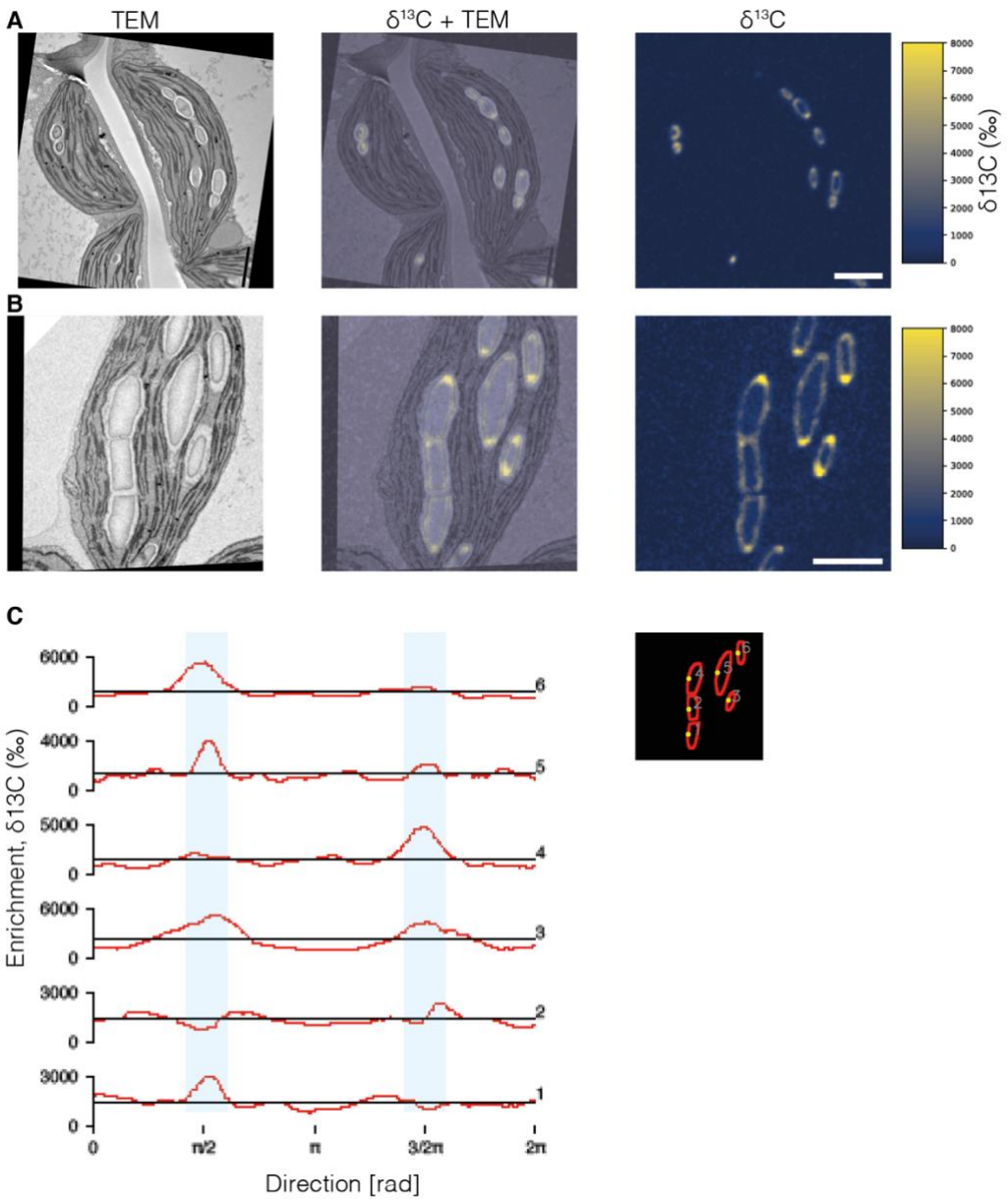

Figure 1.4. Anisotropic starch granule expansion revealed by stable isotope labelling, EM and NanoSIMS imaging. (**A**) Plants subjected to a 4-h night extension photosynthesized for 45 min in normal air, were labelled with a pulse of $^{13}CO_2$ for 15 min, and then harvested immediately for EM and NanoSIMS imaging. (**B**) Plants subjected to a normal night were labelled with a pulse of $13CO_2$ for 1 h at midday then harvested immediately. Scale bars: 2 µm. (**C**) Quantification of ^{13}C-enrichment on the surface of six granules depicted in (**B**). The probing regions (depicted in red in the inset, right) were defined manually with masks over the δ-^{13}C map. Individual circular profiles were extracted anticlockwise from the starting point (yellow). Light blue segments highlight the parts of the profiles corresponding to the granule margins, where most of enrichment is observed. Horizontal lines show the mean enrichment for each profile.

Disrupted starch biosynthesis patterns in Arabidopsis mutants

The availability of Arabidopsis mutants was used to determine which factors control the patterns of starch biosynthesis. First, we analysed the *ss4* mutant, which is defective in the

initiation and growth of granules. The chloroplasts of *ss4* have few large, rounded starch granules (opposed to numerous, lenticular granules in the wild type). SBF-SEM revealed that, after a 4-h night extension, some *ss4* chloroplasts still contained a granule, unlike the wild type (Figure S1.2A). After 15 or 30 min of light, a few small granules were present in addition to the larger granules inherited from the day before (Figure S1.2B and C). These observations, together with the presence of both large and small granules after 8 h (Figure S1.2D) suggests that initiation occurs, albeit at a much-reduced rate. Interestingly, we never observed clusters of granule initials similar to those seen in the wild type (Figure S2E, Figure S3). To study the pattern of granule initiation and growth, we subjected *ss4* plants to an extended night and pulsed them with $^{13}CO_2$ for 15 min in the light, sampling leaves after a 4-h chase (Figure S4). Large granules contained a central ring of ^{13}C-label, indicating that these granules had remained after the extended night and were serving as surfaces for starch re-growth. Interestingly, other granules, sometimes within the same pocket, appeared centrally labelled, consistent with the initiation of new granules, even with pre-existing granules present. We found no evidence of granules containing multiple initials, consistent with the absence of clusters in *ss4* (Figure S2).

We further studied the pattern of granule growth by labelling *ss4* plants with $^{13}CO_2$for 1 h in the middle of the day (after a 12-h night), followed by immediate sampling. The almost uniform, isotropic labelling of the granule surface in *ss4* suggests that SS4 is required for normal anisotropic granule growth (Figure 1.5A) and explains the mutant's rounded granule morphology. The granule initiation phenotype of *ss4* can be rescued by the transgenic expression of a self-glycosylating bacterial glycogen synthase (Lu et al. 2018; Ugalde et al. 2003). Similar ^{13}C-labelling experiments performed on these transgenic plants revealed that each chloroplast contained numerous round granules, that were uniformly labelled. This confirmed that initiation was increased, but that granule growth remained isotropic (Figure 1.5B). When appended to the bacterial glycogen synthase, the non-enzymatic N-terminal domain of the SS4 protein influenced its sub-chloroplastic localization (Lu et al., 2018; Raynaud et al., 2016) and rescued both the granule number and granule morphology phenotypes of the *ss4* mutant (Lu et al., 2018). Labelling experiments on these transgenic plants revealed that each chloroplast contained numerous lenticular granules, with label concentrated on their equatorial regions, similar to the pattern in the wild type (Figure 1.5C). Thus, correct localization of glucan initiating activity by the N-terminus of SS4 is sufficient to guide the overall starch biosynthesis process. This is remarkable because starch is

produced by a suite of biosynthetic enzymes, including but not limited to SS4. In the absence of SS4, these enzymes appear to operate uniformly on the available granule surface.

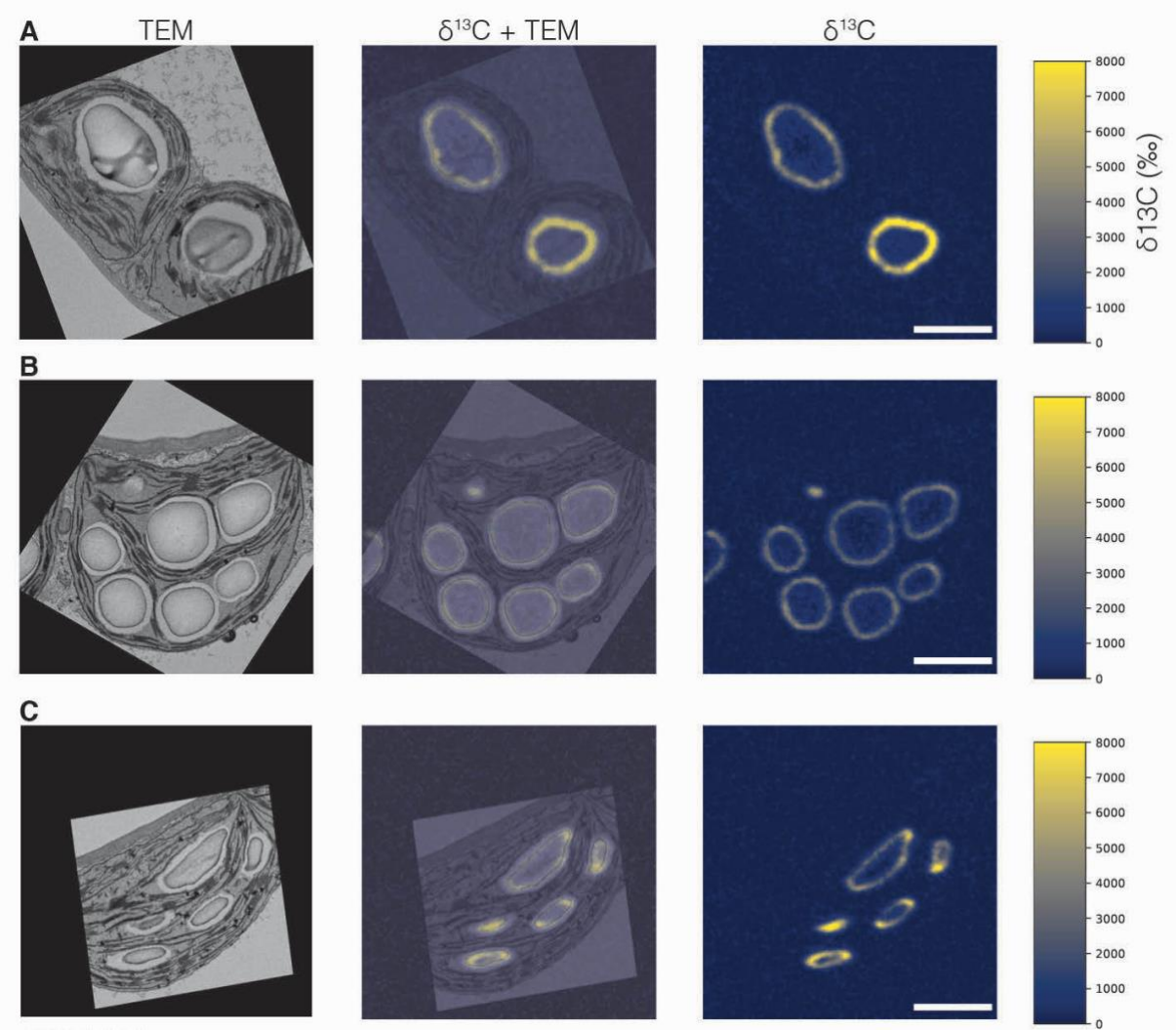

Figure 1.5. Starch granule initiation and growth are controlled by Starch Synthase 4. Plants subjected to a normal night were labelled with a pulse of $^{13}CO_2$ for 1 h at midday then harvested immediately for EM and NanoSIMS imaging. (**A**) Chloroplasts from the *ss4* mutant. (**B**) Chloroplasts from the *ss4* mutant expressing a self-glycosylating glycogen synthase (GS) from A. tumefaciens. (**C**) Chloroplasts expressing the GS fused with the N-terminal of SS4. Scale bars: 2 µm.

Finally, we analysed the synthesis of amylose the minor starch component formed by GBSS. When labelled for 1 h in the middle of the day (after a 12-h night), granules from the amylose-free *gbss* mutant displayed a similar surface-labelling pattern as in the wild type (Figure 1.6A and B). However, when granules were manually segmented into surface and internal core regions, there was less internal enrichment in the *gbss* granules, compared with the wild type (Figure 1.6C). In contrast, granule surface enrichment was slightly higher in

gbss than in the wild type (Figure 1.6C). These data show unambiguously that GBSS-mediated amylose synthesis occurs inside the starch granule matrix in vivo.

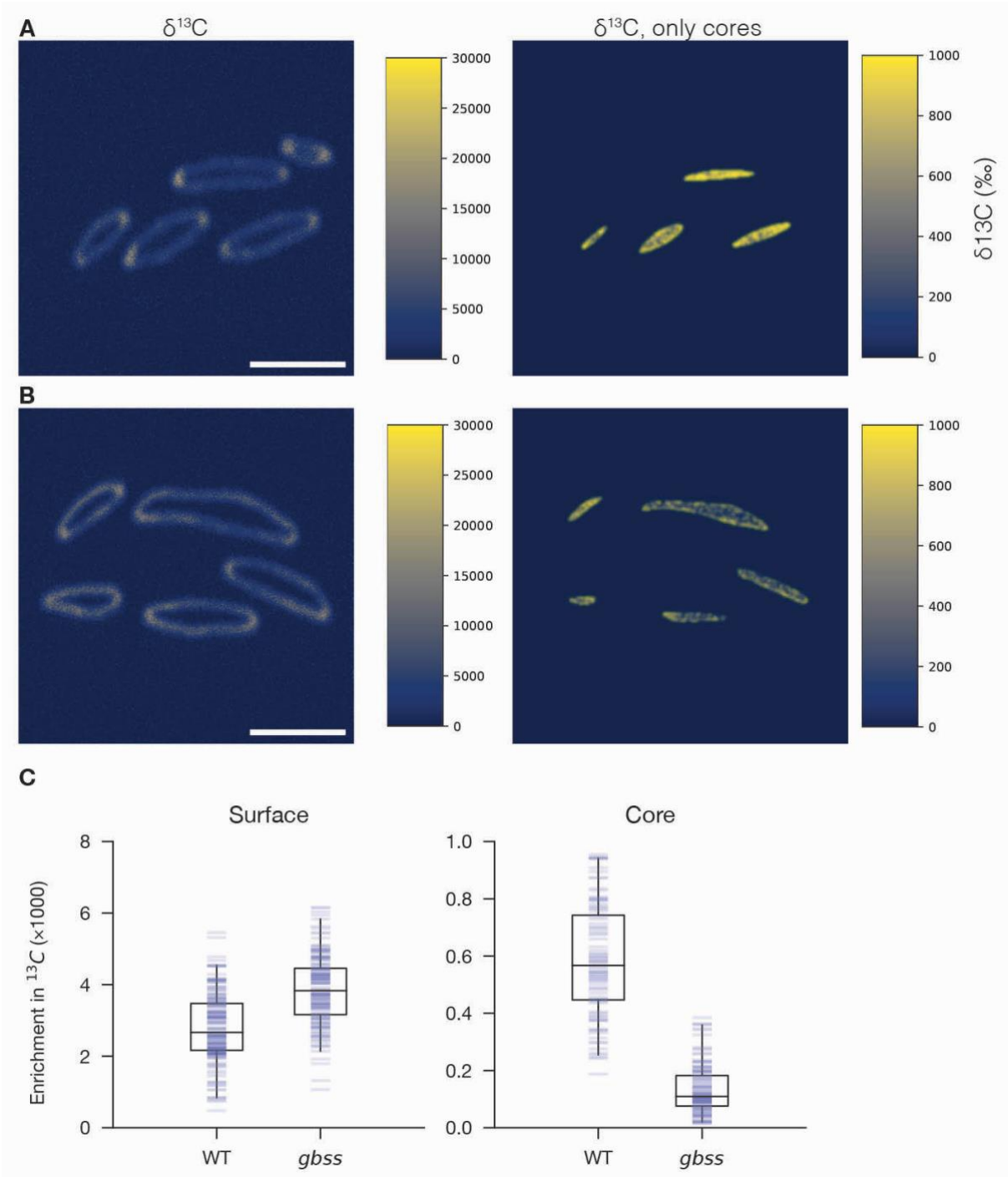

Figure 1.6. Granule Bound Starch Synthase synthesizes amylose in the granule cores. Plants subjected to a normal night were labelled with a pulse of $^{13}CO_2$ for 1 h at midday then harvested immediately for EM and NanoSIMS imaging. Scale bars: 2 µm. (**A**) ^{13}C-enrichment map (left) of starch granules within wild-type chloroplasts. Manually masking the granule surfaces revealed enrichment specifically in the cores (note different ^{13}C-enrichment scales). (**B**) ^{13}C-enrichment map of starch granules (left) and their cores (right) within chloroplasts of the *gbss* mutant. (**C**) Quantification of the ^{13}C-enrichment of granule cores and surfaces overlaid with boxplots representing the 95% CI. N=259 and 269 granules for the wild type and *gbss* mutant, respectively, in each case from three biological replicates.

Discussion

Understanding the in-vivo biosynthesis of biomacromolecules requires genetic, biochemical and cell-biological insight. We have brought together a new combination of experimental methods and analytical techniques to bridge these disciplines in the study of starch—arguably the most important biopolymer produced in plants and therefore a vital agricultural product. As with many biopolymers, starch granule formation is brought about by the concerted actions of numerous enzymes, the coordination of which is evidently genetically controlled, but poorly understood at the cell-biological level. The study of granule initiation in Arabidopsis provides us with a tractable genetic system with which to identify the genes and proteins controlling these processes (Abt et al., 2020; Lu et al., 2018; Roldán et al., 2007; Seung et al., 2017; Seung et al., 2016; Seung, et al., 2018; Vandromme et al. 2019a). By combining high resolution spatio-temporal imaging techniques with genetics, we bridge these disciplines to address previously intractable questions about biopolymer formation in-vivo. Collectively, the parallel initiation followed by fusion and localized starch accumulation challenge the classical view of granule development and illustrate its dependence on the emerging network of proteins that includes both enzymes and scaffolding factors.

There is strong evidence from this work and previous studies that starch granule initiation in chloroplasts occurs at defined sites in-between the thylakoid membranes (Figure 1.1; 18). Some proteins implicated in initiation are themselves partly (SS4, PTST2) or wholly (MFP1) thylakoid-associated and localize to chloroplast subdomains (Gámez-Arjona et al., 2014; Raynaud et al., 2016; Seung, et al., 2018). Our SBF-SEM analysis of de-starched plants, i.e., after 16-h nights, revealed thylakoid-bounded regions differing in appearance to the rest of the stroma, potentially reflecting these subdomains; a hypothesis we are testing with other correlative microscopy methods. Previous models of starch granule biosynthesis generally imply a single point of initiation; when multiple initiations occur, compound starch granules are formed (as seen in the endosperms of some cereals; Li et al., 2017; Yun et al., 2010). This study unambiguously demonstrates that single granules can arise from multiple parallel initiations that subsequently coalesce. In chloroplasts, this pattern of multiple initiations may be functionally important in allowing the rapid establishment of sufficient granule surface area, which is key to the high rate of starch deposition that accompanies photosynthesis. It will be important to determine next whether similar initiation patterns occur in other plant storage organs, such as seeds and tubers, and whether this impacts on starch yields (Gámez-Arjona et al. 2014).

Granule coalescence events raise fundamental, unanswered questions. The arrays of parallel glucan chains in amylopectin molecules that form the 9to 10-nm semi-crystalline lamellar repeats are thought to be radially arranged in starch, giving granules their characteristic birefringence when viewed under polarized light (Pérez and Bertoft, 2010; Zeeman et al., 2002). It is unclear if these semi-crystalline structures are already formed in the observed granule initials. If present, semi-crystalline lamellae are unlikely to be radially oriented considering that, at around 50 nm in diameter, the initials are not much larger than the lamellae themselves. We speculate that a compatible orientation of polymers in adjacent initials may be necessary for them to fuse during subsequent growth. Indeed, not all adjacent granules in the same pockets fuse (perhaps due to opposing orientations of their lamellae) despite the fact that our NanoSIMS imaging revealed deposition of new material onto their flat, abutting surfaces (Figure 1.4A). Alternatively, it is possible that both the initials and larger granules can fuse regardless of their orientations but that, after a certain stage, granule fusion is prevented by the protein factors that establish the pattern of anisotropic granule growth (Figure 1.4B).

The anisotropic deposition of newly synthesized material dictates the way starch granules grow in Arabidopsis chloroplasts into flattened discoids that fill the pockets and lie parallel to the thylakoids. For this to occur, the activities of a suite of enzymes (starch synthases, branching enzymes and debranching enzymes) must be concentrated at the equatorial regions of the granule. In other starch synthesizing tissues, starch granules also take on very specific morphologies. By analogy with the observations made here, we suggest this also happens via the non-random patterns of deposition of new material. Remarkably, our data show that SS4 is critically required for growth anisotropy in Arabidopsis; when missing, newly synthesized starch is deposited almost uniformly onto the granule surface, explaining why the starch granules in *ss4* mutants are near-spherical. We conclude that the presence of this protein—specifically its N-terminal domain required for the protein's correct localization coupled to glucan synthase activity—is crucial for concentrating the activities of the other starch biosynthetic enzymes, including SS1–SS3, BE2 and BE3 and ISA1/2. We propose that a combination of protein-glucan, protein-protein, and protein-lipid interactions underpins this phenomenon. SS4 is known to interact with other proteins, i.e., the fibrillins FBN1a and FBN1b, PTST2 and MRC (Gámez-Arjona et al. 2014; Seung et al., 2017; Seung al., 2018; Vandromme et al., 2019), which themselves have been demonstrated or proposed to have binding capabilities. The PTST-family proteins can bind starch and malto-oligosaccharides,

and, like the putative structural proteins MRC and MFP1, contain predicted coiled-coil motifs that could mediate protein-protein interactions (Seung et al. 2017; Seung et al., 2018; Vandromme et al., 2019). Further, MFP1 and the fibrillins are known to be thylakoid membrane-associated proteins (Seung et al., 2018; Vandromme et al., 2019). Hence, SS4 may serve as a vital link in this interaction network. Other starch biosynthetic enzymes also have predicted glucan and/or protein-interaction domains (Pfister et al., 2016). Indeed, in cereal species, multi-enzyme complexes containing other starch synthase isoforms and branching enzymes have been shown to form (Hennen-Bierwagen et al., 2008; Tetlow et al., 2008). In addition to coordinating their activities, the formation of multi-enzyme complexes could facilitate their collective sub-plastidial localization.

It is also possible that the sites of synthesis may be examples of liquid-liquid phase-separation brought about by many low-affinity protein-protein and protein-glucan interactions. A number of the aforementioned proteins have amino acid regions predicted to be intrinsically disordered—a common feature in proteins capable of condensing into organelles not enveloped by membranes. Starch biosynthetic enzyme activities may be significantly increased by a high local concentrations of glucan substrates within such condensates (while the actions of degradative enzymes might be simultaneously excluded). This type of enzyme stimulation has been demonstrated for GBSS, the activity of which shows biphasic kinetics as soluble glucan substrate concentrations breached a threshold above which viscosity and turbidity increased, signifying the onset of phase transition. This, together with other observations, prompted the hypothesis that GBSS is active within the granule matrix (Denyer et al., 1996; Tatge et al., 1999; Wattebled et al., 2002), which we demonstrate to be correct through isotope labelling and NanoSIMS imaging.

In conclusion, the power of combining genetics with innovative imaging techniques to capture temporal and spatial information with high resolution has allowed us to answer previously intractable questions about starch biosynthesis. This approach, extended to the study of other important biopolymers in-vivo, could enable similar breakthroughs in those fields.

Materials and Methods

Plant material and growth conditions

All experiments were carried out with *Arabidopsis thaliana* L., ecotype Col-0, grown on individual pots of soil (Klasmann-Deilmann Substrate 2) for 35 days in controlled environment cabinets (Percival Scientific, Perry, IA, USA) with a 12-h light (150 µmoles photons m^{-2} s^{-1})/12-h dark regime. The relative humidity was 60% and temperature was 20°C. Plants defective in SS4 (At4g18240) and their transformed lines expressing *Agrobacterium tumefaciens* glycogen synthase linked to the N-terminus of SS4 are described in (Lu et al., 2018). Plants defective in GBSS (At1g32900) are described in (Seung et al., 2015).

Stable isotope labelling

For $^{13}CO_2$ labelling (either at dawn, or after a 4-h night extension for further de-starching) plants were transferred to an airtight chamber within the growth cabinet. Air was passed through the chamber in which CO_2 was substituted with 380 ppm $^{13}CO_2$ (Pangas, Dagmersellen, Switzerland). Labelling to investigate granule initiation was started 5 min before dawn and continued for the first 15 min of the light period. Labelling to investigate granule growth was done for 60 min at midday. Plants were harvested immediately after the $^{13}CO_2$ pulse or transferred to the growth cabinet for a defined chase period.

Serial block face scanning electron microscopy (SBF-SEM)

Samples were taken from the upper quadrant of leaf 6, between the major vein and the leaf margin. Each fixation and staining step were followed by three washing steps with the corresponding buffer. Leaf samples were fixed for 6 h at 20°C, 200 mbar in fixation solution (2.5% [v/v] glutaraldehyde, 2% [v/v] formaldehyde in 0.1 M sodium cacodylate, pH 7.4). Samples were then stained in a medium containing 1.5% (w/v) potassium ferrocyanide, 2% (w/v) osmium tetroxide, 4 mM calcium chloride for 1 h on ice, followed by an incubation in pre-filtered 1% (w/v) thiocarbohydrazide solution (20 min, 20°C) then in 2% (w/v) osmium tetroxide (in 0.1 M sodium cacodylate, pH 7.4, 30 min, 20°C). Samples were then stained with 1% (w/v) uranyl acetate for 12 h at 4°C and then with Walton's lead aspartate for 30 min at 60°C (0.66% [w/v] lead nitrate in 0.4% [w/v] aspartic acid, pH 5.5). Samples were dehydrated with a 6-step ethanol series (50%, 60%, 70%, 80%, 98%, 4 × 100%), followed by 100% acetone, each for 20 min at 4°C. Samples were infiltrated in epoxy resin (Durcupan™ ACM, Sigma-Aldrich, Buchs, SG, Switzerland) with increasing concentrations (25%, 50%,

75%, 3 × 100%) in acetone. The infiltrated samples were cured in molds for 48 h at 60°C. The detailed method is described in (36). The blocks were trimmed, glued on pins and sectioned/scanned ca. 500 times using a scanning electron microscope (FEI Quanta 250, Thermo Fisher Scientific) at 1.8 – 2 kV with an integrated 3View stage and a back-scattered electron detector (Gatan, Pleasanton, CA, USA). The structural features were marked out manually with Amira (ThermoFisher, Waltham MA, USA).

Sample preparation for EM-NanoSIMS imaging

When TEM was used for section imaging, leaf samples were fixed with fixation solution (2.5% [v/v] glutaraldehyde, 2% [w/v] formaldehyde in 0.1 M sodium cacodylate, pH 7.4), stained with 1% (w/v) osmium tetroxide, dehydrated with a 6-step ethanol series, infiltrated with a 4-step (25%, 50%, 75%, 3 × 100%) epoxy resin series in ethanol (Spurr Low Viscosity Embedding Kit, Polysciences Inc, Warrington, PA, USA) and cured for 48 h at 60°C. All steps except the last were microwave-assisted using a BioWave Pro+ (Ted Pella, Redding, CA, USA) and as described in (Abt et al., 2020). Ultrathin sections (70 nm) were transferred onto formvar-coated copper grids (EMS, Hatfield, PA, USA), post-stained with uranyl acetate (10 min) and with lead citrate (10 min). Images were acquired with a transmission electron microscope (JEOL-1400 Plus, JEOL Inc. Peabody, MA, USA) at 120 kV.

When SEM was used for section imaging, samples were processed as for TEM, but osmium staining prior to dehydration and embedding was based on the OTO method (Seligman et al., 1966), adapted as follows. Fixed samples were stained with 3% (w/v) potassium ferrocyanide (II) in 0.1 M sodium cacodylate, pH 7.4, with an equal volume of 4% (w/v) osmium tetroxide solution. Next, samples were incubated with pre-filtered 1% (w/v) thiocarbohydrazide solution and finally stained with 2% (w/v) osmium tetroxide solution. After embedding, 200-nm-thick sections were cut, collected on hydrophilised wafers (PELCO easiGlowTM Glow Discharge Cleaning System), and imaged with a GeminiSEM 500 (ZEISS, Oberkochen, Germany) scanning electron microscope (3 kV) using the back-scattered electron detector.

Nanoscale secondary ion mass spectrometry (NanoSIMS)

Grids previously imaged with TEM or by SEM (semi-thin samples deposited on silicon wafers) were coated with ca. 15 nm gold. Using a NanoSIMS 50L instrument (Hoppe et al., 2013), pre-sputtered regions of interest (ROI) of 20×20 μm^2 or 10×10 μm^2 (256×256 pixels) were scanned with a 16 keV primary Cs^+ beam, focused to a spot size (Gaussian shape, FWHM) of around 100 nm with a pixel dwell time of 5 ms. For each image, the counts for

the secondary ions $^{12}C_2^-$, $^{13}C^{12}C^-$, and $^{14}N^{12}C^-$ were recorded over 5 rasters (planes) in electron multipliers at a mass resolving power of around 9000 (Cameca definition), enough to resolve the ions of interest from potential interferences in the mass spectrum. For each session, three analyses were done on similarly prepared, unlabeled plant material serving as isotopic standard against which ^{13}C-enrichments were reported in the δ-notation, according to the equation:

$$\delta^{13}C\ (‰) = ((C_{mes} / C_{nat}) - 1) \times 10^3,$$

where C_{mes} is the measured $^{12}C^{13}C^-/^{12}C_2^-$ ratio of the sample and C_{nat} is the average $^{12}C^{13}C^-/^{12}C_2^-$ ratio measured in unlabeled samples (isotopic controls).

Using the ImageJ plugin OpenMIMS, ion map files (*.im) were corrected for dead time and aligned using the $^{14}N^{12}C^-$ map, which shared the highest similarity with the corresponding electron micrograph. All further image processing tasks were carried out in Python with the OpenCV bindings. The aligned and accumulated planes of $^{12}C^{13}C^-$ and $^{12}C_2^-$ were used to compute the ^{13}C-enrichment maps (in $\delta^{13}C$) and electron micrographs were then overlaid onto these maps using the $^{14}N^{12}C^-$ map as a reference. To compare the ^{13}C-enrichment in granule cores between the wild type and the *gbss* mutant, the ion maps were manually segmented into three regions: background, granule surface and granule core. For each region, the average value of the enrichment along with the standard deviation was calculated.

Statistical analysis

For each inferential procedure, we used Stan (Gelman et al., 2015) to draw posterior samples from the probability density of generalized linear models (GLM; Gamma likelihood and a normal prior Normal(mu=2, sigma=2)). The parameters were estimated using the Hamiltonian Monte-Carlo NUTS sampler using 4 chains, each with 16,000 iterations. The last 8,000 iterations were used for analysis. The plots were drawn using the Python plot library Matplotlib.

Acknowledgments

We thank Miriam Lucas (ScopeM, ETH Zürich) and Louise Jensen (LGB, EPFL) for guidance with electron microscopy, Florent Plane for NanoSIMS technical support, Federico Massini for help with image segmentation, and Andrea Ruckle for help with plant culture. This work was funded by the Swiss National Science Foundation (grants CR32I3_166487 and 31003A_182570) and by ETH Zurich.

Author contributions

Léo Bürgy: investigation, methodology, formal analysis, visualization, data curation, writing, original draft. Simona Eicke: investigation, methodology, visualization. Christophe Kopp: investigation. Camilla Jenny: investigation. Kuan Jen Lu: resources. Stephane Escrig: methodology. Anders Meibom: conceptualization, methodology, writing, review & editing. Samuel C. Zeeman: conceptualization, supervision, writing, original draft, review & editing.

Competing interests

Authors declare no competing interests.

Data and materials availability

All data are available in the main text, the supplementary materials, and in the ETH Zurich University Archives.

Code availability

Python scripts used during data analysis are available upon request.

Supplementary Materials

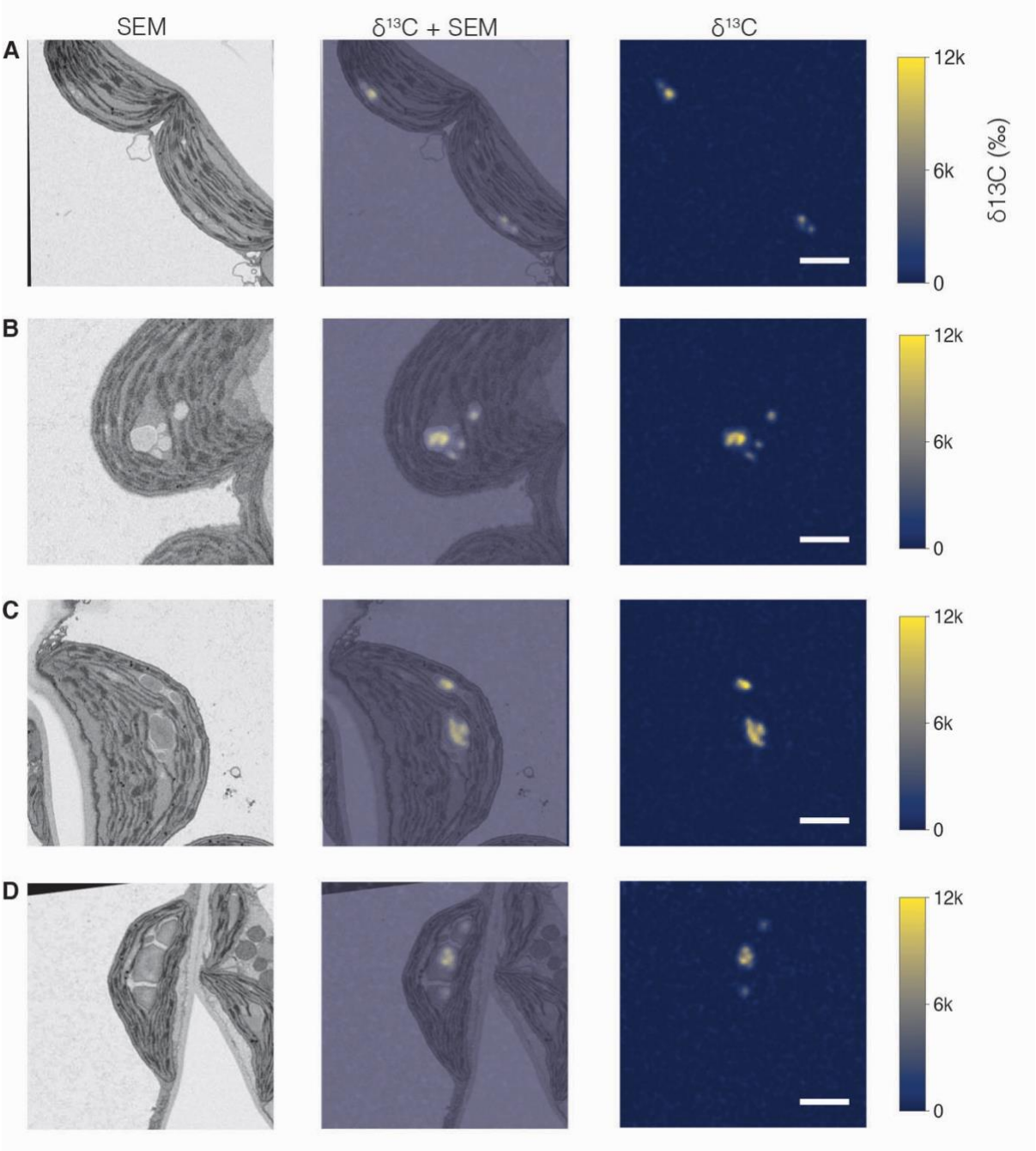

Figure S1.1

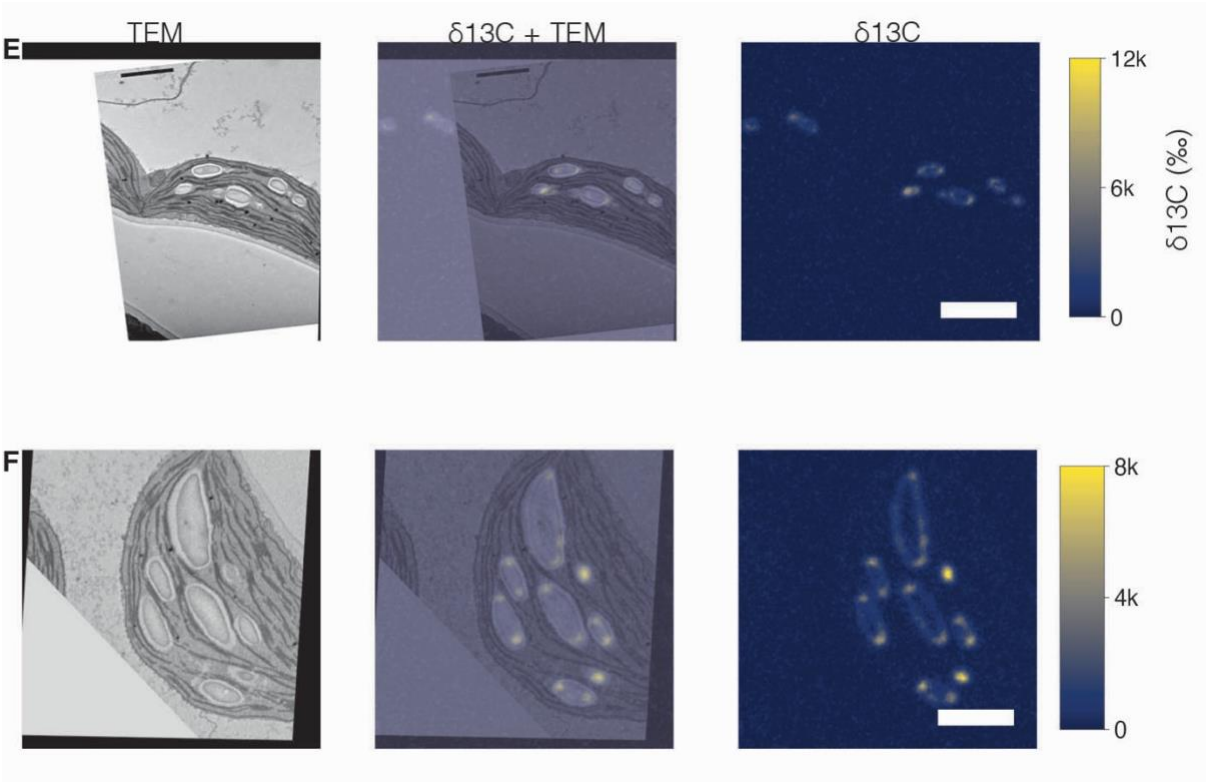

Figure S1.1 (continued)

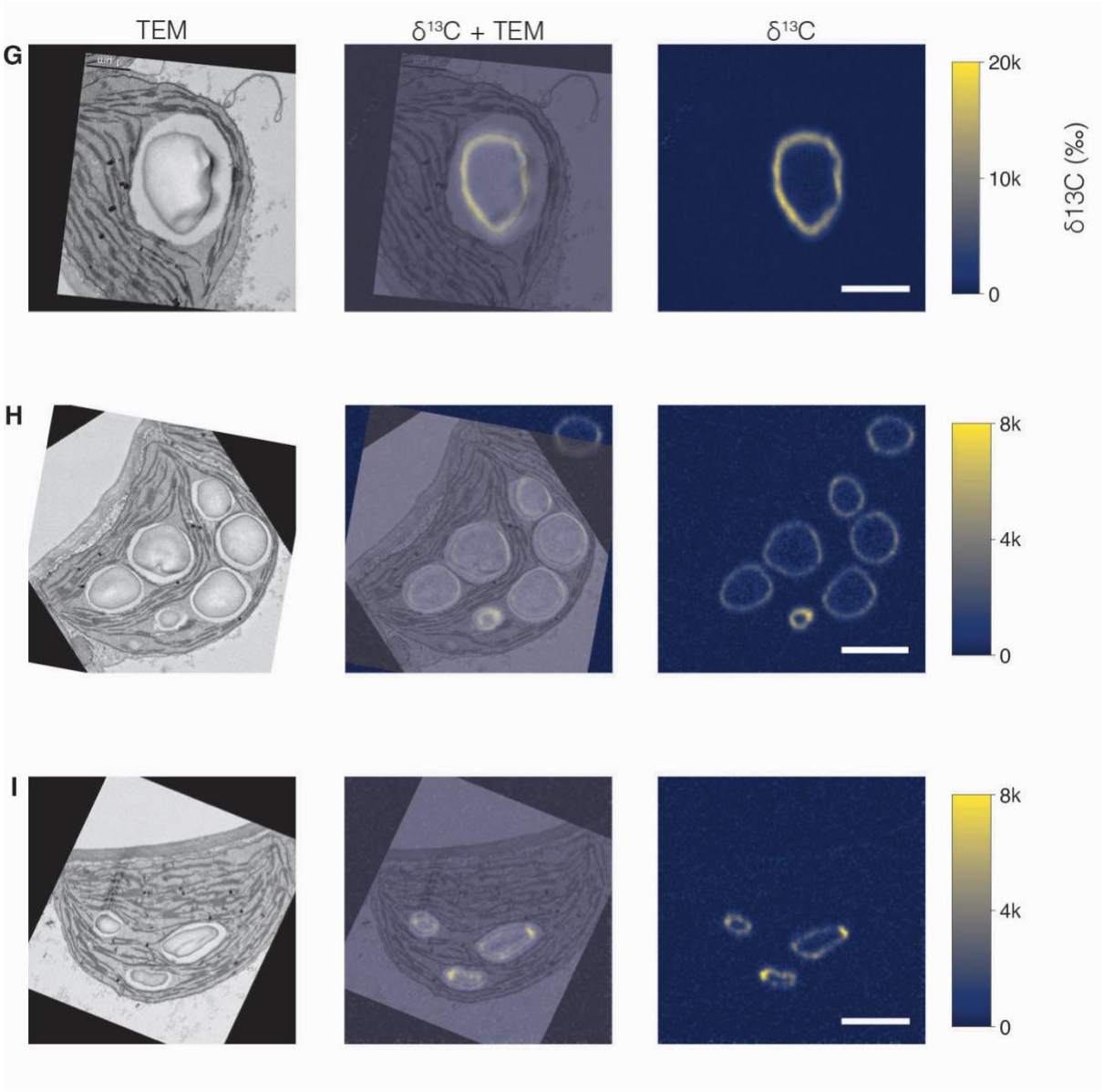

Figure S1.1. Additional examples of starch granule development visualized by $^{13}CO_2$ labelling, EM and NanoSIMS. (**A**–**D**) Additional examples of starch granule coalescence in wild-type chloroplasts, as described in Figure 1.3 **A**–**D**, respectively. (**E**–**F**) Additional examples of anisotropic granule expansion in wild-type chloroplasts, as described in Figure 1.4. (**G**–**I**) Additional examples of aberrant granule initiation and growth in *ss4* mutant chloroplasts (**G**) and the rescue of these phenotypes in the chloroplasts *ss4* plants transformed with A. tumefaciens GS (**H**) or GS fused to the N-terminus of SS4 (**I**), as described in Figure 1.5. Scale bar: 2 µm.

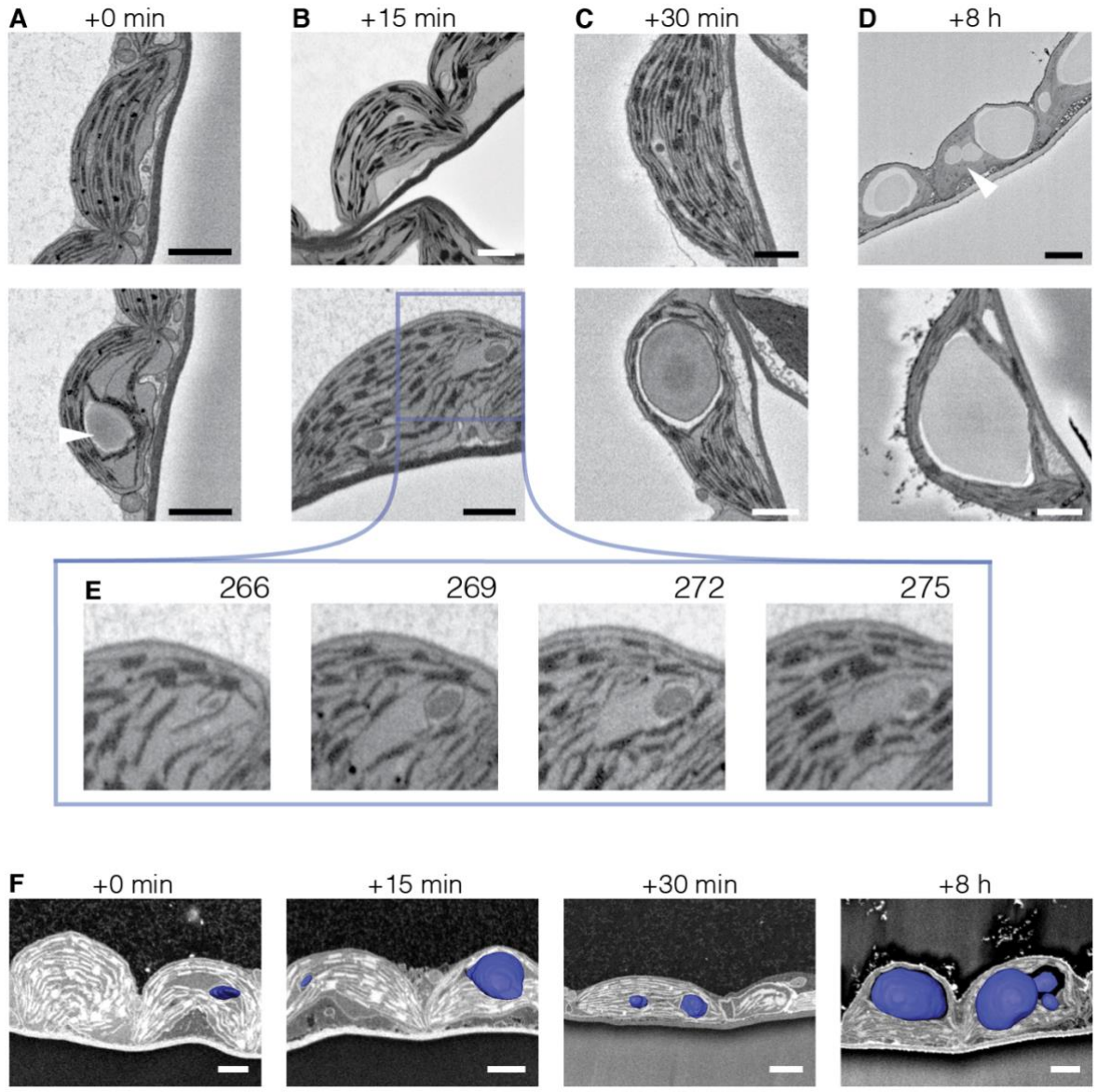

Figure S1.2. The *ss4* mutant displays aberrant starch granule initiation. Chloroplast sections from an SBF-SEM stack (with 50-nm Z-resolution, inverted SEM images) sampled from the mesophyll of fully expanded leaves of 35-day old *ss4* mutant plants grown in a 12 h:12 h diel regime. Few, near-spherical starch granules are present between the thylakoid membranes. (**A**–**D**) Representative chloroplast sections from plants exposed to a prolonged night and harvested (**A**) at the end of the 4-h night extension, with a remaining starch granule visible in the lower panel (white arrowhead), (**B**) after 15 min and (**C**) 30 min light, where both large granules and possible newly-initiated granules could be observed, and (**D**) after 8 h light, where a mixture of large and small granules (white arrowhead) were visible. (**E**) Series of images (with steps of 150 nm in the Z-axis) from the sample stack in (**B**) illustrating a potential newly initiated granule. (**F**) 3D-renderings of representative chloroplasts (non-inverted SEM images) with their starch granules shown in violet. Scale bars: 2 µm.

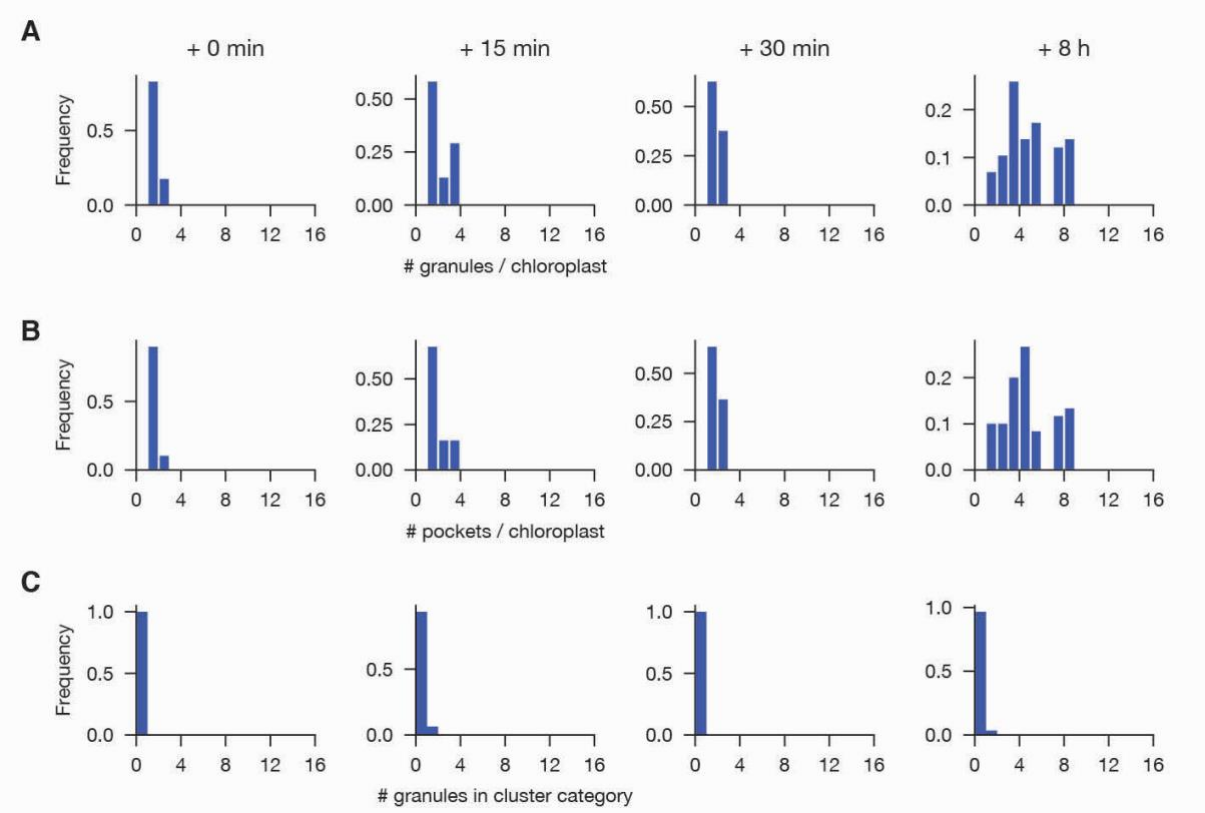

Figure S1.3. Determination of the exact number of starch granules in the *ss4* mutant. Quantitative information was obtained from image stacks as shown in Figure S1.2. (**A**) The number of granules per *ss4* chloroplast. (**B**) The number of starch-containing pockets per *ss4* chloroplast. (**C**) Number of granules in each cluster category. Data in A–C are expressed as frequency distributions. For each time point, two plants from two independent experiments were examined. In total, 37, 30, 27 and 20 chloroplasts were examined, respectively, for the 0-min time point, i.e., the end of the extended night, and for the 15-min, 30-min and 8-h time points during the day.

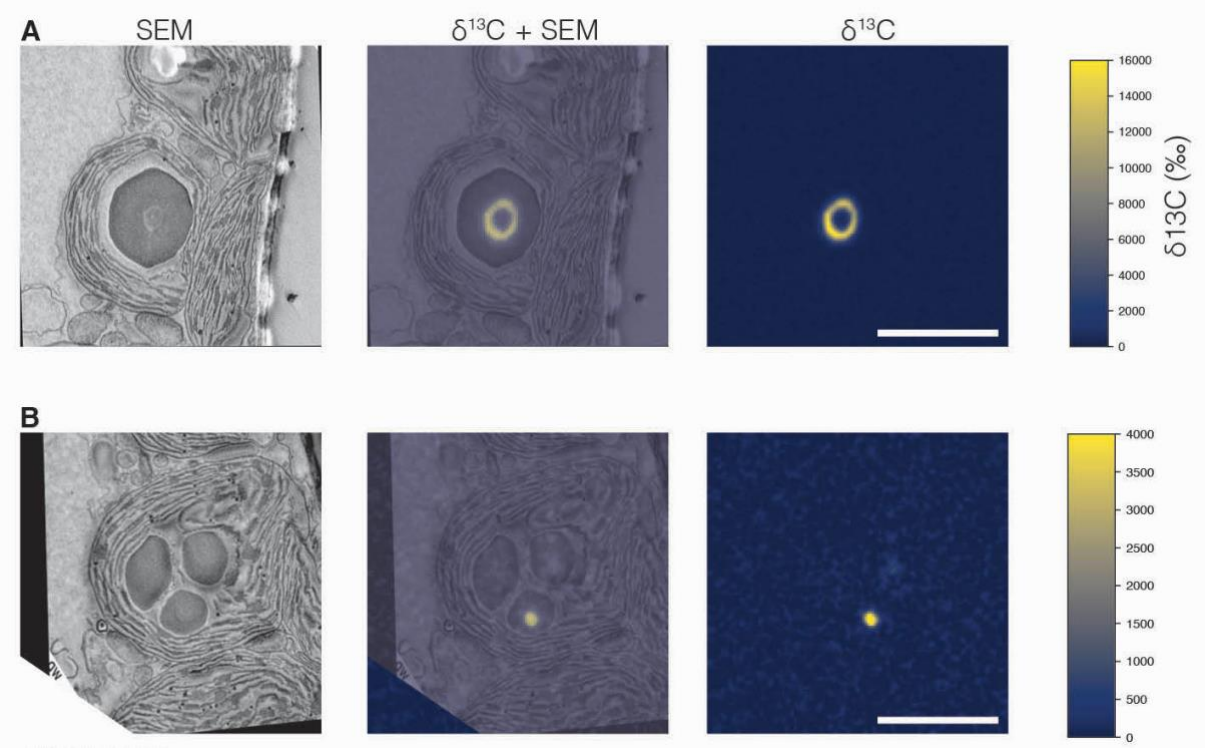

Figure S1.4. Re-expansion of existing starch granules and initiation of new granules in the *ss4* mutant. *ss4* mutant plants were subjected to a 4-h night extension and labelled with a pulse of $^{13}CO_2$ for 15 min in the light, then harvested and fixed for EM and NanoSIMS imaging after a chase of 4 h in air in the light. In some cases (**A**), the ^{13}C-enrichment pattern was indicative of peripheral labelling of a pre-existing granule that remained after the extended night (see Figure S1.2A). In other cases, strong ^{13}C-enrichment was observed at the center of the granule, consistent with the initiation of a new starch granule during the pulse (**B**). Note that since some *ss4* chloroplasts retain starch even after a dark extension, we cannot state with certainty that such granules were newly initiated that day because we do not know the plane of section. If sectioned through their centers, i.e., a great circle spheric section, this would imply new initiation, but if a larger granule was sectioned off-center, i.e., a small circle spheric section, peripheral labelling could be miss-interpreted as a central labelling of a newly initiated granule. However, it is likely that such central labelling would be weak and diffuse. Scale bars: 2 µm.

Supplementary movies

Supplementary Movie S1.1. SBF-SEM reveals that de-starched wild-type chloroplasts produce clusters of starch granule initials in the light. Progression up through one SBF-SEM image stack, after which the direction of the movie reverses, leaving a semi-transparent rendering of the electron density (280 images, 50 nm Z-resolution). Starch granules (annotated in opaque violet) and the starch-containing pockets (annotated in transparent yellow) are embedded within the 3D-renderings. Note the high number of starch granules initials that can occupy a single pocket. For details of the imaged sample, see Figure 1.1G and Figure 1.2D.

Supplementary Movie S1.2. SBF-SEM reveals that clusters of starch granule initials appear to fuse as starch synthesis proceeds. The movie is as described for Supplementary Movie S1.1 (345 images, 50 nm Z-resolution). Note the irregular morphology of larger granules within the pockets that appear to reflect the coalescence of starch granules initials. For details of the imaged sample, see Figure 1.1H and Figure 1.2D.

Supplementary Movie S1.3. SBF-SEM reveals normal lenticular starch granules at the end of the day. The movie is as described for Supplementary Movie S1.1 (360 images, 50 nm Z-resolution). Note the small cluster size compared to earlier time points and the flat surfaces of abutting granules occupying the same pocket. Note also the variation in granule size and the comparatively large number of starch-containing pockets. For details of the imaged sample, see Figure 1.1I and Figure 1.2D.

Supplementary Movie S1.4. Chloroplasts of wild-type mesophyll cells are de-starched after an extended night, as revealed by SBF-SEM. Progression down through one SBF-SEM image stack (414 images, 50 nm Z-resolution) revealing multiple chloroplasts, all devoid of starch. Note the recurrent stromal spaces with a flocculate appearance that may represents sites for future starch granule initiation. For details of the imaged sample, see Figure 1.1F.

Chapter 2

Dissecting the functions starch granule initiation factors.

Leo Bürgy[1], Simona Eicke[1], Clarisse Uwizeye[4], Stephane Escrig[2], Louise Jensen[2], Anders Meibom[2], Samuel C. Zeeman[1*].

[1] Institute of molecular plant biology, ETH Zurich, 8092 Zurich, Switzerland

[2] Laboratory for biological geochemistry, Ecole Polytechnique Fédérale de Lausanne (EPFL), Lausanne, Switzerland

[3] Centre for Advanced Surface Analysis, University of Lausanne, Lausanne, Switzerland

[4] Univ. Grenoble Alpes, CNRS, CEA, INRAe, IRIG-LPCV, Grenoble, France

* Correspondence to: samuel.zeeman@biol.ethz.ch

Author contributions Leo Bürgy conducted most of the experiments. Simona Eicke and Leo Bürgy helped with electron microscopy procedures. Clarisse helped with image segmentation. Anders Meibom and Stephane Escrig provided technical support to acquire NanoSIMS images. Louise helped set up the serial sectioning workflow. Leo Bürgy prepared all the figures with the help of Simona Eicke for the movies and the 3D visualisations and wrote the manuscript together with Samuel C. Zeeman, with input from all authors.

Abstract

The number of starch granules that form in individual plastids within a plant cell is genetically regulated. Granule number is inversely linked to granule size, which is an important functional trait for industrial processes that utilise starch. Relatively little is known about what determines granule initiation and thus their number. However, in the last decade, a number of genes encoding potential initiation factors in Arabidopsis chloroplasts have been identified. When one or more of the encoded proteins are absent, the chloroplasts contain fewer, generally larger, granules. We previously showed that multiple granule initials can form simultaneously in regions between the chloroplast thylakoid membranes and are able to fuse into one. Thus, the final number of starch granules will be influenced by the number of locations in which initials form, the number of initials produced, and whether or not they fuse. Here, we investigated the potential disruption of these process in recently discovered starch granule initiation mutants. We show that some mutants are unable to properly initiate parallel granules, while others are capable of proper initiation, but that these events appear to be incorrectly localised within the chloroplast. We propose hereafter a more dynamic model, that allows plants deficient in either genetic factor to trigger initiation. It further gives insights about the importance of having multiple starch granules in each chloroplast.

Introduction

Most plants store a large fraction of their photosynthetically fixed carbon as transitory starch, a polymer of glucose that forms insoluble, micrometre-scale granules in leaf mesophyll cell chloroplasts. The starch granules grow during the day and degraded again during the night to provide the plant with substrates for respiration and the biosynthesis of further metabolites (Stitt and Smith, 2012). In Arabidopsis, leaf mesophyll cell chloroplasts contain numerous starch granules. Estimates of the number vary depending on whether counts are made on whole segmented chloroplasts (20 in Burgy et al., 2021; 7 in Crumpton-Taylor et al., 2012), or on chloroplast sections (3 in Seung et al., 2018 and Abt et al., 2020). These numerous granules result from (1) the deposition of glucans onto existing starch granules, (2) the initiation of new granules, and (3) the fusion of granules.

It has been proposed that Starch Granule Initiation (SGI) is a spontaneous phenomenon (e.g., Ziegler et al., 2005) but the variations between species and recent discoveries indicate rather that it is under the control of genetic factors. In Arabidopsis chloroplasts, SGI requires the coordinated activity of a set of at least five proteins in addition to the starch biosynthetic enzymes themselves. Mutants defective in these proteins typically have decreased number of granules, while the structure of the starch polymers remains largely unaltered (Roldan et al., 2007, Crumpton-Taylor et al., 2013, Seung et al., 2017, Seung et al., 2018, Vandromme et al., 2019a). Interestingly, in most cases, the ability to accumulate starch does not appear affected, even if the number of granules is reduced, since the starch content measured in those mutants are quite similar to wild type, at least in normal laboratory growth conditions. The fewer granules present are larger than in the wild type and can exhibit abnormal shape, suggesting that the factors that influence initiation, may also influence how granules subsequently grow.

The severity of the phenotype in the SGI mutants vary. STARCH SYNTHASE 4 (SS4), one of the enzymes of starch biosynthesis, has the most striking SGI phenotype; *ss4* chloroplasts contain either no granules or very few nearly spherical granules. In addition, the *ss4* mutant has vastly elevated concentrations of ADP-Glc, presumably accumulating when there is no granule initial that the remaining starch syntheses can use as a substrate. SS4 may affect the initiation process both via its C-terminal enzymatic (glucosyl transferase) domain and via its N-terminal coiled-coil-containing domain (Lu et al., 2018). The latter is required for SS4 to multimerise and interact with other partner proteins that guide its localisation, and presumably therefore the initiation events within the chloroplast (Roldan et al., 2007,

Szydlowski et al., 2009, Lu et al., 2018). SS4 interacts with PROTEIN TARGETING TO STARCH 2 (PTST2; At1g27070), which harbours both a coiled-coil-containing domain with which it interacts with the C-terminal, enzymatic domain SS4, and a family-48 carbohydrate binding module (CBM48). The homolog of PTST2, PTST3 (At5g03420), does not appear to interact with SS4 directly, but it can interact with PTST2. Both *ptst2* and *ptst3* mutants contained fewer granules in their chloroplasts than the wild type. The *ptst2* phenotype is more severe than that of *ptst3*, while the *ptst2ptst3* double mutant shows a strong decrease in granule number, approaching the severity of the *ss4* mutant [Seung et al., 2017].

Two additional interactors, MAR BINDING FILAMENT-LIKE PROTEIN1 (MFP1) and MYOSIN-RESEMBLING CHLOROPLAST PROTEIN (MRC) were recently described (Seung et al., 2018; Vandromme et al., 2019a). Both proteins were identified as direct or indirect interactors of PTST2, while MRC (also called PII) was also independently identified as a direct SS4 interactor. MFP1 and MRC lack known protein domains but contain numerous predicted coiled-coil-containing regions, suggesting that they may be structural or scaffolding proteins (Seung et al., 2018, Vandromme et al., 2019a). Biochemical analyses of fractionated Arabidopsis chloroplasts showed that MFP1 is associated with the thylakoid membrane and microscopic analysis using a fluorescently tagged version of the protein showed that it occurs in patches. MRC behaves as a soluble protein but has a distinct localisation, appearing as a few punctae within the stroma (Seung et al., 2018). The current model for SGI suggests that SS4 elongates the MOS provided by PTST2 (and possibly also by PTST3) into granule initials. Thylakoid associated MFP1 determines the location of PTST2 within the plastid, thus controlling the sites of initiation. The complex of PTST2, SS4 and MRC directed by MFP1 may create a suitable local environment for the initiation of new starch granules, although the precise role of MRC is unclear as yet.

To provide more information about the mechanisms by which starch granules are initiated, we recently implemented a workflow to analyse starch granule development in situ, using complementary nanometre-scale imaging techniques (Chapter 1; Burgy et al., 2021). Here, we deploy these methods to investigate the SGI mutants *ptst2*, *ptst3*, *mrc* and *mfp1* and show that these can be defined as either unable to properly initiate parallel granules (*ss4* and *mrc*) or capable of proper initiation, but that these events are incorrectly localised within the chloroplast (*ptst2*, *ptst3* and *mfp1*).

Results

De-starching SGI mutant chloroplasts with an extended night.

Visualising SGI is facilitated when chloroplasts are previously de-starched with an extended night (Chapter 1; Burgy et al. 2021). To see to which extent the SGI mutants could be de-starched, we prepared material for serial block-face scanning electron microscopy (SBF-SEM), harvesting duplicate samples after a 4-h night extension from the mesophyll of fully expanded leaves of 35-day-old mutant and wild-type plants. Subsequent imaging revealed that, as expected, chloroplasts of the wild type were devoid of starch. Similarly, chloroplasts of *mfp1* contained almost no remaining starch granules but displayed enlarged stromal spaces with less dense stroma inside in between the network of parallel and flattened thylakoid membranes (Figure 2.1A arrowhead at 0h, Figure S2.1A; Supplemental Movie S2.1). In *mrc*, all chloroplasts were free of starch (Figure 2.1B; Table 1; Supplemental Movie S2.4) in one replicate, with enlarged stromal spaces also present. In the second replicate some chloroplasts still contained one starch granule, which was often very thin and curved (2–8 μm in diameter, 0.5–1 μm thick; Figure S2.1B, arrowhead). In *ptst2*, one replicate was de-starched, again with enlarged stromal gaps (Figure 2.1C), but in the second replicate, half of the chloroplasts contained thin residual granules (Figure S2.1C; Supplemental Movie S2.7). In some cases, chloroplasts that were constricted in their middle— presumably undergoing fission—still had long granules that appeared to be preventing division (Figure S2.1C, arrowheads). In *ptst3*, almost no remaining starch was observed, but several stromal gaps were evident (Figure 2.1D; Figure S2.1D; Supplemental Movie S2.11). In both *ss4* replicates, chloroplasts often contained one remaining near-spherical starch granule (Figure 2.1E; Figure S2.1E; Supplemental Movie S2.16–17). Curiously, the granules were in close contact with surrounding thylakoid membranes, which appeared slightly dissociated from the rest of the thylakoid network (Figure S2.1E, arrowhead).

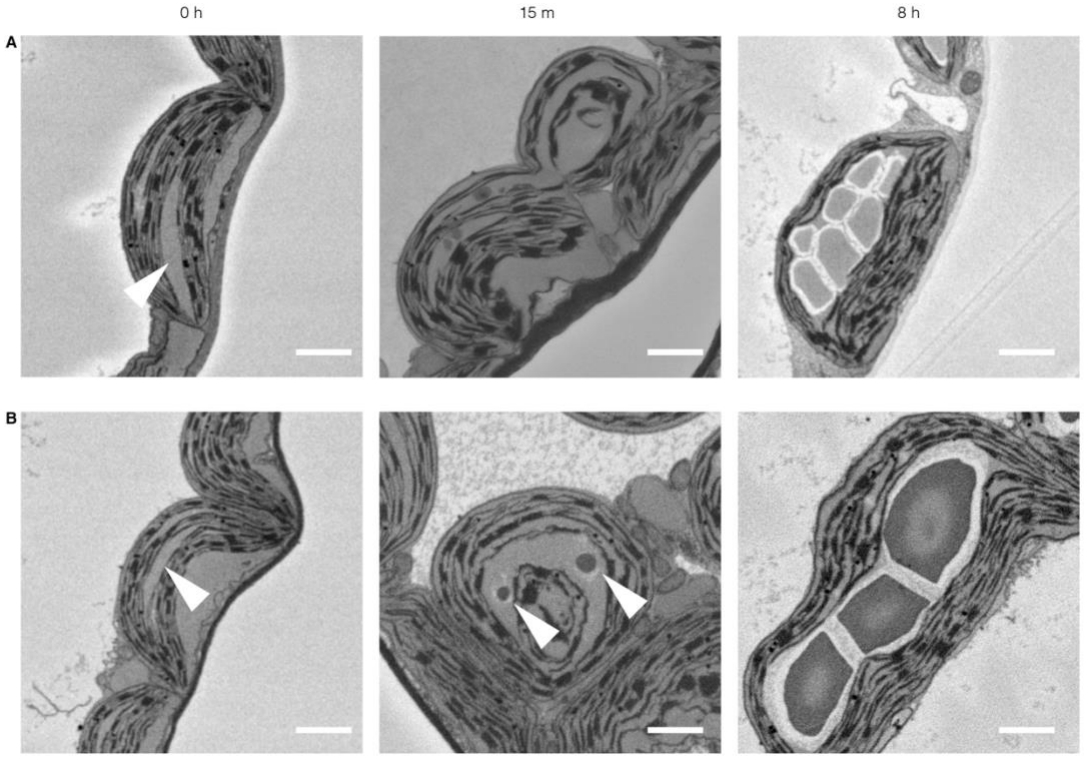

Figure 2.1. See legend on next page

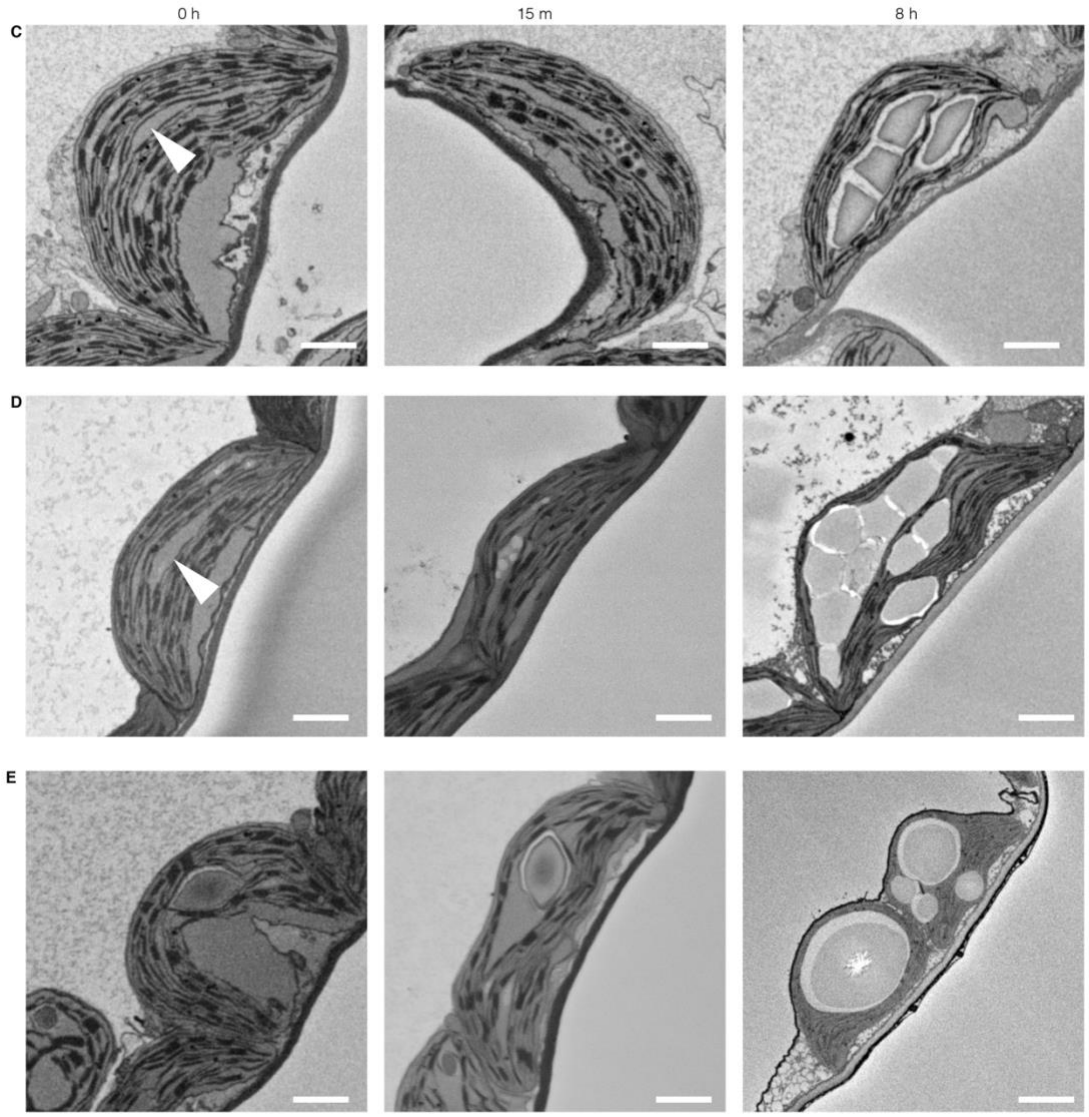

Figure 2.1 Chloroplast sections from an SBF-SEM stack (with 50-nm Z-resolution, inverted SEM images) sampled from the mesophyll of fully expanded leaves of 35-day old Arabidopsis plants grown in a 12h:12h diel regime. Starch granules appear as dark-grey disks between thylakoid membranes. (A–E), Representative chloroplast sections from plants (A, *mfp1*; B, *mrc*; C, *ptst2;* D, *ptst3*; E, *ss4*) exposed to a prolonged night and harvested at the end of the 4-h night extension (first column), after 15 min light (second column) and after 8 h light (third column). Note the numerous starch initials after 15 min light in A, C and D. Note the distant initials within the same stromal pocket after 15 min light (B, arrowheads). In the first column, the arrowheads indicate the stromal gap where starch granules may later initiate. Further presentations of these data are given in supplemental movies S2.1–21 (see Movie description in Supplementary material). Scale bars: 2 µm. Data for wild-type and *ss4* come from SBF-SEM stacks in Chapter 1; Burgy et al., 2021.

Genotype	Light (h)	Replicate 1		Replicate 2	
		Count	Percentage	Count	Percentage
WT*	0	6	100	6	100
	0.25	8	0	14	0
	8	12	0	15	0
mfp1	0	10	100	12	100
	0.25	18	0	6	0
	8	3	0	12	0
mrc-3	0	11	100	15	40
	0.25	27	3.7	6	0
	8	7	0	4	0
ptst2-7	0	12	100	8	37.5
	0.25	12	16.7	17	17.6
	8	8	37.5	10	20
ptst3-5	0	7	100	11	81.8
	0.25	10	0	9	0
	8	11	0	12	0
ss4*	0	12	41.7	25	44
	0.25	14	7.1	16	37.5
	8	12	16.7	14	7.1

Table 2.1. Percentages of empty chloroplasts immediately after a 4-h night extension (light=0), or after a subsequent 15 min (light=0.25) or 8 h light. For each of the two biological replicates, the count of full chloroplasts examined is given (between 3 and 27). *Data for wild-type and *ss4* come from SBF-SEM stacks in Chapter 1; Burgy et al., 2021.

To see whether the remaining starch observed at the microscopic scale was reflected at macroscopic scale, we measured the starch content of whole rosettes by quantifying the glucose released after treating extracted insoluble material with α-amylase and amyloglucosidase (see methods; Figure 2.2A-E). At the end of the 4-h night extension, wild-type plants contained a very low starch concentration of 0.19 ± 0.06 mg/g FW (n=5). Although the starch content is not zero, no starch initials could be seen in the mesophyll chloroplasts (Chapter 1; Burgy et al. 2021). Thus, it is possible that this represents background glucose released by the enzymatic treatment from other, non-starch sources, or starch present elsewhere in the rosette (e.g., guard cells; Horrer et al., 2016). While the starch values for SGI mutants were also low, the mean values were higher that the wild type; *ss4* values were almost five-fold higher, and statistically significant. The values for *ptst2*, *ptst3* and *mrc* values were approximately three-fold higher and the *mfp1* value was two-fold higher, but these differences did not differ significantly from the wild type. These data, including the variation observed, are consistent with the microscopic observations (Figure 2.1) and suggest that when starch granule numbers are decreased, it has a small, but

detectable effect on its turnover, which confirms older reports (Seung et al., 2017). We also visualized starch in the rosettes at the end of the night by I_2/KI staining. The starch in the rosettes of the SGI mutants was below the level of detection using this qualitative method, except in *ss4*, which stained for starch in its older leaves, as previously reported (Figure 2.2F).

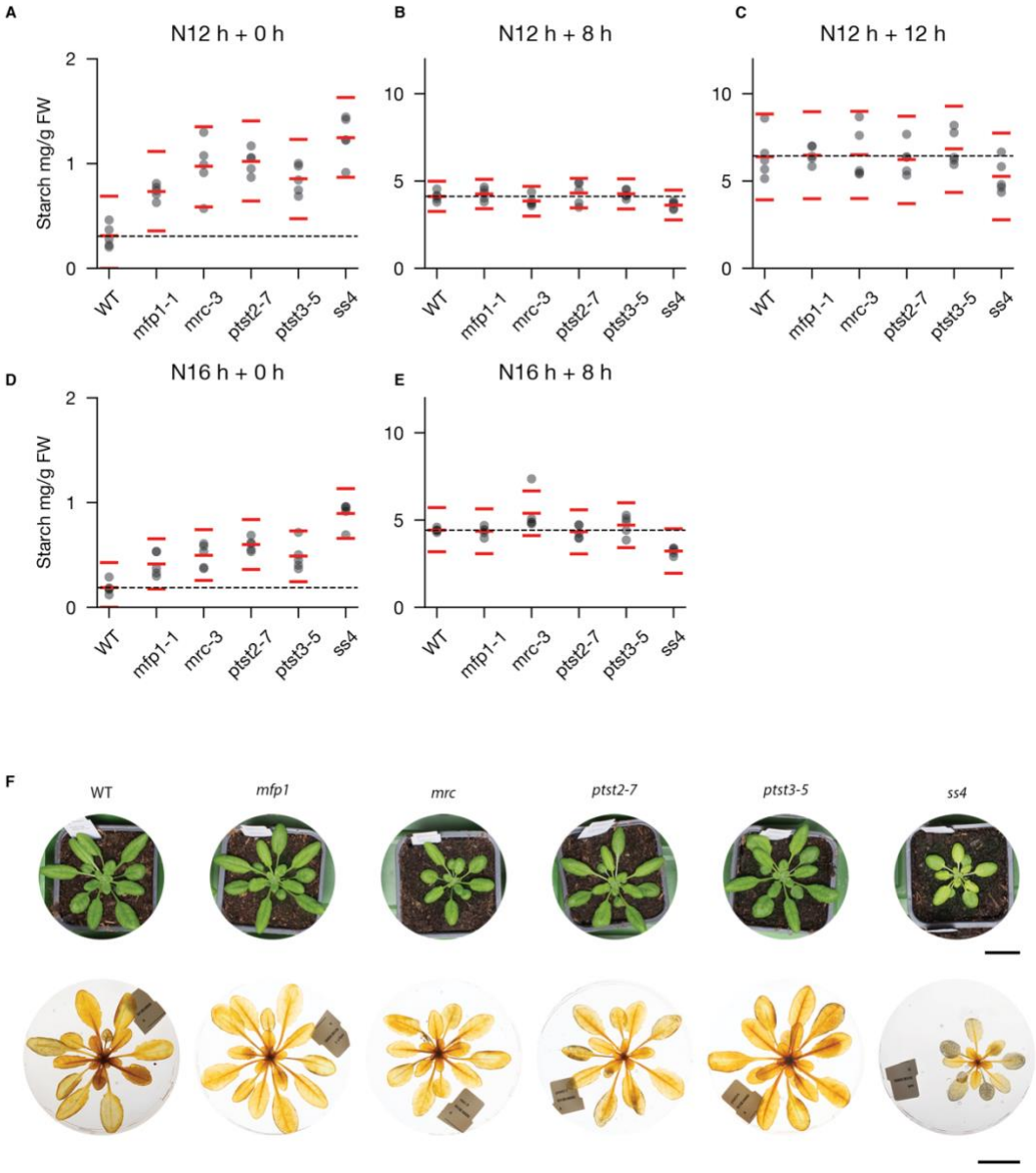

Figure 2.2 Starch concentrations in WT and in the SGI mutants. (**A**–**E**) Starch concentrations after a normal night (N12h) and harvested immediately (**A**), after 8 h day (**B**) and 12 h day (**C**). Starch concentrations after a 4-h night extension (N16h) and harvested immediately (**D**) and after 8 h day (**E**). Each solid point represents one of 5 replicate plants; the dashed line represents the average of wild type and the red bars represent the 2.5%, 50% and 95% C.I. bounds (from bottom to top, respectively) of each line. The lower bounds of the C.I. were clipped to zero. **F**, Representative 5-week-old de-starched rosettes (fresh, top row and stained for starch, bottom row). Scale bars: 20 mm.

Parallel granule initiation is defective in some SGI mutants.

We checked whether SGI mutants were able to produce clusters of starch granule initials in parallel, as observed for the wild type. Plants were given a brief exposure to light (15 min) after the 4-h night extension, then harvested and prepared for SBF-SEM. Evaluation of the cluster sizes in the resultant image stacks (Figure 2.1) revealed two classes of mutants: *mfp1*, *ptst2* and *ptst3* were able to create parallel initials, while *mrc* and *ss4* appeared defective in this process (Figure 2.3B). In *mfp1* plants, chloroplasts contained an average of 4.6 granule initials in each stromal pocket, with one containing as many as 19 initials (Figure 2.3B; Table 2; Supplemental Movie S2.2). The initials were nearly spherical, and the clusters often had a central, larger aggregate of starch, that may be the result of early fusion (Figure S2.1A, arrowhead). However, compared with the wild type, there were fewer clusters per chloroplast. In *mrc* plants, chloroplasts either contained small, round, isolated granules that were presumably freshly initiated (Figure 2.1B; Supplemental Movie S2.5), or larger granules that resembled those found at the end of the prolonged night (Figure S2.1B). In contrast to *mfp1*, the small granules did not form clusters with more than two initials (1.7 on average) (Fig 1B, centre, arrowheads), but similarly to *mfp1* there were only few clusters per chloroplast.

In *ptst2* and *ptst3* plants, chloroplasts contained clusters of round initials with an average of 6 and 2.4 initials per pocket, respectively. The *ptst2* mutant had the largest cluster size of all plants examined in this experiment, with a maximum of 37 initials clustering in one pocket (Figure 2.3B; Supplemental Movie S2.8–9). There were again examples of chloroplasts in *ptst2* where larger residual granules were apparently obstructing division (Figure S2.1C). In *ptst3*, a maximum of 16 initials in one pocket was observed (Figure 2.3B; Supplemental Movie S2.13–14). Like *mfp1* and *mrc*, both of the *ptst* mutants appeared to have fewer clusters per chloroplasts than the wild type. As expected, *ss4* had the most severe phenotype, which was consistent with what we previously reported (Chapter 1; Burgy et al. 2021). Many chloroplasts were empty of starch and most of those that contained starch had one large granule, however, some also contained, smaller, potentially newly initiated granules (Figure 2.3B; Supplemental Movie S2.18–19).

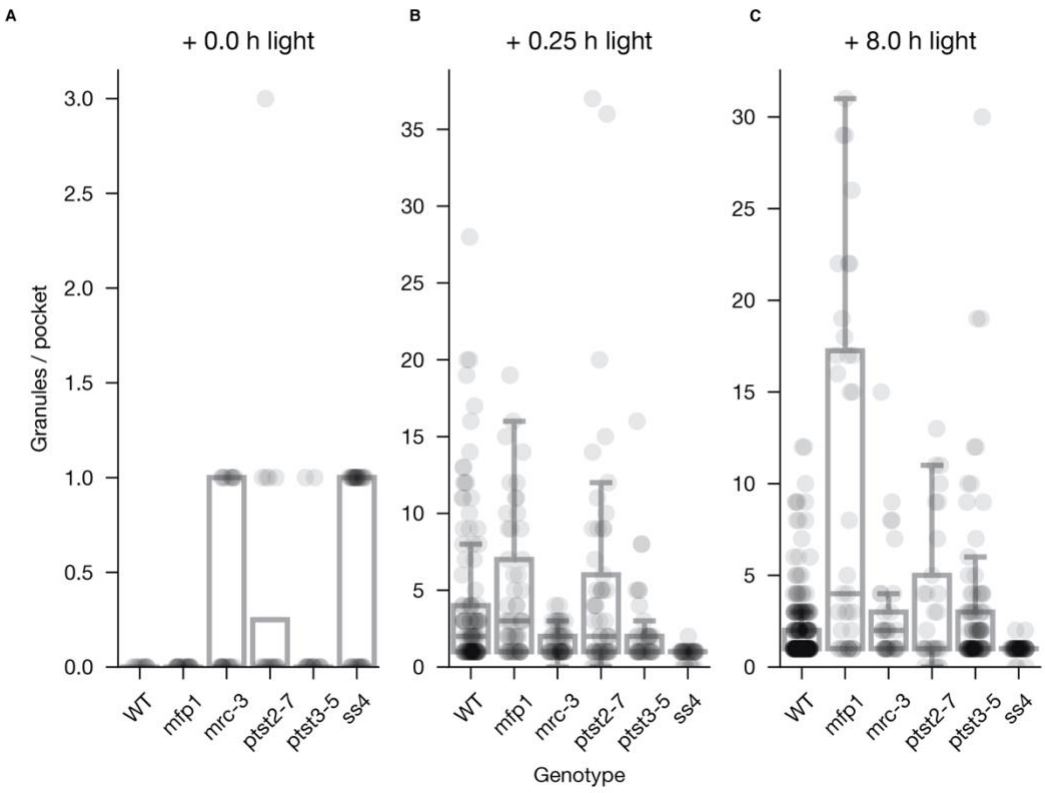

Figure 2.3: Number of starch granules per pocket after the 4-h night extension (**A**), followed by 15 min day (**B**) and after 8 h day (**C**). The number of starch granules per pocket was evaluated from entire chloroplasts from the SBF-SEM stacks displayed in Figure 2.1. Each point represents a cluster. When the chloroplasts had no starch, they are represented with a single "0-cluster". Boxplots are overlaid to ease the interpretation of the spread. Data from wild type and *ss4* come from SBF-SEM stacks in Chapter 1; Burgy et al., 2021.

Genotype	Light (h)	Number of clusters per chloroplast (avg)	Number of granules per pocket (avg)	Number of granules per chloroplast (avg)
WT*	**0**	-	-	-
	0.25	5.1	4.3	21.6
	8	11	2	20.1
mfp1	**0**	-	-	-
	0.25	2	4.6	9.4
	8	2.4	8.9	21.1
mrc-3	**0**	1	1	1
	0.25	1.4	1.7	2.3
	8	3.3	2.9	9.7
ptst2	**0**	1	1.4	1.4
	0.25	2	6	12.2
	8	1.8	3.9	7.2
ptst3	**0**	1	1	1
	0.25	2	2.4	4.8
	8	4.1	3	12.3
ss4*	**0**	1.1	1	1.1
	0.25	1.3	1	1.3
	8	2.4	1	2.5

Table 2.2. Average number of clusters, average cluster size and average granule number per chloroplast. The absence of average (-) indicates that no observed chloroplast had starch. *Data from wild-type and *ss4* come from SBF-SEM stacks in Chapter 1; Burgy et al., 2021.

Changes in granule numbers during the day

We next performed SBF-SEM analysis on plants exposed to light to an 8 h day after the 4-h night extension, again quantifying the numbers of starch granules (Table 2). In the wild type, the coalescence previously reported had resulted in smaller numbers of granules per stromal pocket (from 4.3 down to 2), while the number of occupied pockets had increased (from 5.1 to 11), indicative on further initiation during the day. In *mfp1*, the chloroplasts contained a comparable number of granules to the wild type. However, the number of clusters was substantially lower than in wild type (2.4 rather than 11) similar to what was present at the start of the day. In addition, the cluster size was larger than in wild type (8.9 rather than 2), and higher than at the start of the day (Figure 2.3A; Supplemental Movie S2.3), such that the average number of granules per chloroplast was twice that after 15 min light.

All other SGI mutants had fewer granules in total, ranging from over 12 in *ptst3* to less than 3 in *ss4*. In *mrc*, the number of occupied pockets was low, as was the number of granules per pocket, but both values were slightly higher than after 15 min light. In *ptst2*, the number of occupied pockets appeared unchanged, but the number of granules per pocket decreased as in

the wild type, rather than increasing as in *mfp1*. In *ptst3*, the number of occupied pockets increased, though not as much as in wild type, while the number of granules per pocket increase little is at all (Figure 2.3B, C). The *ss4* mutant still displayed the strongest phenotype, almost always had just 1 granule per pocket, although we observed an increase in the number of pockets occupied. After 8 h of light, starch concentrations in all mutants were comparable to the wild type, which had 4.42 ± 0.11 mg/g FW (Figure 2.2B and E). The mean starch value for *mrc* was slightly higher than the wild type (5.39 ± 1.11 mg/g FW) while that of *ss4* was slightly lower (3.21 ± 0.2 mg/g FW), but these differences were not statistically significant.

Sub-chloroplastic localisation

The numerical data above need to be treated with some caution when considered alone, given the relatively low numbers of biological replicates and chloroplasts analysed using this meticulous, yet low-throughput approach. However, careful inspection of the SBF-SEM stacks revealed distinctive features in the different SGI mutants, in particular to tell apart the separate starch granules within a cluster. If they were observed with lower resolution imaging techniques, they would be most likely be considered as one single long granule.

We investigate the influence of the SGI proteins upon the location of initiation events by examining the chloroplasts in 3D. In *mfp1*, both after 15 min and 8 h day, the majority of the granules were clustered in one or two pockets in the middle of the thylakoid membrane network (Figure 2.1A; Supplemental Movies S2.2–S2.3). Furthermore, some granules were occasionally present on the margin of the chloroplast, that is, between the inner membrane of the chloroplast and the thylakoids. This was not observed in the wild type, suggesting mis-localisation of granule initiation in *mfp1*. After 8 hours light, granules clustered in one pocket were tessellated in all three dimensions. In some places, there was little or no gap between the granules, potentially suggesting fusion events. In *mrc*, the clusters were much smaller and less frequent, and single granules often occupied an entire stromal pocket (Supplemental Movies S2.5-S2.6). Occasionally, in large stromal pockets that contained more than one granule, they were located far from each other. No granules were observed outside of the thylakoid network. Thus, as indicated from the quantitative data, this qualitative inspection confirmed that the *mfp1* and *mrc* phenotypes were quite different from each other.

In *ptst2*, the numerous initials observed after 15 min light were mostly present in very few pockets, which were generally located in the middle of the chloroplasts (Supplemental

Movies S2.8-S2.9). Further, these large stromal pockets often contained more than one group of initials that were far apart from each other. In both of these ways, the *ptst2* phenotype resembled that of *mfp1*. After 8 h, we often observed a central cluster together with one isolated granule in the periphery (Supplemental Movies S2.10).

Interestingly, a significant fraction of the chloroplasts in *ptst2* were still devoid of starch granules, even after 8 h light. In *ptst3*, the somewhat weaker phenotype after 15 min light was characterised by granule-containing stromal pockets distributed throughout the chloroplast (Supplemental Movies S2.13-S2.14). In one case, a cluster was present between the thylakoids and the envelope. After 8 h light, there was a mix of large and small granules, separated from each other, and clusters of medium-sized granules (Supplemental Movies S2.15).

In *ss4*, most chloroplasts that contained starch after the 4-h night extension had only one granule, located within the thylakoid membrane network. After 15 minutes day, small separate granules surrounded by swirling thylakoid membrane were occasionally visible. No clusters were observed at all at this stage, but after 8 h light some chloroplasts contained both large granules smaller ones that were occasionally adjacent. However, a substantial fraction of chloroplasts only contained one or two large granules, and some remained empty (Supplemental Movies S2.18-S2.21).

Isotopic labelling of starch at the time of granule initiation

To start to examine the dynamics of starch accumulation in the SGI mutants, we conducted an experiment to label the carbon assimilated into starch at the start of the day. Therefore, we pulsed plants, previously subject to a 4-h night extension, with $^{13}CO_2$ air for 15 min in the light. We sampled the mesophyll after a chase period (4 h, in unlabelled air in the light) to allow potential starch granule coalescence to occur, as was observed in the wild type (Chapter 1; Burgy et al., 2021). Fixed, embedded tissue was prepared as serial sections for inspection by SEM and NanoSIMS.

In *mfp1*, parallel initiation occurring in stromal pockets was evident both as centrally labelled, abutting, unfused granules, but also as larger granules that contained a larger area of labelling with several maxima of label intensity, indicative of starch granules that had fused (Figure 2.4A, arrowhead). In *mrc*, we observed two labelling patterns. First, uneven labelling could be observed in a flattened pattern in the middle of granules, suggesting a "planar" enrichment. Either this represents the fusion of new initials arranged as a disc, or alternatively

it could reflect the re-enlargement of a residual, thinned granule. The second pattern more clearly reflected starch accumulation onto pre-existing granules. Interestingly, neighbouring granules appeared to show both anisotropic (Figure 2.4B, second row, arrowhead) and isotropic accumulation. This is most likely due to the relative orientations of the granules: reconstructions of the chloroplast volume from SEM images of the serial sections showed that a round granule labelled with an isotropic 'ring' was in fact a flattened granule sectioned equatorially (see Figure 2.4B inset, orthogonal view).

In *ptst2*, we could observe uneven labelling in a flattened pattern in the middle of granule, as for *mrc*, in addition to centrally labelled granules (Figure 2.4C). In *ptst3*, we could not see any evident clustered labelled initials embedded into one granule. Nonetheless, the central enrichment seemed to be structured with a less enriched centre, albeit unlikely resulting from accumulation onto a pre-existing granule, due to the size and shape. It was interesting that NanoSIMS inspection of serial sections revealed that two starch granules, initiated simultaneously had enlarged into separate granules without coalescing (Figure 2.4D). Another section appeared to capture multiple initials coalescing.

In *ss4*, new initiations could be detected as well as uneven, ring like enrichment patterns (Figure 2.4E, arrowheads). We excluded that we had missed the granule centre through the analysis of serial sections. This suggests either that this large granule had been produced during the chase period or, perhaps less likely, that this chloroplast was quiescent in terms of starch synthesis during the labelling period.

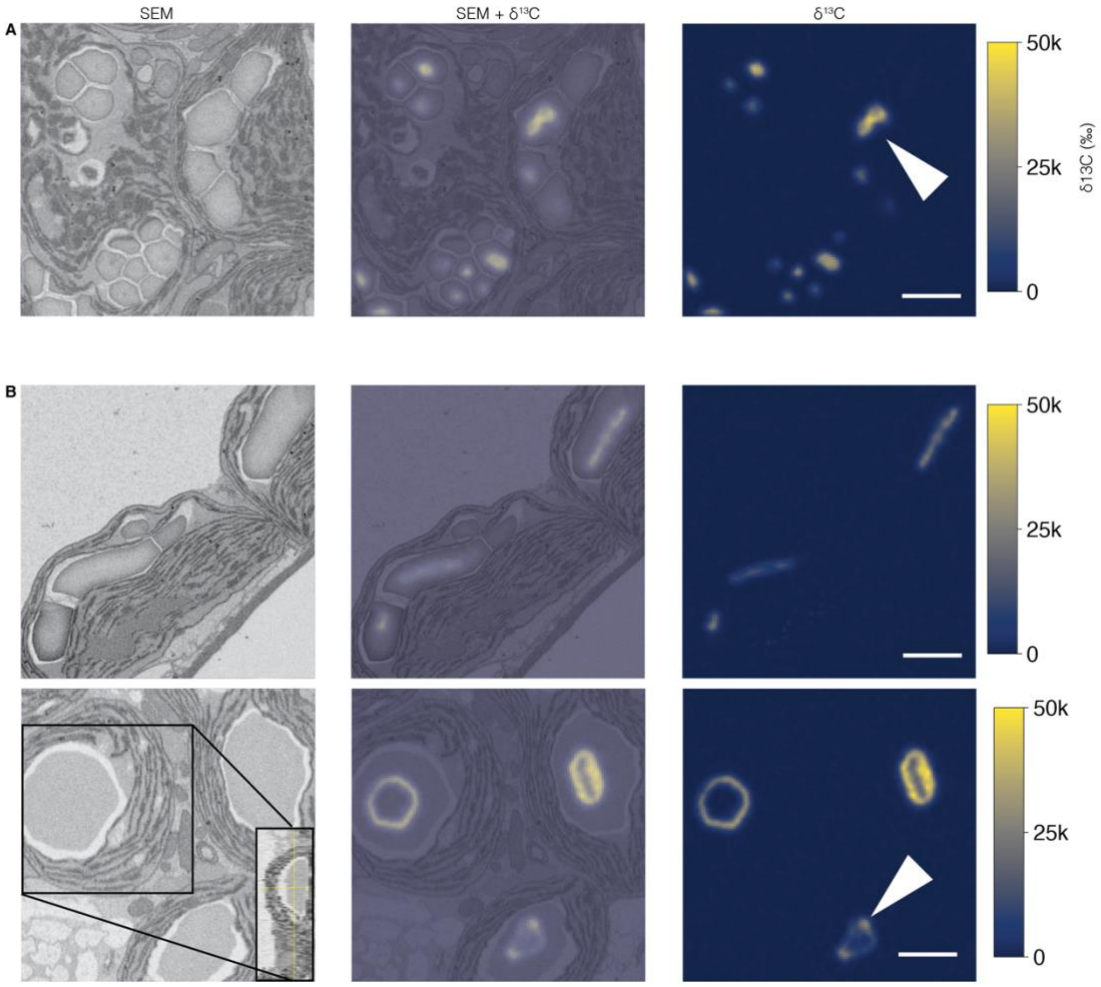

Figure 2.4

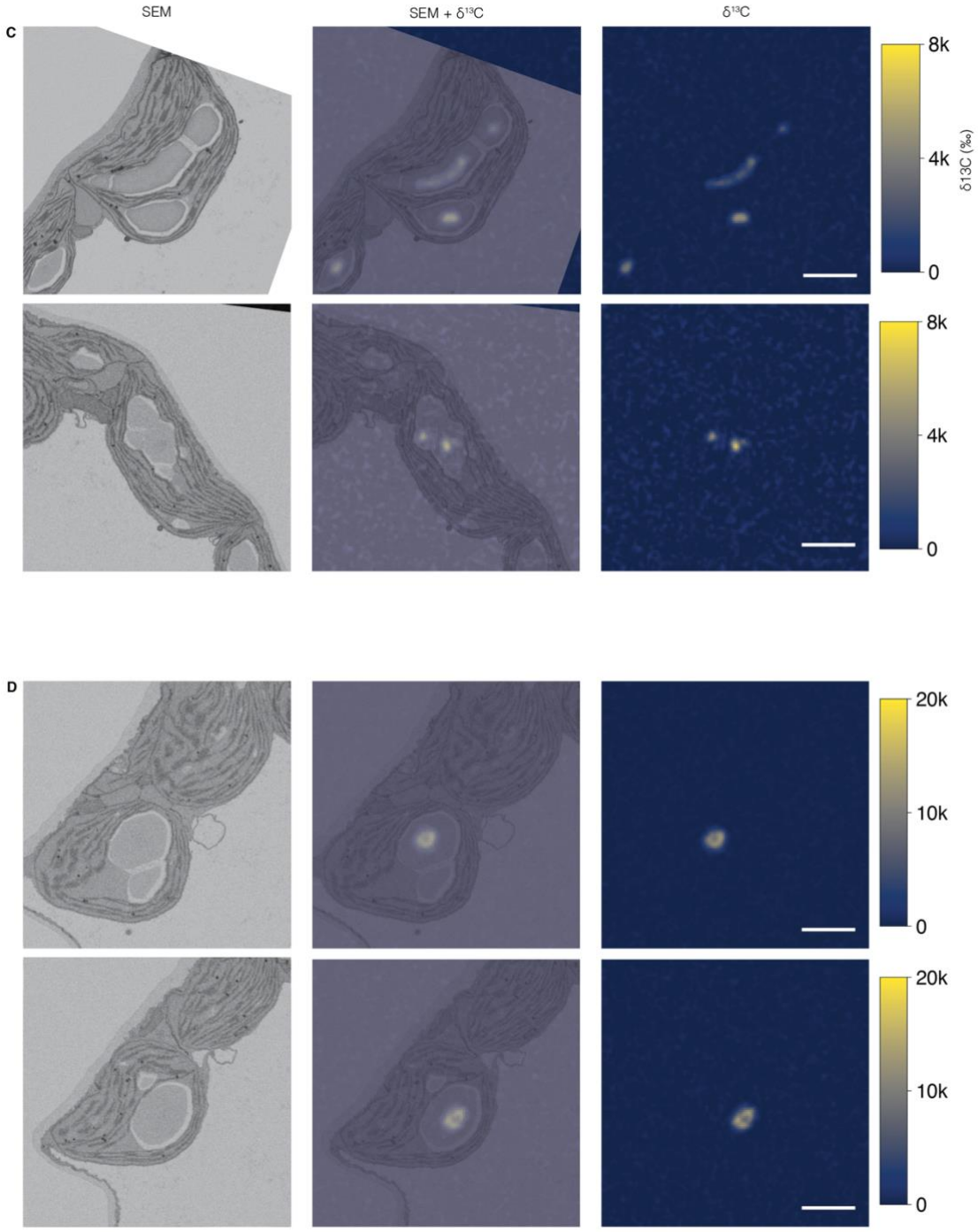

Figure 2.4 (continued)

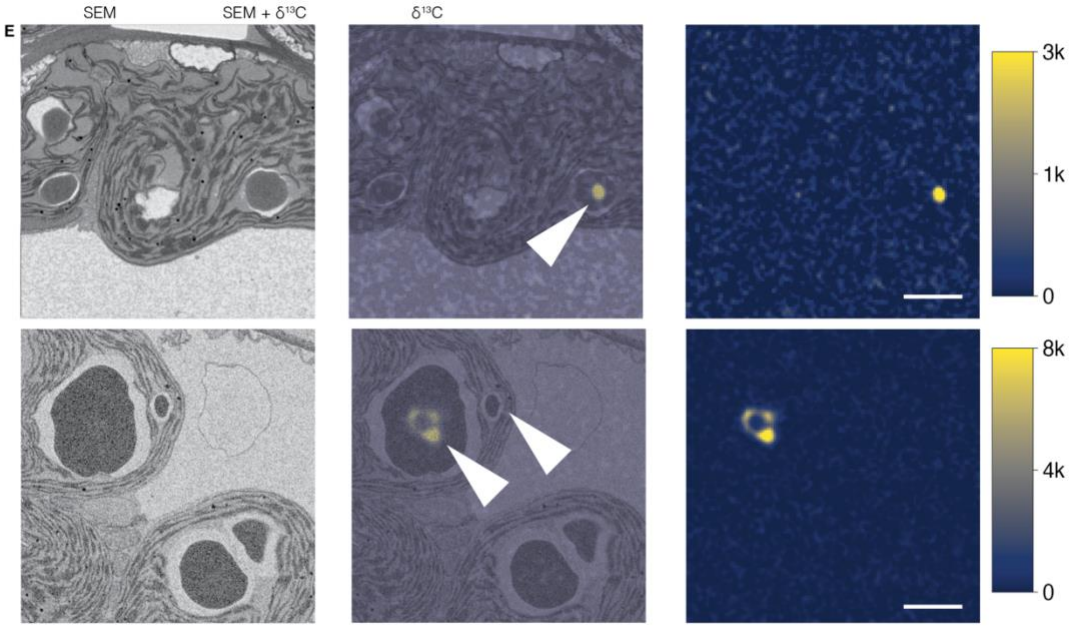

Figure 2.4 (continued)

Figure 2.4. Development of starch granule initials tracked with stable isotope labelling, EM and NanoSIMS imaging. Plants subjected to a 4-h night extension were labelled with a pulse of $^{13}CO_2$ for 15 min in the light, then harvested after a chase of 4 h in normal air in the light (**A**, *mfp1*; **B**, *mrc*; **C**, *ptst2*; **D** *ptst3*; **E**, *ss4*). In each case, samples were fixed and embedded for EM and NanoSIMS imaging. The electron micrograph (right, inverted SEM image) and the enrichment map (left) and their overlay (centre) are shown. Granules were imaged where their diameter was the largest and serial images were acquired both with SEM and NanoSIMS to ensure that no hidden enrichment was not captured in the section. The ^{13}C-enrichment is reported as per mille. **A**, Note the multiple labelled initials in each stromal space, with increasing degree of coalescence during the chase in normal air. Note in A the coalescence event (A, arrowhead). **B**, Thin internal labelling (top row). The map of the sectioned chloroplasts (B, bottom row, inset), where the orthogonal position is indicated with the yellow crosshair. Anisotropic growth was detected in one *mrc* granule (arrowhead). **C**, Central, thin labelling with a neighbouring centrally labelled granule. Dense cluster of abutting granules with multiple initials. **D**, Same chloroplast (top and bottom row) imaged at two different depth in the stack showing two labelled granules within the same pocket. **E**, *ss4* starch granules were either initiated during the pulse (E, top row, arrowhead), before the pulse (E, bottom row, left arrowhead) or after the pulse (E, bottom row, right arrowhead). Scale bar: 2 µm.

Discussion

The recently described SGI mutants reportedly decrease the number of granules per chloroplasts without measurable alterations in internal starch structure, and with little or no effects on overall starch content (Seung et al., 2017; Seung et al., 2018; Vandromme et al., 2019a); also confirmed here through rosette staining and starch measurements). The number of starch granules in a chloroplast is the most obvious metric to evaluate the importance of these genetic factors in the process of SGI. Yet, an immediate conclusion of the work presented here is that acquiring this number is not as simple a matter as it might seem at first. It is likely that many light or fluorescence microscopy methods used to ascertain granule numbers will yield underestimates when many granules are appressed into the same stromal spaces.

One aspect that is hard to evaluate only from light- or 2D-electronmicrograph is the hidden fraction of the chloroplast that is cut off from the section (which will be the majority of the chloroplast volume). This can easily result in wrong interpretations. From a stereological perspective, the size and shape of the granules relative to the chloroplast will influence the number of granules that are visible in a given chloroplast section. Indeed, we often observed in the SBF-SEM stacks that two neighbouring chloroplasts were indeed the one, but due to its concave borders it appeared as two distinct plastids on certain cross-sections. Similarly, larger granules were observed with protrusions, which in some sections could appear as two granules. Some granules seemed to be spanning a blocked chloroplast division events (FIGURE S2.1C, middle, arrowhead). Theoretically, on certain sections this could appear as two granules in two separate chloroplasts!

Indeed, the analysis of SGI mutants presented here indicates that the respective proteins may participate either in SGI in its strictest sense, or in dictating where in the chloroplast SGI occurs—or perhaps both. The ability to produce multiple starch granule initials in parallel is still evident in *mfp1*, *ptst2* and *ptst3*, even if its frequency and/or position is affected. This is an important observation since it means that SGI either may be compromised only slightly, or may be functioning quite normally, but not in the correct sub-chloroplastic locations. Indeed, *mfp1* was described as having fewer starch granules per chloroplast than the wild type, using light microscopy (Seung et al., 2018; Abt et al., 2020). Yet the data presented here suggest that it has as many as the wild type, just differently localised within the chloroplast. In contrast, SGI capability appears genuinely compromised when either MRC or SS4 are lost.

Some mutants could not be fully de-starched

Our data show that the starch content of the SGI mutants is unaffected at the end of the day, but that it does seem to vary at dawn (Figure 2.2). In a regular day-night alternation, the residual starch concentration at dawn appeared slightly, but usually significantly higher than in wild type (Figure 2.2A) (Seung et al., 2017; Seung et al., 2018; this work). Not all SGI mutations had the same impact on the residual starch concentration. It was the highest in *ss4*, similarly high in *mrc*, *ptst2* and *ptst3*, and lowest in *mfp1* yet still twice that of the wild type. These trends were similar to what was previously reported (Seung et al., 2017; Seung et al., 2018; Lu et al., 2018).

When plants were exposed to the 4-h night extension, starch contents were lower in all genotypes, but this pattern of elevated starch in the mutants was maintained (Figure 2.2D). Although the decreases in magnitude meant that the differences measured were not statistically significant (except for *ss4*), and that no differences could be discerned with iodine staining (Figure 2.2F, bottom row), the fact that granules remained at the delayed dawn suggest that the starch is less rapidly degraded in the mutants. The reasons for this are not immediately obvious, although for *ss4*, where this phenomenon is most obvious, it was proposed that surface area:volume ratio is important, potentially limiting the accessible surface available to the degradation enzymes. Presently, it is not known whether the activities of the degradation enzymes act uniformly across the surface of the starch granules, or whether their activities are directed towards certain locations, as we showed to be the case for the starch biosynthetic enzymes (Chapter 1; Burgy et al., 2021). If their actions are directed, then the argument about limited surface area may be less tenable. At one extreme, it is plausible that some granules could be preferentially degraded, leaving others intact. To test that hypothesis, it would be interesting to mark the exterior of the starch granule (by $^{13}CO_2$ labelling at dusk) and see whether they are all degraded during the subsequent night. If so, the labelled exterior should be lost, but if not, some granules would remain labelled.

Not all observed regions examined by SBF-SEM after the extended night contained the same proportion of de-starched chloroplasts, pointing to a substantial variability. This can be seen in *ss4* by iodine staining, where the older leaves contain more starch (Figure 2.2F and Ragel et al., 2013), but there could also be variation within a leaf. There was also variation in the starch contents at the whole plant level (Figure 2.2). The presence of residual starch in the SGI mutants clearly makes the subsequent analysis of initiation more difficult, since it is necessary to distinguish between residual granules and those newly initiated. In future

experiments, this could be addressed by extending the dark period in the SGI mutants. However, this has an inherent risk, since a protracted time in the dark could induce starvation responses, affecting starch production upon re-illumination. Thus, controls such as in Figure 2.2, where starch accumulation rates were shown to be normal in plants treated with an extended night would be very important.

Parallel initiation vs localisation.

As mentioned, the relevance of any new genetic factor in SGI follows from observing a change in granule number in chloroplast sections (Roldan et al., 2007; Seung et al., 2017; Seung et al., 2018; Vandromme et al., 2019a). However, a given granule number can be the result of a variety of processes and does not depend solely on SGI capacity. First, as established above, it is necessary to be able to make precise counts and be attune to the many pitfalls inherent to low resolution/higher throughput methods. Second, when chloroplasts increase in volume (e.g., when failing to divide because of large obstructing granules, as observed in our analyses) granule count increases, and it was shown previously in the pioneering study of Crumpton-Taylor et al. (2012) that large chloroplasts have more granules. Third, granule initials coalesce, and the extent to which this happens will clearly influence granule numbers. That said, it is abundantly obvious from the images and movies presented here that not all abutting granules fuse. This needs further investigation using the methods developed here. It is also possible that specific granules are degraded, even during net starch accumulation. Although unlikely, this possibility is also difficult to exclude.

Our investigation shed new light on the mechanisms of SGI. First, it supports the notion that MFP1 is an anchor that served to determine where initiation occurs yet suggests that initiation capacity per se is unaffected. We suggest that, when MFP1 is absent, the initiation complex may operate in fewer sites within the chloroplast, where it initiates many granules, leading to the observed density of initials (Figure 2.1A, S2.1A). The occasional observation of granules between the thylakoids and the envelope is consistent with this idea of mis-localisation. Our preliminary NanoSIMS experiments with *mfp1* suggest that coalescence of clustered granule initials can occur, even if the SBF-SEM stacks also revealed that single large pockets could contain multiple clusters that were distant from each other. This likely leads to the stromal pockets containing unusually high numbers of abutting granules, visible at the end of the day.

Our data also change our viewpoint on other SGI proteins, such as PTST2. Despite its proposed role in offering substrates to SS4, and thereby being important for the initiation

process, this mutant has some similarities to *mfp1*, in that clusters of granule initials could be seen by SBF-SEM. Thus, SGI still operates, possibly due to the presence of the homologous PTST3. We know that MFP1 defines the partial membrane localisation of PTST2, which may in turn serve as a link to the other SGI proteins. When PTST2 is missing, this link could be broken, explaining the similarities in these two mutant phenotypes (assuming that PTST3 cannot fulfil this role). Nevertheless, our preliminary numbers suggest the *ptst2* ends up with fewer starch granules at the end of the day, possibly because initiations are less frequent, or because PTST2 plays as yet unknown roles (e.g., in preventing neighbouring granules from coalescing). Unfortunately, our first isotope labelling experiments with *ptst2* were not sufficient to distinguish coalescence events from granule re-expansion, but further experiments will be able to resolve this question. The *ptst3* phenotype could also be seen to fit the model outlined above. Despite having a lower frequency of initiation, and fewer granules at the end of the day, the granules appeared more scattered in the chloroplasts, which could be interpreted as MFP1 and PTST2 still serving to localise the SGI process, which is compromised in its function by the loss of PTST3. This model needs testing, and sensible next steps would be to obtain further information on predicted function of PTST3. It would also be sensible to analyse the *ptst2ptst3* double mutant, the phenotype of which is more severe than either of the single mutants, and reportedly more similar to that of *ss4*.

Interestingly, the *mrc* mutant phenotype already has conspicuous similarities to that of *ss4*. We detected far fewer initials in *mrc* at the start of the day than in *mfp1* and the *ptst* mutants, and most initials were isolated, as in *ss4*. This is consistent with the previous suggestion that MRC is required for SS4 function in some way—perhaps bringing it to the same locations as the other SGI proteins. Nevertheless, at the end of the day *mrc* was able to produce more starch granules than *ss4*, meaning that SS4 is not completely inactive in its absence. Furthermore, the granules in *mrc* at the end of the day appear more similar to those of the wild type than of *ss4*. This could mean that the function of SS4 in directing the anisotropic growth of established starch granules (Chapter 1; Burgy et al., 2021) is impaired less by the loss of MRC than by its ability to contribute to granule initiation.

In conclusion, the patterns that emerges from a close examination both with higher temporal and spatial resolution reveals that the number of granules is only the tip of the iceberg to understand the mechanisms of SGI. No genetic factor appears to act in exactly the same way, but this work gives major clues as the combination of related events that occur: protein localisation, parallel initiation, coalescence, and granule growth.

Material and methods

Plant material and growth conditions

All experiments were carried out with *Arabidopsis thaliana* L., ecotype Col-0, grown on individual pots of soil (Klasmann-Deilmann Substrate 2) for 35 days in controlled environment cabinets (Percival Scientific, Perry, IA, USA) with a 12-h light (150 µmoles photons m^{-2} s^{-1})/12-h dark regime. The relative humidity was 60% and temperature was 20°C. Plants defective in SS4 are described in (Lu et al., 2018). Plants defective in MFP1 and MRC are described in (Seung et al., 2018). Plants defective in PTST2 and PTST3 are described in (Seung et al., 2017).

Starch concentration

35-d Arabidopsis rosettes (n = 5) were frozen in liquid nitrogen and homogenised in cold 0.7 M $HClO_4$ solution using a Genogrinder (SpexSamplePrep, Metuchen, NJ, USA). The insoluble material was collected by centrifugation and washed in 80% (v/v) ethanol and resuspended in water as previously described by Seung et al. (2017). Starch was quantified using an enzyme-based spectrophotometric assay as previously described by Smith and Zeeman (2006).

in situ staining of starch

Whole rosettes were harvested and immediately bleached with hot 70% (v/v) ethanol for 2 days, then washed with water, stained for starch with iodine/potassium iodide solution (I_2/KI; 1 g I_2 and 2 g KI diluted in a total volume of 300 mL distilled water) for 10 min and washed shortly in water twice. Rosettes were photographed using front and back light in water.

SBF-SEM

→ Chapter 1; Burgy et al., 2021

SIP

→ Chapter 1; Burgy et al., 2021

SEM

→ Chapter 1; Burgy et al., 2021

Serial sectioning

Semi-thin sections (200 nm) were glued with contact glue thinned with L-limonene and ribbons of 20 sections were collected onto hydrophilised silicon wafers. The ribbons were analysed by scanning electron microscopy (using the backscattered electrons at a voltage of 2

kV of a Zeiss Gemini500), imaging first section 10 in order to identify chloroplasts that were centrally sectioned. These same chloroplasts were then imaged on all sections of the ribbon. The use of serial sections enabled 3D reconstruction of the granule, but also allowed the sections to be probed with the NanoSIMS for 3D reconstruction of the isotopic labelling, removing ambiguity regarding the plane of section of the granule. In practice, typically only the three most central sections of the starch granules labelled at dawn were imaged with the NanoSIMS.

NanoSIMS

→ Chapter 1; Burgy et al., 2021

Statistical analysis

To quantify the magnitude of the change in starch concentrations between the different genotypes, we modelled the starch concentration in each genotype y_{starch}, genotype as normally distributed with mean starch concentration $\mu_{genotype}$ and a constant standard deviation σ.

$$\sigma \sim \text{Half} - \text{Normal}(0, 10),$$

$$\mu_{genotype} \sim \text{Normal}(5,3),$$

$$y_{starch,genotype} \mid \mu_{genotype}, \sigma \sim \text{Normal}(\mu_{genotype}, \sigma).$$

We used Bayesian inference with Stan (Gelman et al. 2015) to sample the posterior and ran 4 chains for 4000 iterations with the random seed = 1993. Finally, we extracted the 95-% credible intervals and plotted them onto the plot of the starch concentration.

Stan model:

```
data {
    int<lower=1> N;
    vector[N] y;
    int<lower=1> G;
    int<upper=G> genotype[N];
}
parameters {
    real<lower=0> sigma;
    vector<lower=0>[G] mu;
```

```
}
model {
    sigma ~ normal(0, 10);
    mu ~ normal(5, 3);
    for (i in 1:N) {
        y[i] ~ normal(mu[genotype[i]], sigma);
      }
}
generated quantities {
    vector[G] y_mean;
    vector[G] y_pred;
    for (i in 1:G)
        y_mean[i] = mu[i];
    for (i in 1:G)
        y_pred[i] = normal_rng(y_mean[i], sigma);
}
```

Supplementary materials

Supplemental Movie S2.1: SBF-SEM of de-starched (4-h night extension) *mfp1* chloroplasts. Progression up through one SBF-SEM image stack. Note the stromal gaps. For details of the imaged sample, see first column of Figure 1A and Figure 3A.

Supplemental Movie S2.2: SBF-SEM of de-starched *mfp1* chloroplasts exposed to 15 min light. Progression up through one SBF-SEM image stack. Note the high number of starch granules initials that can occupy a single pocket. For details of the imaged sample, see Figure 1A and Figure 3B.

Supplemental Movie S2.3: SBF-SEM of de-starched *mfp1* chloroplasts exposed to 8 h light. Progression up through one SBF-SEM image stack. For details of the imaged sample, see Figure 1A and Figure 3C.

Supplemental Movie S2.4: SBF-SEM of *mrc* chloroplasts exposed to a 4-h night extension. Progression up through one SBF-SEM image stack. Note the stromal gaps and the remaining starch granules. For details of the imaged sample, see Figure 1B and Figure 3A.

Supplemental Movie S2.5: SBF-SEM of de-starched *mrc* chloroplasts exposed to 15 min light. Progression up through one SBF-SEM image stack. For details of the imaged sample, see Figure 1B and Figure 3B.

Supplemental Movie S2.6: SBF-SEM of de-starched *mrc* chloroplasts exposed to 8h light. Progression up through one SBF-SEM image stack. For details of the imaged sample, see Figure 1B and Figure 3C.

Supplemental Movie S2.7: SBF-SEM of *ptst2* chloroplasts after a 4-h night extension. Progression up through one SBF-SEM image stack. Note the stromal gaps and the remaining starch. For details of the imaged sample, Figure 1C and Figure 3A.

Supplemental Movie S2.8: SBF-SEM of de-starched *ptst2* chloroplasts exposed to 15 min light. Progression up through one SBF-SEM image stack. Note the stromal gaps and the remaining starch. For details of the imaged sample, see Figure 1C and Figure 3B.

Supplemental Movie S2.9: SBF-SEM of de-starched *ptst2* chloroplasts exposed to 15 min light. Progression up through one SBF-SEM image stack. For details of the imaged sample, see Figure 1C and Figure 3B.

Supplemental Movie S2.10: SBF-SEM of de-starched *ptst2* chloroplasts exposed to 8 h light. Progression up through one SBF-SEM image stack. For details of the imaged sample, see Figure 1C and Figure 3C.

Supplemental Movie S2.11: SBF-SEM of *ptst3* chloroplasts exposed to a 4-h night extension. Progression up through one SBF-SEM image stack. Note the stromal gaps. For details of the imaged sample, see Figure 1D and Figure 3A.

Supplemental Movie S2.12: SBF-SEM of *ptst3* chloroplasts exposed to a 4-h night extension. Progression up through one SBF-SEM image stack. Note the stromal gaps. For details of the imaged sample, see Figure 1D and Figure 3A.

Supplemental Movie S2.13: SBF-SEM of de-starched *ptst3* chloroplasts exposed to 15 min light. Progression up through one SBF-SEM image stack. For details of the imaged sample, see Figure 1D and Figure 3B.

Supplemental Movie S2.14: SBF-SEM of de-starched *ptst3* chloroplasts exposed to 15 min light. Progression up through one SBF-SEM image stack. For details of the imaged sample, see Figure 1D and Figure 3B.

Supplemental Movie S2.15: SBF-SEM of de-starched *ptst3* chloroplasts exposed to 8 h light. Progression up through one SBF-SEM image stack. For details of the imaged sample, see Figure 1D and Figure 3C.

Supplemental Movie S2.16: SBF-SEM of de-starched *ss4* chloroplasts. Progression up through one SBF-SEM image stack. Note the stromal gaps. For details of the imaged sample, see Figure 1E and Figure 3A.

Supplemental Movie S2.17: SBF-SEM of de-starched *ss4* chloroplasts. Progression up through one SBF-SEM image stack. Note the stromal gaps. For details of the imaged sample, see Figure 1E and Figure 3A.

Supplemental Movie S2.18: SBF-SEM of de-starched *ss4* chloroplasts exposed to 15 min light. Progression up through one SBF-SEM image stack. For details of the imaged sample, see Figure 1E and Figure 3B.

Supplemental Movie S2.19: SBF-SEM of de-starched *ss4* chloroplasts exposed to 15 min light. Progression up through one SBF-SEM image stack. For details of the imaged sample, see Figure 1B and Figure 3B.

Supplemental Movie S2.20: SBF-SEM of de-starched *ss4* chloroplasts exposed to 8 h light. Progression up through one SBF-SEM image stack. For details of the imaged sample, see Figure 1E and Figure 3C.

Supplemental Movie S2.21: SBF-SEM of de-starched *ss4* chloroplasts exposed to 8 h light. Progression up through one SBF-SEM image stack. For details of the imaged sample, see Figure 1E and Figure 3C.

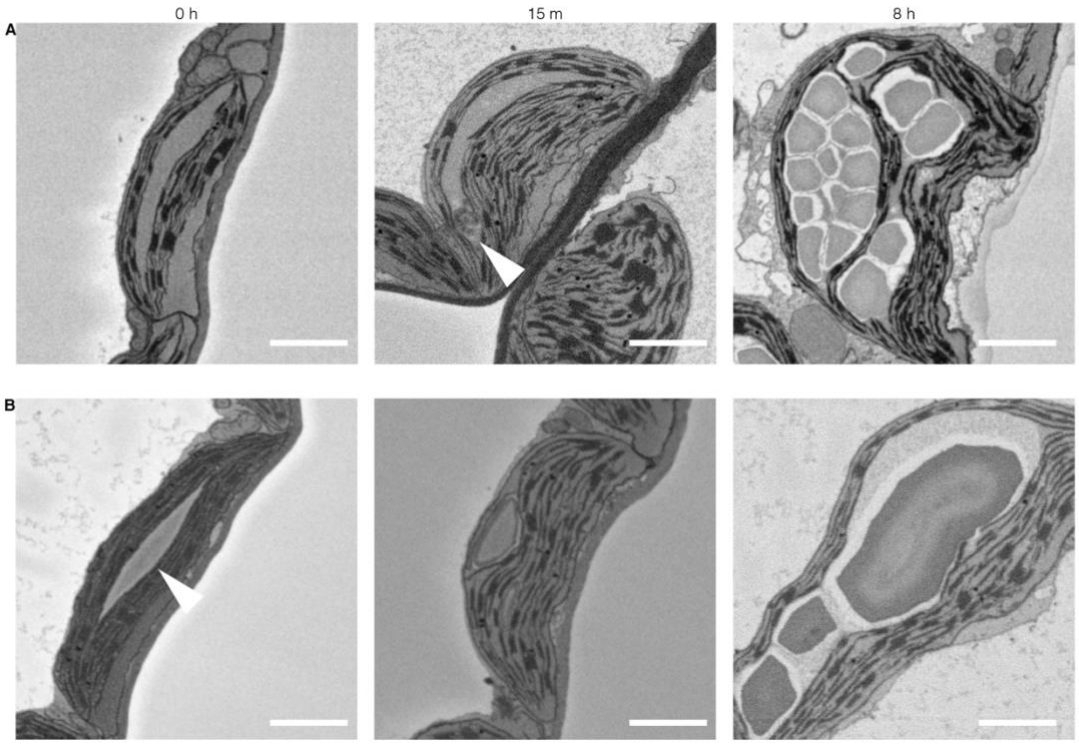

Figure S2.1. See legend on next page.

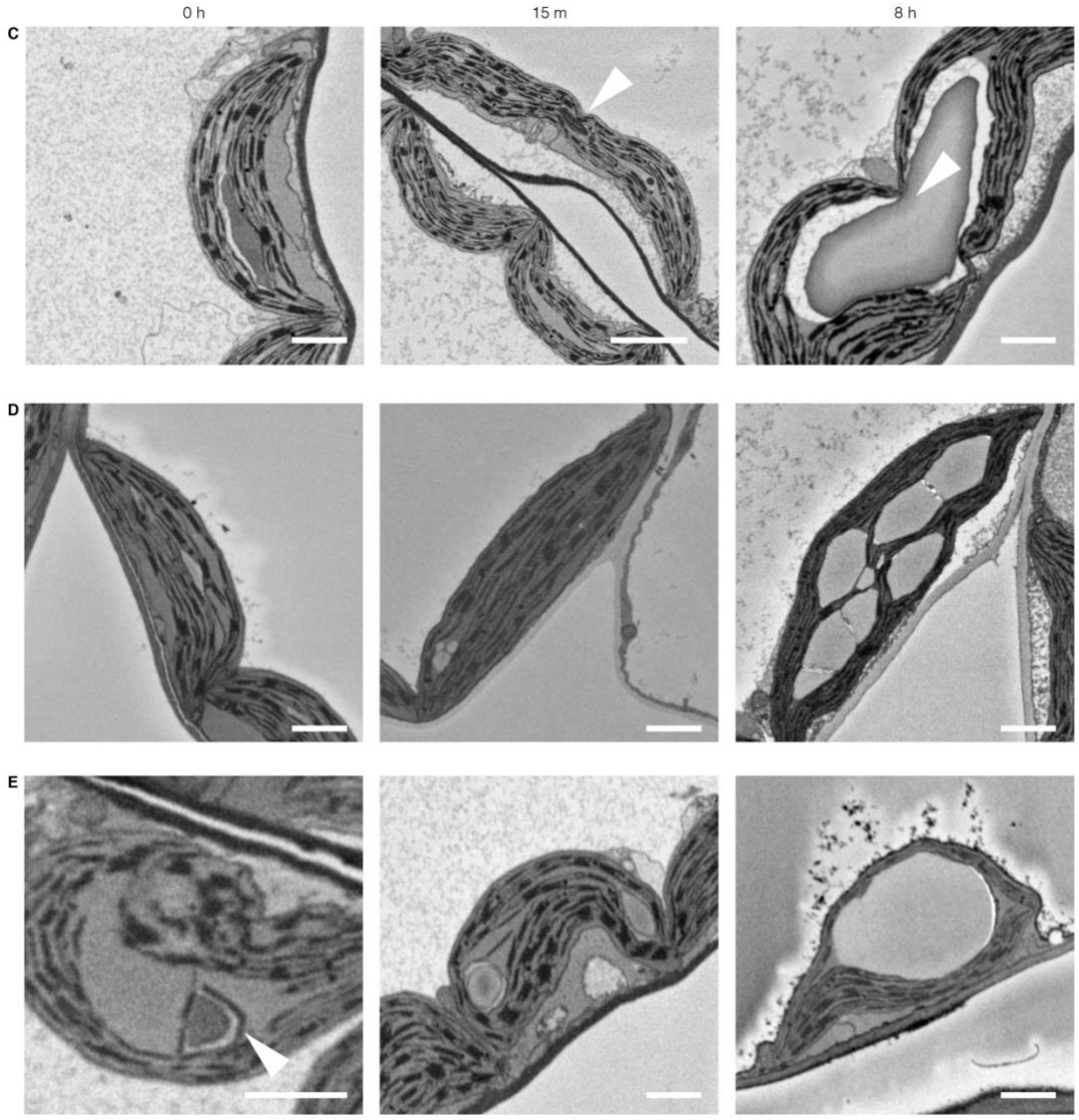

Figure S2.1. Diversity of situations in SBF-SEM stacks. Chloroplast sections from an SBF-SEM stack (with 50-nm Z-resolution, inverted SEM images) sampled from the mesophyll of fully expanded leaves of 35-day old Arabidopsis plants grown in a 12h:12h diel regime. Starch granules appear as dark-grey disks between thylakoid membranes. (**A**–**E**), Chloroplast sections from plants (**A**, *mfp1*; **B**, *mrc*; **C**, *ptst2;* **D**, *ptst3*; **E**, *ss4*) exposed to a prolonged night and harvested at the end of the 4-h night extension (left column), after 15 min light (central column) and after 8 h light (right column). Note in A the enlarged stromal pocket (left), the location of the cluster (centre, arrowhead) and the numerous starch granule that cluster into few pockets (right). Note in B the remaining thin granule (left) and the heterogeneous appearance of the large starch granule (right). Note in C the residual starch granule (left) and the starch granules at the apparent division site of the chloroplast (centre and right, arrowheads). Note in D the abutting granules tightly packed into stromal pockets (right). Note in E the protruding thylakoid mesh that seem to wrap around the starch granule (left, arrowhead). Further presentations of these data are given in Supplemental Movies. Scale bars: 2 µm.

General discussion

The complexity of starch granule development is reflected in the increasing number of genetic factors and their intrinsic coordination. However, understanding the development of starch granules requires not only genetic, but also biochemical and cell-biological insight. The aim of this work was to push forward our understanding of starch granule initiation, at the cell biological level, with a focus on in situ quantitative imaging. We developed new combinations of experimental methods and analytical techniques which, together with genetic and biochemical knowledge, help answer fundamental and previously intractable questions regarding starch granule biosynthesis. Capturing the dynamics of starch granule development, first in the wild type, then in SGI mutants, brings new perspectives that help to explain the modus operandi of the protein factors involved and starts to uncover the molecular mechanisms.

First, I showed that chloroplasts don't simply initiate isolated new granules. Rather, multiple starch initials can coalesce, then grow as a single granule. This parallel initiation followed by fusion challenges the classical view of granule initiation at a single point—the 'hilum'. This doesn't mean that individual granules cannot be initiated—indeed I observed isolated granules early in the day. However, it is possible that even these started as more than one initial and fused prior to sampling. Granule coalescence events raise the question to whether the semi-crystalline structures typically associated with starch are already formed in the observed granule initials. This will likely require other methods, such as cryo-EM tomography to resolve. Further, my work illustrates the dependence of this process on certain proteins, notably MRC and the emerging network that includes both enzymes and scaffolding factors.

Second, anisotropic starch granule growth observed during the day strengthens the link with their flattened shape. This phenomenon could also help explain the diversity of starch granule shapes observed in different plants. The presence of anisotropic growth is probably the result of the formation of complexes between starch biosynthetic enzymes that concentrate in specific regions within plastids, similarly to what was described in amyloplasts (Tetlow et al., 2008; Bierwagen et al., 2008). Those complexes could act on starch granule development

through their anchoring in the thylakoids and help trigger liquid-liquid phase separation. Further, they could help shape and maintain the orientation and curvature of thylakoids.

Third, this work and previous studies that starch granule initiation in chloroplasts occurs at defined sites in-between the thylakoid membranes, where the multiple initiations occur, and one or more starch granules are formed. I also demonstrated that among the recently discovered SGI mutants are plants that appear unable to properly localised the parallel initiation granules within the chloroplast (notably the *mfp1* mutant). These findings provide nuance as to how these proteins influence SGI.

Improving the description of granule numbers and morphologies

Starch granules are challenging to study as the structural features range from the nanometric to the sub-millimetric scale. When describing number of starch granules in situ, evaluation is usually done on sections of leaf and reported per chloroplast section. The ease and throughput of this approach are offset by the fact that number of granules is prone to error and will inevitably underestimate the actual number of granules per chloroplast.

With SBF-SEM we see all the granule in each chloroplast and, with it, more complexity that requires more precise characterisation. New units were necessary to deal with parallel initiation within stromal spaces and to quantify such phenomena. We therefore introduced the term “cluster size” to measure the number of granules that are present in close proximity in a single stromal pocket, i.e., not separated by thylakoid membrane. These stromal pockets are easy to see when filled with starch (e.g., in wild-type chloroplasts harvested at the end of the day), but they are also evident when there is no starch present. However, in some cases, stromal pockets were more difficult to define since they sometimes have a convoluted geometry. Indeed, in some mutants, large stromal pockets contained within them two or more distinct clusters of granule initials that were far from each other. These situations are biologically relevant but are not well characterised using the stromal pocket concept that was sufficient for the wild type.

These new metrics may be difficult to implement in practice as the boundaries of pocket may not be well defined. In addition, the pockets can only really be defined by the presence of starch granules within them. Nonetheless, the reason for the distinct appearance of the plastid stroma in pockets where we predict granules will form will require further investigations to confirm that they are indeed sites for new initiation events. Ideally, it will be possible to develop molecular markers for such regions—perhaps using some of the proteins we already

know, such as MFP1. Some proteins are known to be involved in the curvature of membranes. This raises the question whether coiled-coil containing proteins could be recruited to maintain the thylakoid in a specific conformation, even in the absence of starch granules. MFP1 and MRC are potential candidates but other, yet unknown factors should not be excluded.

Characterising granule morphology

Starch granule morphology is most often assessed by the visual examination of extracted starch granules imaged via LM or SEM. The visual assessment is fast both in data acquisition and interpretation, but the accuracy of the latter depends on experimenter's appreciation. Small changes between two conditions are likely to go undetected, thus limiting the potential for discovery. Further, extraction and purification remove information about the location starch in the tissue and the plastid. For instance, the polyhedral starch granules observed in cassava or rice are unlikely to adopt this shape freely. These granules most probably grow toward each other and abut in a confined space. Therefore, granules from homogenised tissues show their internal, planar faces, hence the term polyhedral. This mandates that examination of extracted granules is accompanied by complementary in situ microscopical analyses. Two-dimensional LM or TEM of sectioned material can easily show individual granules within the plastids, but suffer other limitations, as mentioned above.

Using SBF-SEM, though labour intensive, addresses both issues since the starch granules are imaged both in situ and in 3D. In that setting, useful geometric parameters can be computed from segmented granules such as the volume, the surface area, the diameter as well as the convexity and the sphericity. In addition, provided that other plastid structures (e.g., chloroplast thylakoids) are preserved and segmented, the arrangement of the granules with respect to them can be computed.

A second approach to describing extracted starch granules is flow cytometry. This technique provides high throughput and requires only tiny quantities, allowing specific tissues to be analysed. The interpretation of the output signal, though not straightforward, yields information about the circumscribed radius of the granules (size) via the forward scattering of the laser light, but can also yield insight into granule shape via the side scattering. For example, the degree of sphericity or regularity can be estimated via the breadth of bimodality of the side scattering peaks, since non-spherical granules can pass the laser light in different orientations.

Why do chloroplasts produce multiple, flat starch granules?

Given the high variability in the morphology of starch granules, it may seem difficult to model the process of granule growth. Theoretically, granules would expand radially in the absence of any constraint, producing spheres. In practice, some starch granules are spherical, but often this is not the case. In leaves, the granules are almost always flattened discoid shaped. This work has shown that in wild-type Arabidopsis chloroplasts, this results from constraints on radial growth, i.e., SS4-dependent anisotropic growth. Preferential growth along the equatorial axes occurs at the expense of polar growth. This raises obvious questions as to what advantage producing multiple granules of this shape per chloroplast offers the plant.

Together with the fact that new starch granules are initiated, the characteristic lenticular shape of chloroplasts starch granules leads to the hypothesis that the chloroplasts may seek to maximise the accumulation surface. Indeed, a flattened spheroid will have more surface area per unit volume than a sphere with the same volume. This is probably not important for deposition, which my data suggest is not limited by the surface available. However, it may be important for starch degradation, which, as discussed in the preceding chapter, may occur over the entire granule surface. Thus, the flattened morphology could contribute to the efficient adaptation of carbon fluxes, that vary between the day and night. In contrast, the starch in amyloplasts of storage organs, in which circadian oscillations of accumulation and degradation do not occur, the granules are typically not flat.

Alternatively, one could view the flattened shape of the granules as a consequence of the physical constraint of thylakoid membrane network, which in turn could be shaped by other physical forces within the plant cell. This could lead to the physical exclusion of the biosynthetic enzymes from where the thylakoids push against the granule surface, concentrating them around the equator. However, this explanation seems unlikely: in the early hours of the day, anisotropic growth of small granules could be observed. Furthermore, in the *ss4* mutant near-spherical granules are formed—presumably under similar physical conditions as in the wild type.

Partitioning the granules and SGI apparatus over plastid division cycles

The large thin granules we sometimes observed in the middle of dumbbell-shaped chloroplasts seemed to be perturbing correct chloroplast division in some of the SGI mutants. This already suggests one potential advantage to accumulating starch as multiple starch

granules rather than as one large granule, assuming that this would impair division and have a negative impact on the plant. Interestingly, the chloroplasts of younger leaves, whose cells were still expanding and chloroplasts still dividing, were observed to have a higher number of chloroplasts in their leaves (Crumpton et al., 2012, Abt et al., 2020).

When the granules are fewer but smaller in equatorial diameter, like in *ss4*, the division process can presumably proceed more readily, but would yields one daughter chloroplast with one large granule and another that does not contain any granule. In contrast, *mrc* starch granules whose diameters can be similar to that of the chloroplast, cannot divide. This could result in a more consistent, albeit reduced number of granules per chloroplast. Interestingly, a significant number of granules in *ss4* remain starchless at the end of the day, a phenomenon also seen in *ptst2*. One possibility is that when the SGI apparatus is mis-localised, plastid division could yield 'impotent' chloroplasts where the apparatus ends up all in one daughter plastid.

Thus, from a broader perspective, the reason that chloroplasts produce multiple granules could be that it is beneficial for them when dividing, to distributing both the granules and the proteins responsible for their production between the two sibling plastids. This would be in addition to benefit that many smaller starch granules would be less likely to get in the way of division. These questions could benefit from the combination of in situ immunolabelling and EM correlative imaging to image the location of each of the factors. This imaging should also be combined with a refined temporal resolution; proteins may well be mostly active at certain time points instead of being constantly present. Further, even if present constantly, their distribution might vary strongly, with condensing phases to catalyse the initiation events.

NanoSIMS to investigate the carbon metabolism

The NanoSIMS, in a normal setting, operates at room temperature and ultra-high vacuum (10^{-9}–10^{-10} Torr), requiring samples to be fixed and embedded in resin to render it inert. During this sample preparation, the label that has been assimilated in cellular structures is fixed, but not that in the soluble fraction. In this study, we used this to our advantage since it enhances the contrast in enrichment between the starch and the surrounding cellular compartment, but it also overlooks fundamental aspects of cellular processes.

Recently, a new method has been proposed to reconciliate the requirements of the NanoSIMS without altering the sample during the fixation and embedding. In this method, the sample is high-pressure frozen and cryo sectioned. The thin sections are then thawed and dried prior to

SEM imaging and NanoSIMS analysis. Because of the gentle chemical fixation, the antigenicity of the sample allows immuno-fluorescence microscopy and immuno-EM to be performed. By better preserving the solutes in place, the method captures the distribution of the label in both soluble and insoluble fractions. The much lower carbon content substantially changes the sample's chemical composition in comparison with plastic sections. As a consequence, the cyanide (CN^-) and the carbide (C_2^-) counts are higher in the cryo-fixed sections, although the increases observed are dependent on the subcellular structure and density (Loussert et al., 2020). The resulting workflow contributes to a better integration of complementary imaging technique to resolve important pathways that mainly occur in the soluble fraction of the tissue.

Regarding starch granule development, cryo-based EM and NanoSIMS are promising for several reasons. First, the absence of shrinkage of starch granules will present a more realistic picture of the granule-granule and granule thylakoid interfaces. The small initials that coalesce are suspected to be even less distinguishable from each other; skipping the dehydration could alleviate this problem. Unsurprisingly, recent results applying these methods to dinoflagellates, yielded ionic images very different to those from the plastic sections. It would be interesting to examine the detail distribution of the label in the stroma, for instance in the vicinity of the stromal pockets or to evaluate the abundance and location of the soluble precursor of starch. This could help understand the link between the soluble labelled photoassimilates and the location of SGI proteins with the expanding granules. However, use of such techniques on the air-filled mesophyll of leaves would likely be labour intensive and technically demanding since high-pressure freezing of such tissues is more challenging in comparison to isolated cells.

In this project, we mainly used NanoSIMS to test for the presence or the absence of a signal within the granule or on its surface. To a lesser extent, we used it in a more quantitative way to measure the anisotropic growth. As the labels can be present in the granule but not captured in the thin section, we applied the technique used in array tomography (that is the serial sectioning) to preserve consecutive slices of the volume of interest. The use of the serial NanoSIMS has proven very efficient to preserve the z-structure and to speed up and aid in the process of interpretation, since the labels can be analysed in the context of a stack of semi-thin sections (is it the middle of the granules? is it the single granule within that chloroplast? etc.). Further, NanoSIMS could be used to compare partitioning into starch across granules. In that context, preliminary observations from the SGI mutants pointed

towards a link between the number of granules present and the strength of the enrichment, the latter being much stronger when fewer granules are available, due to the deficient initiation machinery (see Chapter 1; NanoSIMS of *mrc*).

Despite the successful application of NanoSIMS to study the development of starch granules, the tiny size of starch granule initials pushes the NanoSIMS resolution limits to its maximum. There are good chances that the small initials that form rapidly in the first minutes of the day may already have coalesced after 15 minutes or that they may be too close together for us to resolve their individual isotopic signals with the NanoSIMS. That could explain why the enrichment is so strong in some SGI mutants, and why, despite seeing clusters of granules by SBF-SEM the initial NanoSIMS did not always provide us with evidence of subsequent coalescence. To address this problem, further experiments will be needed, where one could de-starch the plants more thoroughly, pulse the plant for shorter periods (e.g., 5 minutes rather than 15), and sample the tissue after different chase periods (e.g., from 10 minutes to several hours).

So far, the NanoSIMS was applied to mark the sites of starch accumulation – specifically to mark the time of initiation of new granules. However, it is possible that not all granules grow at the same rate or, and I occasionally observed that some granules appeared not to be labelled, raising the question of whether every starch granule is actively elaborated. Therefore, it would be interesting to perform further experiments to label starch granules at the end of the day and check the possible absence of labelled starch (implying a lack of synthesis), or conversely to see is some label is retained after incubation in the dark (implying a lack of degradation). Further, young plants could be pulsed with $^{13}CO_2$ and sampled only after a chase period day rather than hours to investigate the turnover of starch over the plant's lifetime.

High resolution and high throughput imaging

In this work, we extracted a number of valuable parameters directly from SBF-SEM image stacks that captured the chloroplasts. This allows whole chloroplasts to be observed at great lateral and depth resolution, making it possible to study with great detail the granule initiation and its association with the thylakoids. However, the high resolution is associated with a loss in overview (only a few tens of micrometres inside the leaf) and most of the imaged volume is empty of chloroplasts, not to mention the low throughput.

One approach to try and address that limitation would be to extract intact chloroplasts from leaves. The risk of disrupting them is obviously high but, if successful, would lead to a substantial concentration. A second approach to increase the number of granules analysed with NanoSIMS would be to extract and embed them in agarose. The analysis of serial sections containing several hundreds of chloroplasts or starch granules could dramatically improve the throughput at the NanoSIMS stage, even if at the expense of the structural information with respect to the cell or the chloroplast. Indeed, some of the replication that would help to support or extend the experiments conducted in this thesis could be approached in this way.

This thesis contains examples of manual segmentation, done image by image along the z-axis but the fact that one pixel is labelled on one section means it has a high probability of being labelled on the previous and the next slices. Machine semantic segmentation is increasingly changing the way biological tissues are analysed, but extrapolation in the third dimension remains challenging. Nevertheless, a successful attempt at extending the U-Net architecture (Ronneberger et al., 2015) to use 3D-images has been recently published (Ciceket al., 2016). We are confident that the machine segmentation of starch granules could become a routine technique and efforts should be implemented. One bottleneck is the elaboration of the training data set, a resource not always available for the structures of interest. Fortunately, the manually segmented stacks for starch we have created could be directly used as training example. However, one technical difficulty we encountered consists in cutting high resolution image stacks into manageable chunks (sub-image) so that processing times are reasonable. The small images need, in a second step, to be reconstructed. Semantic image segmentation often yields sooner good performances with fewer images than in object recognition. This is because, in the former case, in each of the training image, every pixel is one label. (In our case, starch marked on one image spans several pixels: a patch of 10 pixels in radius contains already more than 300 labelled pixels.) In contrast, in the latter case, each training image is associated with a single label—the object presence or absence.

To conclude, the work presented here has attempted to harness the power of several technique to unveil the complex mechanisms of SGI. With further technical, experimental and image processing advances, it is likely that this attempt will be enhanced in terms of throughput, allowing more samples to be analysed and some of the new hypotheses we have formulated to be rigorously tested.

References

ABAD, Marta C., BINDERUP, Kim, RIOS-STEINER, Jorge, ARNI, Raghuvir K., PREISS, Jack and GEIGER, James H. "The X-ray crystallographic structure of *Escherichia coli* branching enzyme". *Journal of Biological Chemistry*. 2002, vol. 277, p. 42164–42170.

ABT, Melanie R., PFISTER, Barbara, SHARMA, Mayank, EICKE, Simona, BURGY, Leo, NEALE, Isabel, SEUNG, David and ZEEMAN, Samuel C. "STARCH SYNTHASE 5, a noncanonical starch synthase-like protein, promotes starch granule initiation in Arabidopsis". *Plant Cell*. 2020, vol. 32, p. 2543–2565.

ALBERT, Sahradha, WIETRZYNSKI, Wojciech, LEE, Chia Wei, SCHAFFER, Miroslava, BECK, Florian, SCHULLER, Jan M., SALOMÉ, Patrice A., PLITZKO, Jürgen M., BAUMEISTER, Wolfgang and ENGEL, Benjamin D. "Direct visualization of degradation microcompartments at the ER membrane". *Proceedings of the National Academy of Sciences*. 2020, vol. 117, p. 1069–1080.

BAHAJI, Abdellatif, LI, Jun, OVECKA, Miroslav, EZQUER, Ignacio, MUÑOZ, Francisco J., BAROJA-FERNÁNDEZ, Edurne, ROMERO, Jose M., ALMAGRO, Goizeder, MONTERO, Manuel, HIDALGO, Maite, SESMA, Maria T. and POZUETA-ROMERO, Javier. "Arabidopsis thaliana mutants lacking ADP-glucose pyrophosphorylase accumulate starch and wild-type ADP-glucose content: further evidence for the occurrence of important sources, other than ADP-glucose pyrophosphorylase, of ADP-glucose linked to leaf starch biosynthesis". *Plant and Cell Physiology*. 2011, vol. 52, p. 1162–1176.

BALL, Steven, GUAN, Han Ping, JAMES, Martha, MYERS, Alan, KEELING, Peter, MOUILLE, Gregory, BULÉON, Alain, COLONNA, Paul and PREISS, Jack. "From glycogen to amylopectin: A model for the biogenesis of the plant starch granule". *Cell*. 1996, vol. 86, p. 349–352.

BALL, Steven G. and MORELL, Matthew K. "From bacterial glycogen to starch: understanding the biogenesis of the plant starch granule". *Annual Review of Plant Biology*. 2003, vol. 54, p. 207–233.

BALLICORA, Miguel A, FRUEAUF, Jeremiah B, FU, Yingbin, SCHÜRMANN, Peter and PREISS, Jack. "Activation of the potato tuber ADP-glucose pyrophosphorylase by thioredoxin". *Journal of Biological Chemistry*. 2000, vol. 275, no. 2, p. 1315–1320.

BALLICORA, Miguel A., IGLESIAS, Alberto A. and PREISS, Jack. "ADP-glucose pyrophosphorylase: a regulatory enzyme for plant starch synthesis". *Photosynthesis research*. 2004, vol. 79, p. 1–24.

BARRATT, D. H. Paul, DERBYSHIRE, Paul, FINDLAY, Kim, PIKE, Marilyn, WELLNER, Nikolaus, LUNN, John, FEIL, Regina, SIMPSON, Clare, MAULE, Andrew J. and SMITH, Alison M. "Normal growth of Arabidopsis requires cytosolic invertase but not sucrose synthase". *Proceedings of the National Academy of Sciences*. 2009, vol. 106, p. 13124–13129.

BERG, Jeremy M., TYMOCZKO, John L. and STRYER, Lubert. *Biochemistry*. W.H. Freeman, 2002.

BERTOFT, Eric, PIYACHOMKWAN, Kuakoon, CHATAKANONDA, Pathama and SRIROTH, Klanarong. "Internal unit chain composition in amylopectins". *Carbohydrate Polymers*. 2008, vol. 74, p. 527–543.

BLANSHARD, J. M. V., BATES, D. R., MUHR, A. H., WORCESTER, D. L. and HIGGINS, J. S. "Small-angle neutron scattering studies of starch granule structure". *Carbohydrate Polymers*. 1984, vol. 4, p. 427–442.

BORASTON, Alisdair B., BOLAM, David N., GILBERT, Harry J. and DAVIES, Gideon J. "Carbohydrate-binding modules: fine-tuning polysaccharide recognition". *Biochemical Journal*. 2004, vol. 382, p. 769–781.

BRADSKI, Gary. "The OpenCV Library". *Dr. Dobb's Journal of Software Tools*. 2000,

BRAKENHOFF, G. and NANNINGA G. "Three-dimensional confocal fluorescence microscopy". *Methods in Cell Biology*. 1989, vol. 30, p. 379–398.

BRIARTY, LG, HUGHES, CE and EVERS, AD. "The developing endosperm of wheat—a stereological analysis". *Annals of Botany*. 1979, vol. 44, no. 6, p. 641–658.

BRUST, Henrike, ORZECHOWSKI, Slawomir, FETTKE, Joerg and STEUP, Martin. "Starch synthesizing reactions and paths: *in vitro* and *in vivo* studies". *Journal of Applied Glycoscience*. 2013, vol. 60, p. 3–20.

BULEON, Alain, COLONNA, Paul, PLANCHOT, Veronique and BALL, Steven. "Starch granules: structure and biosynthesis". *International journal of biological macromolecules*. 1998, vol. 23, no. 2, p. 85–112.

BULL, Simon E., SEUNG, David, CHANEZ, Christelle, MEHTA, Devang, KUON, Joel-Elias, TRUERNIT, Elisabeth, HOCHMUTH, Anton, ZURKIRCHEN, Irene, ZEEMAN, Samuel C., GRUISSEM, Wilhelm and VANDERSCHUREN, Herve. "Accelerated *ex situ* breeding of GBSS-and PTST1-edited cassava for modified starch". *Science Advances*. 2018, vol. 4, p. eaat6086.

BURGY, Leo, EICKE, Simona, KOPP, Christophe, LU, Kuan-Jen, ESCRIG, Stephane, MEIBOM, Anders and ZEEMAN, Samuel C. "Starch is formed by coalescence of granule initials and directed anisotropic growth, controlled by the non-enzymatic domain of STARCH SYNTHASE 4". *submitted to Nature Communications*. 2021,

BURNS, Margaret S. "Applications of secondary ion mass spectrometry (SIMS) in biological research: a review". *Journal of Microscopy*. 1982, vol. 127, p. 237–258.

BURTON, Rachel A., JENNER, Helen, CARRANGIS, Luke, FAHY, Brendan, FINCHER, Geoffrey B., HYLTON, Chris, LAURIE, David A., PARKER, Mary, WAITE, Darren, WEGEN, Sonja Van, VERHOEVEN, Tamara and DENYER, Kay. "Starch granule initiation and growth are altered in barley mutants that lack isoamylase activity". *The Plant Journal*. 2002, vol. 31, p. 97–112.

BUSCHIAZZO, Alej, RO, UGALDE, Juan E., GUERIN, Marcelo E., SHEPARD, William, UGALDE, Rodolfo A. and ALZARI, Pedro M. "Crystal structure of glycogen synthase: homologous enzymes catalyse glycogen synthesis and degradation". *The EMBO Journal*. 2004, vol. 23, p. 3196–3205.

BUSSI, Yuval, SHIMONI, Eyal, WEINER, Allon, KAPON, Ruti, CHARUVI, Dana, NEVO, Reinat, EFRATI, Efi and REICH, Ziv. "Fundamental helical geometry consolidates the plant photosynthetic membrane". *Proceedings of the National Academy of Sciences*. 2019, vol. 116, p. 22366–22375.

BUSTOS, Regla, FAHY, Brendan, HYLTON, Christopher M., SEALE, Robert, NEBANE, N. Mir, A, EDWARDS, Anne, MARTIN, Cathie and SMITH, Alison M. "Starch granule initiation is controlled by a hetero-multimeric isoamylase in potato tubers". *Proceedings of the National Academy of Sciences*. 2004, vol. 101, p. 2215–2220.

BUTTROSE, M. S. "The influence of environment on the shell structure of starch granules". *The Journal of Cell Biology*. 1962, vol. 14, p. 159–167.

CALLAGHAN, Paul T., LELIEVRE, John and LEWIS, James A. "A comparison of the size and shape of $$-limit dextrin and amylopectin using pulsed field-gradient nuclear magnetic resonance and analytical ultracentrifugation". *Carbohydrate Research*. 1987,

CASPAR, Timothy, HUBER, Steven C. and SOMERVILLE, Chris. "Alterations in growth, photosynthesis, and respiration in a starchless mutant of *Arabidopsis thaliana* deficient in chloroplast phosphoglucomutase activity". *Plant Physiology*. 1985, vol. 79, p. 11–17.

CASTAING, R., JOUFFREY, B. and SLODZIAN, G. "Sur les possibilités d'analyse locale d'un échantillon par utilisation de son émission ionique secondaire". *Comptes Rendus Hebdomadaires des Séances de L'Académie des Sciences*. 1960, vol. 251, p. 1010–1012.

CHATTERJEE, Manash, BERBEZY, Pierre, VYAS, Darshna, COATES, Steve and BARSBY, Tina. "Reduced expression of a protein homologous to glycogenin leads to reduction of starch content in Arabidopsis leaves". *Plant Science*. 2005, vol. 168, no. 2, p. 501–509.

CHAWLA, Mrinalini, VERMA, Vibha, KAPOOR, Meenu and KAPOOR, Sanjay. "A novel application of periodic acid–Schiff (PAS) staining and fluorescence imaging for analysing tapetum and microspore development". *Histochemistry and cell biology*. 2017, vol. 147, no. 1, p. 103–110.

CHIA, Tansy, CHIRICO, Marcella, KING, Rob, RAMIREZ-GONZALEZ, Ricardo, SACCOMANNO, Benedetta, SEUNG, David, SIMMONDS, James, TRICK, Martin, UAUY, Cristobal, VERHOEVEN, Tamara and TRAFFORD, Kay. "A carbohydrate-binding protein, B-GRANULE CONTENT 1, influences starch granule size distribution in a dose-dependent manner in polyploid wheat". *Journal of Experimental Botany*. 2020, vol. 71, p. 105–115.

CICEK, Ozgün, ABDULKADIR, Ahmed, LIENKAMP, Soeren S., BROX, Thomas and RONNEBERGER, Olaf. 3D U-Net: learning dense volumetric segmentation from sparse annotation. 2016.p. 424–432.

CLÉDAT, Dominique, BATTU, Serge, MOKRINI, Redouane and CARDOT, Philippe J. P. "Rice starch granule characterization by flow cytometry scattering techniques hyphenated with sedimentation field-flow fractionation". *Journal of Chromatography*. 2004, vol. 1049, p. 131–138.

COLLIEX, Christian. "The "father" of microanalysis: Raymond Castaing, creator of a generation of scientific instruments, still in worldwide operation". *Comptes Rendus Physique*. 2019, vol. 20, p. 746–755.

COPEL, Les and HARDY, Karen. "Archaeological starch". *Agronomy*. 2018, vol. 8, no. 1, p. 4.

CRUMPTON-TAYLOR, Matilda, GRANDISON, Scott, PNG, Kenneth M. Y., BUSHBY, Andrew J. and SMITH, Alison M. "Control of starch granule numbers in Arabidopsis chloroplasts". *Plant Physiology*. 2012, vol. 158, p. 905–916.

CRUMPTON-TAYLOR, Matilda, PIKE, Marilyn, LU, Kuan-Jen, HYLTON, Christopher M., FEIL, Regina, EICKE, Simona, LUNN, John E., ZEEMAN, Samuel C. and SMITH, Alison M. "Starch synthase 4 is essential for coordination of starch granule formation with chloroplast division during Arabidopsis leaf expansion". *New Phytologist*. 2013, vol. 200, p. 1064–1075.

CUESTA-SEIJO, Jose A., NIELSEN, Morten M., RUZANSKI, Christian, KRUCEWICZ, Katarzyna, BEEREN, Sophie R., RYDHAL, Maja G., YOSHIMURA, Yayoi, STRIEBECK, Alex, ER, MOTAWIA, Mohammed S., WILLATS, William G. T. and PALCIC, Monica M. "In vitro biochemical characterization of all barley endosperm starch synthases". *Frontiers in Plant Science*. 2016, vol. 6, p. 1265.

DELATTE, Thierry, TREVISAN, Martine, PARKER, Mary L. and ZEEMAN, Samuel C. "Arabidopsis mutants *isa1* and *isa2* have identical phenotypes and lack the same multimeric isoamylase, which influences the branch point distribution of amylopectin during starch synthesis". *The Plant Journal*. 2005, vol. 41, p. 815–830.

DELVALLÉ, David, DUMEZ, Sylvain, WATTEBLED, Fabrice, ROLDÁN, Isaac, PLANCHOT, Véronique, BERBEZY, Pierre, COLONNA, Paul, VYAS, Darshna, CHATTERJEE, Manash, BALL, Steven, MÉRIDA, Angel and D'HULST, Christophe. "SOLUBLE STARCH SYNTHASE I: a major determinant for the synthesis of amylopectin in *Arabidopsis thaliana* leaves". *Plant Journal*. 2005, vol. 43, p. 398–412.

DENYER, Kay, CLARKE, Belinda, HYLTON, Christopher, TATGE, Helma and SMITH, Alison M. "The elongation of amylose and amylopectin chains in isolated starch granules". *The Plant Journal*. 1996, vol. 10, no. 6, p. 1135–1143.

DENYER, Kay, WAITE, Darren, MOTAWIA, Saddik, MØLLER, Birger Lindberg and SMITH, Alison M. "GRANULE-BOUND STARCH SYNTHASE I in isolated starch granules elongates malto-oligosaccharides processively". *Biochemical Journal*. 1999, vol. 340, no. 1, p. 183–191.

DENYER, Kay, JOHNSON, Philip, ZEEMAN, Samuel and SMITH, Alison M. "The control of amylose synthesis". *Journal of Plant Physiology*. 2001, vol. 158, no. 4, p. 479–487.

DHUGGA, Kanwarpal S., TIWARI, Suresh C. and RAY, Peter M. "A reversibly glycosylated polypeptide (rgp1) possibly involved in plant cell wall synthesis: purification, gene cloning, and trans-Golgi localization". *Proceedings of the National Academy of Sciences*. 1997, vol. 94, p. 7679–7684.

DUMEZ, Sylvain, WATTEBLED, Fabrice, DAUVILLEE, David, DELVALLE, David, PLANCHOT, Véronique, BALL, Steven G. and D'HULST, Christophe. "Mutants of Arabidopsis lacking STARCH BRANCHING ENZYME II substitute plastidial starch synthesis by cytoplasmic maltose accumulation". *The Plant Cell*. 2006, vol. 18, p. 2694–2709.

EDWARDS, Anne, BORTHAKUR, Alip, BORNEMANN, Stephen, VENAIL, Julien, DENYER, Kay, WAITE, Darren, FULTON, Dan, SMITH, Alison and MARTIN, Cathie. "Specificity of starch synthase isoforms from potato". *European Journal of Biochemistry*. 1999, vol. 266, p. 724–736.

EGEA, Isabel, BARSAN, Cristina, BIAN, Wanping, PURGATTO, Eduardo, LATCHÉ, Alain, CHERVIN, Christian, BOUZAYEN, Mondher and PECH, Jean-Claude. "Chromoplast differentiation: current status and perspectives". *Plant and Cell Physiology*. 2010, vol. 51, no. 10, p. 1601–1611.

EGEA, Isabel, BIAN, Wanping, BARSAN, Cristina, JAUNEAU, Alain, PECH, Jean-Claude, LATCHÉ, Alain, LI, Zhengguo and CHERVIN, Christian. "Chloroplast to chromoplast transition in tomato fruit: spectral confocal microscopy analyses of carotenoids and chlorophylls in isolated plastids and time-lapse recording on intact live tissue". *Annals of Botany*. 2011, vol. 108, p. 291–297.

ENGEL, Benjamin D, LUDINGTON, William B and MARSHALL, Wallace F. "Intra-flagellar transport particle size scales inversely with flagellar length: revisiting the balance-point length control model". *Journal of Cell Biology*. 2009, vol. 187, no. 1, p. 81–89.

ENGEL, Benjamin D., SCHAFFER, Miroslava, CUELLAR, Luis Kuhn, VILLA, Elizabeth, PLITZKO, Jürgen M. and BAUMEISTER, Wolfgang. "Native architecture of the Chlamydomonas chloroplast revealed by *in situ* cryo-electron tomography". *eLife*. 2015, vol. 4, p. e04889.

ENGLYST, H.N., KINGMAN, S.M. and CUMMINGS, J.H. "Classification and measurement of nutritionally important starch fractions". *European Journal of Clinical Nutrition*. 1992, vol. 46, no. SUPPL. 2, p. 33-50.

ESPADA, Joaquin. "Enzymic synthesis of adenosine diphosphate glucose from glucose 1-phosphate and adenosine triphosphate". *Journal of Biological Chemistry*. 1962, vol. 237, p. 3577–3581.

FERNANDEZ, Olivier, ISHIHARA, Hirofumi, GEORGE, Gavin M., MENGIN, Virginie, FLIS, Anna, SUMNER, Dean, ARRIVAULT, Stéphanie, FEIL, Regina, LUNN, John E., ZEEMAN, Samuel C., SMITH, Alison M. and STITT, Mark. "Leaf starch turnover occurs in long days and in falling light at the end of the day". *Plant Physiology*. 2017, vol. 174, p. 2199–2212.

FLÜTSCH, Sabrina, DISTEFANO, Luca and SANTELIA, Diana. "Quantification of starch in guard cells of *Arabidopsis thaliana*". *Bio-protocol*. 2018, vol. 8, no. 13,

FRAGU, P., BRIANÇON, C., FOURRÉ, C., CLERC, J., CASIRAGHI, O., JEUSSET, J., OMRI, F. and HALPERN, S. "SIMS microscopy in the biomedical field". *Biology of the Cell*. 1992, vol. 74, no. C, p. 5-18.

FRAGU, Philippe and KAHN, Edmond. "Secondary ion mass spectrometry (SIMS) microscopy: A new tool for pharmacological studies in humans". *Microscopy Research and Technique*. 1997, vol. 36, p. 296–300.

FRENCH, D., SMITH, E. E. and WHELAN, W. J. "The structural analysis and enzymic synthesis of a pentasaccharide alpha-limit dextrin formed from amylopectin by *Bacillus subtilis* alpha-amylase". *Carbohydrate Research*. 1972, vol. 22, p. 123–134.

FU, Yingbin, BALLICORA, Miguel A., LEYKAM, Joseph F. and PREISS, Jack. "Mechanism of reductive activation of potato tuber ADP-glucose pyrophosphorylase". *Journal of Biological Chemistry*. 1998, vol. 273, p. 25045–25052.

FUJITA, Naoko, KUBO, Akiko, SUH, Dong-Soon, WONG, Kit-Sum, JANE, Jay-Lin, OZAWA, Kenjiro, TAKAIWA, Fumio, INABA, Yumiko and NAKAMURA, Yasunori. "Antisense inhibition of isoamylase alters the structure of amylopectin and the physicochemical properties of starch in rice endosperm". *Plant and Cell Physiology*. 2003, vol. 44, p. 607–618.

FUJITA, Naoko, HANASHIRO, Isao, SUZUKI, Sachi, HIGUCHI, Toshiyuki, TOYOSAWA, Yoshiko, UTSUMI, Yoshinori, ITOH, Rumiko, AIHARA, Satomi and NAKAMURA, Yasunori. "Elongated phytoglycogen chain length in transgenic rice endosperm expressing active starch synthase IIa affects the altered solubility and crystallinity of the storage α-glucan". *Journal of Experimental Botany*. 2012, vol. 63, p. 5859–5872.

GÁMEZ-ARJONA, Francisco M., RAYNAUD, Sandy, RAGEL, Paula and MÉRIDA, Angel. "Starch synthase 4 is located in the thylakoid membrane and interacts with plastoglobule-associated proteins in Arabidopsis". *Plant Journal*. 2014, vol. 80, p. 305–316.

GÁMEZ-ARJONA, Francisco Manuel, DE LA CONCEPCION, Juan Carlos, RAYNAUD, Sandy, and MÉRIDA, Angel. "*Arabidopsis thaliana* plastoglobule-associated fibrillin 1a interacts with fibrillin 1b *in vivo*". *FEBS Letters*. 2014, vol. 588, p. 2800–2804.

GAO, Ming, WANAT, Jennifer, STINARD, Philip S., JAMES, Martha G. and MYERS, Alan M. "Characterization of *dull1*, a maize gene coding for a novel starch synthase". *The Plant Cell*. 1998, vol. 10, p. 399–412.

GELMAN, Andrew, LEE, Daniel and GUO, Jiqiang. "Stan: a probabilistic programming language for Bayesian inference and optimization". *Journal of Educational and Behavioral Statistics*. 2015, vol. 40, no. 5, p. 530–543.

GERNAT, C., RADOSTA, S., DAMASCHUN, G. and SCHIERBAUM, F. "Supramolecular structure of legume starches revealed by X-ray scattering". *Starch-Stärke*. 1990, vol. 42, p. 175–178.

GINDULLIS, Frank and MEIER, Iris. "Matrix attachment region binding protein MFP1 is localized in discrete domains at the nuclear envelope". *Plant Cell*. 1999, vol. 11, p. 1117–1128.

GUAN, Han Ping and PREISS, Jack. "Differentiation of the properties of the branching isozymes from maize (*Zea mays*)". *Plant Physiology*. 1993, vol. 102, p. 1269–1273.

GUILLEN, Daniel, SANCHEZ, Sergio and RODRIGUEZ-SANOJA, Romina. "Carbohydrate-binding domains: multiplicity of biological roles". *Applied Microbiology and Biotechnology*. 2010, vol. 85, p. 1241–1249.

HÄUSLER, Rainer E., SCHLIEBEN, Nils Helge, SCHULZ, Burkhard and FLÜGGE, Ulf-Ingo. "Compensation of decreased triose phosphate/phosphate translocator activity by accelerated starch turnover and glucose transport in transgenic tobacco". *Planta*. 1998, vol. 204, p. 366–376.

HE, Cuiwen, HU, Xuchen, JUNG, Rachel S., WESTON, Thomas A., S, OVAL, Norma P., TONTONOZ, Peter, KILBURN, Matthew R., FONG, Loren G., YOUNG, Stephen G. and JIANG, Haibo. "High-resolution imaging and quantification of plasma membrane cholesterol by NanoSIMS". *Proceedings of the National Academy of Sciences*. 2017, vol. 114, p. 2000–2005.

HELDT, Hans W., CHON, Chong Ja, MARONDE, Dorothea, HEROLD, Alice, STANKOVIC, Zivko S., WALKER, David A., KRAMINER, Anna, KIRK, Martha R. and HEBER, Ulrich. "Role of orthophosphate and other factors in the regulation of starch formation in leaves and isolated chloroplasts". *Plant Physiology*. 1977, vol. 59, p. 1146–1155.

HELLE, Stanislas, BRAY, Fabrice, VERBEKE, Jérémy, DEVASSINE, Stéphanie, COURSEAUX, Adeline, FACON, Maud, TOKARSKI, Caroline, ROLANDO, Christian and SZYDLOWSKI, Nicolas. "Proteome analysis of potato starch reveals the presence of new starch metabolic proteins as well as multiple protease inhibitors". *Frontiers in Plant Science*. 2018, vol. 9, p. 746.

HENNEN-BIERWAGEN, Tracie A., LIU, Fushan, MARSH, Rebekah S., KIM, Seungtaek, GAN, Qinglei, TETLOW, Ian J., EMES, Michael J., JAMES, Martha G. and MYERS, Alan M. "Starch biosynthetic enzymes from developing maize endosperm associate in multi-subunit complexes". *Plant Physiology*. 2008, vol. 146, no. 4, p. 1892–1908.

HENNEN-BIERWAGEN, Tracie A., LIN, Qiaohui, GRIMAUD, Florent, PLANCHOT, Véronique, KEELING, Peter L., JAMES, Martha G. and MYERS, Alan M. "Proteins from multiple metabolic pathways associate with starch biosynthetic enzymes in high molecular weight complexes: a model for regulation of carbon allocation in maize amyloplasts". *Plant Physiology*. 2009, vol. 149, p. 1541–1559.

HINDIE, E., BLAISE, G. and GALLE, P. *Origin of the cyanide secondary ions emitted from biological tissue under 10 keV Caesium bombardment*. 1990. p. 335–338.

HINDIE, Elif, COULOMB, Bernard and GALLE, Pierre. "SIMS microscopy: a tool to measure the intracellular concentration of ^{14}C-labelled molecules". *Biology of the Cell*. 1992, vol. 74, p. 89–92.

HIZUKURI, Susumu. "Polymodal distribution of the chain lengths of amylopectins, and its significance". *Carbohydrate Research*. 1986, vol. 147, p. 342–347.

HOPPE, Peter, COHEN, Stephanie and MEIBOM, Anders. "NanoSIMS: technical aspects and applications in cosmochemistry and biological geochemistry". *Geostandards and Geoanalytical Research*. 2013, vol. 37, no. 2, p. 111–154.

HORRER, Daniel, FLÜTSCH, Sabrina, PAZMINO, Diana, MATTHEWS, Jack S. A., THALMANN, Matthias, NIGRO, Arianna, LEONHARDT, Nathalie, LAWSON, Tracy and SANTELIA, Diana. "Blue light induces a distinct starch degradation pathway in guard cells for stomatal opening". *Current Biology*. 2016, vol. 26, no. 3, p. 362–370.

HOWITT, Crispin A., RAHMAN, Sadequr and MORELL, Matthew K. "Expression of bacterial starch-binding domains in Arabidopsis increases starch granule size". *Functional Plant Biology*. 2006, vol. 33, p. 257–266.

HUNTER, John D. "Matplotlib: a 2D graphics environment". *IEEE Annals of the History of Computing*. 2007, vol. 9, no. 03, p. 90–95.

HWANG, Seon Kap, KOPER, Kaan, SATOH, Hikaru and OKITA, Thomas W. "Rice endosperm starch phosphorylase (PHO1) assembles with disproportioning enzyme (DPE1) to form a protein complex that enhances synthesis of malto-oligosaccharides". *Journal of Biological Chemistry*. 2016, vol. 291, p. 19994–20007.

IWAI, Masakazu, ROTH, Melissa S. and NIYOGI, Krishna K. "Sub diffraction-resolution live-cell imaging for visualizing thylakoid membranes". *Plant Journal*. 2018, vol. 96, p. 233–243.

JANE, Jay-Lin, KASEMSUWAN, Tunyawat, LEAS, Sharon, ZOBEL, Henzy and ROBYT, John F. "Anthology of starch granule morphology by scanning electron microscopy". *Starch-Stärke*. 1994, vol. 46, no. 4, p. 121–129.

JANECEK, Stefan, SVENSSON, Birte and MACGREGOR, Ann. "Structural and evolutionary aspects of two families of non-catalytic domains present in starch and glycogen binding proteins from microbes, plants and animals". *Enzyme and Microbial Technology*. 2011, vol. 49, p. 429–440.

JANECEK, Stefan, SVENSSON, Birte and MACGREGOR, E. Ann. "α-Amylase: an enzyme specificity found in various families of glycoside hydrolases". *Cellular and Molecular Life Sciences*. 2014, vol. 71, p. 1149–1170.

JENSEN, Louise Helene Soegaard, CHENG, T., PLANE, Florent Olivier Vivien, ESCRIG, Stéphane, COMMENT, A., VAN DEN BRAND, B. and MEIBOM, Anders. "Sample preparation for CryoNanoSIMS". *81st IUVSTA Workshop*, 2019,

JEONG, Sun Yong, ROSE, Annkatrin and MEIER, Iris. "MFP1 is a thylakoid-associated, nucleoid-binding protein with a coiled-coil structure". *Nucleic Acids Research*. 2003, vol. 31, p. 5175–5185.

KAWAGOE, Yasushi, AKIKO KUBO, HIKARU SATOH, FUMIO TAKAIWA and YASUNORI NAKAMURA. "Roles of isoamylase and ADP-glucose pyrophosphorylase in starch granule synthesis in rice endosperm". *Plant Journal*. 2005, vol. 42, p. 164–174.

KOCH, Karen. "Sucrose metabolism: regulatory mechanisms and pivotal roles in sugar sensing and plant development". *Current Opinion in Plant Biology*. 2004, vol. 7, p. 235–246.

KOLBE, Anna, TIESSEN, Axel, SCHLUEPMANN, Henriette, PAUL, Matthew, ULRICH, Silke and GEIGENBERGER, Peter. "Trehalose 6-phosphate regulates starch synthesis via posttranslational redox activation of ADP-glucose pyrophosphorylase". *Proceedings of the National Academy of Sciences*. 2005, vol. 102, p. 11118–11123.

KOPP, C., WISZTORSKI, M., REVEL, J., MEHIRI, M., DANI, V., CAPRON, L., CARETTE, D., FOURNIER, I., MASSI, L., MOUAJJAH, D., PAGNOTTA, S., PRIOUZEAU, F., SALZET, M. MEIBOM, A., SABOURAULT, C. "MALDI-MS and NanoSIMS imaging techniques to study cnidarian–dinoflagellate symbioses". *Zoology*. 2015, vol. 118, p. 125–131.

KREIS, Martin. "Primer dependent and independent forms of soluble starch synthetase from developing barley endosperms". *Planta*. 1980, vol. 148, p. 412–416.

KRISMAN, Clara R. and BARENGO, Renée. "A precursor of glycogen biosynthesis: α-1, 4-glucan-protein". *European Journal of Biochemistry*. 1975, vol. 52, p. 117–123.

KRUGER, Nicholas J and SCOTT, Peter. "Integration of cytosolic and plastidial carbon metabolism by fructose 2, 6-bisphosphate". *Journal of Experimental Botany*. 1995, p. 1325–1333.

KUBO, Akiko, COLLEONI, Christophe, DINGES, Jason R., LIN, Qiaohui, LAPPE, Ryan R., RIVENBARK, Joshua G., MEYER, Alex, J., er, BALL, Steven G., JAMES, Martha G., HENNEN-BIERWAGEN, Tracie A. and MYERS, Alan M. "Functions of heteromeric and homomeric isoamylase-type starch-debranching enzymes in developing maize endosperm". *Plant Physiology*. 2010, vol. 153, p. 956–969.

LARONDELLE, Yvan, MERTENS, Emmanuel, SCHAFTINGEN, Emile Van and HENRI-GÉRY, H. E. R. S. "Purification and properties of spinach leaf phosphofructokinase 2/fructose 2, 6-bisphosphatase". *European Journal of Biochemistry*. 1986, vol. 161, p. 351–357.

LARSON, Mark E., FALCONER, Daniel J., MYERS, Alan M. and BARB, Adam W. "Direct characterization of the maize starch synthase IIa product shows maltodextrin elongation occurs at the non-reducing end". *Journal of Biological Chemistry*. 2016, vol. 291, p. 24951–24960.

LEE, E. Y. C. and WHELAN, W. J. "Glycogen and starch debranching enzymes". *Enzymes*. 1971,

LELOIR, L. F., FEKETE, M. A. De and CARDINI, C. E. "Starch and oligosaccharide synthesis from uridine diphosphate glucose.". *The Journal of Biological Chemistry*. 1961, vol. 236, p. 636–641.

LETERRIER, Marina, HOLAPPA, Lynn D., BROGLIE, Karen E. and BECKLES, Diane M. "Cloning, characterisation and comparative analysis of a STARCH SYNTHASE IV gene in wheat: functional and evolutionary implications". *BMC Plant Biology*. 2008, vol. 8, p. 98.

LHUISSIER, F., LEFEBVRE, F., GIBOUIN, D., DEMARTY, M., THELLIER, M. and RIPOLL, C. "Secondary ion mass spectrometry imaging of the fixation of ^{15}N-labelled NO in pollen grains.". *Journal of Microscopy*. 2000, vol. 198, no. 2, p. 108–115.

LI, Sanfeng, WEI, Xiangjin, REN, Yulong, QIU, Jiehua, JIAO, Guiai, GUO, Xiuping, TANG, Shaoqing, WAN, Jianmin and HU, Peisong. "*OsBT1* encodes an ADP-glucose transporter involved in starch synthesis and compound granule formation in rice endosperm". *Scientific Reports*. 2017, vol. 7, no. 1, p. 1–13.

LIN, Tsan-Piao, CASPAR, Timothy, SOMERVILLE, Chris R. and PREISS, Jack. "A starch deficient mutant of *Arabidopsis thaliana* with low ADP-glucose pyrophosphorylase activity lacks one of the two subunits of the enzyme". *Plant Physiology*. 1988, vol. 88, p. 1175–1181.

LINDEN, James C. and SCHILLING, N. "*De novo* maltotriose biosynthesis from the reducing end by *Spinacia oleracea* chloroplasts". *Plant Physiology*. 1984, vol. 74, p. 795–799.

LIU, Fushan, ROMANOVA, Nadya, LEE, Elizabeth A., AHMED, Regina, EVANS, Martin, GILBERT, Elliot P., MORELL, Matthew K., EMES, Michael J. and TETLOW, Ian J. "Glucan affinity of STARCH SYNTHASE IIa determines binding of STARCH SYNTHASE I and STARCH-BRANCHING ENZYME IIb to starch granules". *Biochemical Journal*. 2012, vol. 448, p. 373–387.

LOHMEIER-VOGEL, Elke M., KERK, David, NIMICK, Mhairi, WROBEL, Susan, VICKERMAN, Lori, MUENCH, Douglas G. and MOORHEAD, Greg Bg. "Arabidopsis At5g39790 encodes a chloroplast-localized, carbohydrate-binding, coiled-coil domain-containing putative scaffold protein". *BMC Plant Biology*. 2008, vol. 8,

LOMAKO, Joseph, LOMAKO, Wieslawa M. and WHELAN, William J. "A self-glucosylating protein is the primer for rabbit muscle glycogen biosynthesis". *The FASEB journal*. 1988, vol. 2, p. 3097–3103.

LOMBARD, Vincent, RAMULU, Hemalatha Golaconda, DRULA, Elodie, COUTINHO, Pedro M. and HENRISSAT, Bernard. "The carbohydrate-active enzymes database (CAZy) in 2013". *Nucleic Acids Research*. 2014, vol. 42, p. D490–D495.

LOUSSERT-FONTA, Céline, TOULLEC, Gaëlle, PARAECATTIL, Arun Aby, JEANGROS, Quentin, KRUEGER, Thomas, ESCRIG, Stephane and MEIBOM, Anders. "Correlation of fluorescence microscopy, electron microscopy, and NanoSIMS stable isotope imaging on a single tissue section". *Communications Biology*. 2020, vol. 3, no. 1, p. 1–9.

LU, Kuan-Jen, PFISTER, Barbara, JENNY, Camilla, EICKE, Simona and ZEEMAN, Samuel C. "Distinct functions of STARCH SYNTHASE 4 domains in starch granule formation". *Plant Physiology*. 2018, vol. 176, p. 566–581.

MACKINDER, Luke C. M., CHEN, Chris, LEIB, Ryan D., PATENA, Weronika, BLUM, Sean R., RODMAN, Matthew, RAMUNDO, Silvia, ADAMS, Christopher M. and JONIKAS, Martin C. "A spatial interactome reveals the protein organization of the algal CO_2-concentrating mechanism". *Cell*. 2017, vol. 171, p. 133-147.e14.

MALINOVA, Irina and FETTKE, Joerg. "Reduced starch granule number per chloroplast in the *dpe2/phs1* mutant is dependent on initiation of starch degradation". Wagner L. Araujo. *PLOS ONE*. 2017, vol. 12, p. e0187985.

MANNERS, David J. "Recent developments in our understanding of amylopectin structure". *Carbohydrate Polymers*. 1989,

MARKHAM, Jonathan E. and KRUGER, Nicholas J. "Kinetic properties of bifunctional 6-phosphofructo-2-kinase/fructose-2, 6-bisphosphatase from spinach leaves". *European Journal of Biochemistry*. 2002, vol. 269, p. 1267–1277.

MATSUSHIMA, Ryo, YAMASHITA, Jun, KARIYAMA, Shungo, ENOMOTO, Takashi and SAKAMOTO, Wataru. "A phylogenetic re-evaluation of morphological variations of starch grains among *Poaceae* species". *Journal of Applied Glycoscience*. 2013, vol. 60, no. 1, p. 37–44.

MCCORMICK, Alistair J. and KRUGER, Nicholas J. "Lack of fructose 2, 6-bisphosphate compromises photosynthesis and growth in Arabidopsis in fluctuating environments". *The Plant Journal*. 2015, vol. 81, no. 5, p. 670–683.

MEIER, Iris, PHELAN, Tom, GRUISSEM, Wilhelm, SPIKER, Steven and SCHNEIDER, Dagmar. "MFP1: a novel plant filament-like protein with affinity for matrix attachment region DNA". *Plant Cell*. 1996, vol. 8, p. 2105–2115.

MICHALSKA, Justyna, ZAUBER, Henrik, BUCHANAN, Bob B., CEJUDO, Francisco J. and GEIGENBERGER, Peter. "NTRC links built-in thioredoxin to light and sucrose in regulating starch synthesis in chloroplasts and amyloplasts". *Proceedings of the National Academy of Sciences*. 2009, vol. 106, p. 9908–9913.

MORRISON, W. R. and SCOTT, D. C. "Measurement of the dimensions of wheat starch granule populations using a Coulter counter with 100-channel analyser". *Journal of Cereal Science*. 1986, vol. 4, p. 13–21.

MUGFORD, Sam T., FERN, EZ, Olivier, BRINTON, Jemima, FLIS, Anna, KROHN, Nicole, ENCKE, Beatrice, FEIL, Regina, SULPICE, Ronan, LUNN, John E., STITT, Mark and SMITH, Alison M. "Regulatory properties of ADP-glucose pyrophosphorylase are required for adjustment of leaf starch synthesis in different photoperiods". *Plant Physiology*. 2014, vol. 166, p. 1733–1747.

MUKERJEA, Rupendra and ROBYT, John F. "Tests for the mechanism of starch biosynthesis: *de novo* synthesis or an amylogenin primer synthesis". *Carbohydrate Research*. 2013, vol. 372, p. 55–59.

MYERS, Alan M., MORELL, Matthew K., JAMES, Martha G. and BALL, Steven G. "Recent progress toward understanding biosynthesis of the amylopectin crystal". *Plant Physiology*. 2000, vol. 122, p. 989–997.

NAKAMURA, Yasunori, UTSUMI, Yoshinori, SAWADA, Takayuki, AIHARA, Satomi, UTSUMI, Chikako, YOSHIDA, Mayumi and KITAMURA, Shinichi. "Characterization of the reactions of starch branching enzymes from rice endosperm". *Plant and Cell Physiology*. 2010, vol. 51, p. 776–794.

NIELSEN, Tom Hamborg, RUNG, Jesper Henrik and VILLADSEN, Dorthe. "Fructose-2,6-bisphosphate: a traffic signal in plant metabolism". *Trends in Plant Science*. 2004, vol. 9, p. 556–563.

NIELSEN, Morten M., RUZANSKI, Christian, KRUCEWICZ, Katarzyna, STRIEBECK, Alex, ER, CENCI, Ugo, BALL, Steven G., PALCIC, Monica M. and CUESTA-SEIJO, Jose A. "Crystal structures of the catalytic domain of *Arabidopsis thaliana* starch synthase IV, of granule bound starch synthase from CLg1 and of granule bound starch synthase I of *Cyanophora paradoxa* illustrate substrate recognition in starch synthases". *Frontiers in Plant Science*. 2018, vol. 9, p. 1138.

NIKUNI, Z. and FUKUI, T. "Experimental method for starch". *Tanpakushitsu kakusan koso. Protein, nucleic acid, enzyme*. 1969, vol. 14, p. 943–948.

NIKUNI, Z. "Studies on starch granules". *Starch-Stärke*. 1978, vol. 30, p. 105–111.

OKAR, David A. and LANGE, Alex J. "Fructose-2, 6-bisphosphate and control of carbohydrate metabolism in eukaryotes". *Biofactors*. 1999, vol. 10, p. 1–14.

OOSTERGETEL, Gerrit T. and VAN BRUGGEN, Ernst F. J. "On the origin of a low angle spacing in starch". *Starch-Stärke*. 1989, vol. 41, p. 331–335.

PAWLEY, James. *Handbook of biological confocal microscopy*. Springer Science & Business Media, 2006.

PENG, Cheng, WANG, Yihua, LIU, Feng, REN, Yulong, ZHOU, Kunneng, LV, Jia, ZHENG, Ming, ZHAO, Shaolu, ZHANG, Long, WANG, CHUNMING, Jiang, LING, Zhang, XIN, Guo, XIUPING, Bao, YIQUN and WAN, Jianmin. "FLOURY ENDOSPERM 6 encodes a CBM 48 domain-containing protein involved in compound granule formation and starch synthesis in rice endosperm". *The Plant Journal*. 2014, vol. 77, p. 917–930.

PÉREZ, Serge, BALDWIN, Paul M. and GALLANT, Daniel J. *Structural features of starch granules I*. Elsevier, 2009, 149–192.

PÉREZ, Serge and BERTOFT, Eric. "The molecular structures of starch components and their contribution to the architecture of starch granules: A comprehensive review". *Starch-Stärke*. 2010, vol. 62, no. 8, p. 389–420.

PEREZ-MORAL, Natalia, PLANKEELE, Jean-Michel, DOMONEY, Claire and WARREN, Frederick J. "Ultra-high performance liquid chromatography-size exclusion chromatography (UPLC-SEC) as an efficient tool for the rapid and highly informative characterisation of biopolymers". *Carbohydrate Polymers*. 2018, vol. 196, p. 422–426.

PERNICE, Mathieu, DUNN, Simon R, TONK, Linda, DOVE, Sophie, DOMART-COULON, Isabelle, HOPPE, Peter, SCHINTLMEISTER, Arno, WAGNER, Michael and MEIBOM, Anders. "A nanoscale secondary ion mass spectrometry study of dinoflagellate functional diversity in reef-building corals". *Environmental microbiology*. 2015, vol. 17, no. 10, p. 3570–3580.

PETER, ERL, R. and LECHENE, C. "Measure of carbon and nitrogen stable isotope ratios in cultured cells". *Journal of the American Society for Mass Spectrometry*. 2004, vol. 15, p. 478–485.

PFISTER, Barbara, LU, Kuan-Jen, EICKE, Simona, FEIL, Regina, LUNN, John E., STREB, Sebastian and ZEEMAN, Samuel C. "Genetic evidence that chain length and branch point distributions are linked determinants of starch granule formation in Arabidopsis". *Plant Physiology*. 2014, vol. 165, p. 1457–1474.

PFISTER, Barbara, SANCHEZ-FERRER, Antoni, DIAZ, Ana, LU, Kuanjen, OTTO, Caroline, HOLLER, Mirko, SHAIK, Farooque Razvi, MEIER, Florence, MEZZENGA, Raffaele and ZEEMAN, Samuel C. "Recreating the synthesis of starch granules in yeast". *eLife*. 2016, vol. 5, p. e15552.

PFISTER, Barbara and ZEEMAN, Samuel C. "Formation of starch in plant cells". *Cellular and Molecular Life Sciences*. 2016, vol. 73, p. 2781–2807.

PILLING, Emma and SMITH, Alison M. "Growth ring formation in the starch granules of potato tubers". *Plant Physiology*. 2003, vol. 132, p. 365–371.

PIPERNO, Dolores R., RANERE, Anthony J., HOLST, Irene and HANSELL, Patricia. "Starch grains reveal early root crop horticulture in the Panamanian tropical forest". *Nature*. 2000, vol. 407, no. 6806, p. 894–897.

PIPITONE, Rosa, EICKE, Simona, PFISTER, Barbara, GLAUSER, Gaetan, FALCONET, Denis, UWIZEYE, Clarisse, PRALON, Thibaut, ZEEMAN, Samuel C., KESSLER, Felix and DEMARSY, Emilie. "Two distinct phases of chloroplast biogenesis during de-etiolation in *Arabidopsis thaliana*". *bioRxiv*. 2020,

PITCHER, Julie, SMYTHE, Carl and COHEN, Philip. "Glycogenin is the priming glucosyltransferase required for the initiation of glycogen biogenesis in rabbit skeletal muscle". *European Journal of Biochemistry*. 1988, vol. 176, p. 391–395.

RAGEL, Paula, STREB, Sebastian, FEIL, Regina, SAHRAWY, Mariam, ANNUNZIATA, Maria Grazia, LUNN, John E., ZEEMAN, Samuel C. and MÉRIDA, Angel. "Loss of starch granule initiation has a deleterious effect on the growth of Arabidopsis plants due to an accumulation of ADP-glucose". *Plant Physiology*. 2013, vol. 163, p. 75–85.

RAHMAN, Sadequr, REGINA, Ahmed, LI, Zhongyi, MUKAI, Yasuhiko, YAMAMOTO, Maki, KOSAR-HASHEMI, Behjat, ABRAHAMS, Sharon and MORELL, Matthew K. "Comparison of starch-branching enzyme genes reveals evolutionary relationships among isoforms. characterization of a gene for starch-branching enzyme IIa from the wheat genome donor *Aegilops tauschii*". *Plant Physiology*. 2001, vol. 125, no. 3, p. 1314–1324.

RAYNAUD, S, Y, RAGEL, Paula, ROJAS, Tomás and MÉRIDA, Angel. "The N-terminal part of *Arabidopsis thaliana* starch synthase 4 determines the localisation and activity of the enzyme". *Journal of Biological Chemistry*. 2016, vol. 291, p. 10759–10771.

RENNIE, Emilie A., HANSEN, Sara Fasmer, BAIDOO, Edward E. K., HADI, Masood Z., KEASLING, Jay D. and SCHELLER, Henrik Vibe. "Three members of the Arabidopsis glycosyltransferase family 8 are xylan glucuronosyltransferases". *Plant Physiology*. 2012, vol. 159, p. 1408–1417.

RIESMEIER, Jorg W., FLÜGGE, Uwe. I., SCHULZ, Burkhard, HEINEKE, Dieter, HELDT, Hans-Walter, LOTHAR, Willmitzer and FROMMER, Wolf B. "Antisense repression of the chloroplast triose phosphate translocator affects carbon partitioning in transgenic potato plants". *Proceedings of the National Academy of Sciences*. 1993, vol. 90, p. 6160–6164.

ROBINSON, Carol V., SALI, Andrej and BAUMEISTER, Wolfgang. "The molecular sociology of the cell". *Nature*. 2007, vol. 450, p. 973–982.

ROLDÁN, Isaac, WATTEBLED, Fabrice, LUCAS, M. Mercedes, DELVALLÉ, David, PLANCHOT, Veronique, JIMÉNEZ, Sebastian, PÉREZ, Ricardo, BALL, Steven, D'HULST, Christophe and MÉRIDA, Angel. "The phenotype of soluble starch synthase IV defective mutants of *Arabidopsis thaliana* suggests a novel function of elongation enzymes in the control of starch granule formation". *The Plant Journal*. 2007, vol. 49, p. 492–504.

ROLL-SABATÉ, Agnès, COLONNA, Paul, MENDEZ-MONTEALVO, Maria Guadalupe and PLANCHOT, Véronique. "Branching features of amylopectins and glycogen determined by asymmetrical flow field flow fractionation coupled with multiangle laser light scattering". *Biomacromolecules*. 2007, vol. 8, p. 2520–2532.

RONNEBERGER, Olaf, FISCHER, Philipp and BROX, Thomas. U-net: convolutional networks for biomedical image segmentation. *arxiv*, 2015.p. 234–241.

ROTHSCHILD, Andrea, T and ECARZ, Juana S. "UDP-glucose:protein transglucosylase in developing maize endosperm". *Plant Science*. 1994, vol. 97, p. 119–127.

RUAN, Yong-Ling. "Signaling role of sucrose metabolism in development". *Molecular Plant*. 2012, vol. 5, p. 763–765.

SAITO, Mika, TANAKA, Tsuyoshi, SATO, Kazuhiro, VRINTEN, Patricia and NAKAMURA, Toshiki. "A single nucleotide polymorphism in the "*fra*" gene results in fractured starch granules in barley". *Theoretical and Applied Genetics*. 2018, vol. 131, p. 353–364.

SATOH, Hikaru, SHIBAHARA, Kensuke, TOKUNAGA, Takashi, NISHI, Aiko, TASAKI, Mikako, HWANG, Seon-Kap, OKITA, Thomas W, KANEKO, Nanae, FUJITA, Naoko, YOSHIDA, Mayumi, HOSAKA, Yuko, SATO, Aya, UTSUMI, Yoshinori, OHDAN, Takashi and NAKAMURA, Yasunori. "Mutation of the plastidial α-glucan phosphorylase gene in rice affects the synthesis and structure of starch in the endosperm". *The Plant Cell*. 2008, vol. 20, no. 7, p. 1833–1849.

SCHAFFER, Miroslava, MAHAMID, Julia, ENGEL, Benjamin D., LAUGKS, Tim, BAUMEISTER, Wolfgang and PLITZKO, Jürgen M. "Optimized cryo-focused ion beam sample preparation aimed at *in situ* structural studies of membrane proteins". *Journal of Structural Biology*. 2017, vol. 197, p. 73–82.

SCHNEIDER, Anja, HÄUSLER, Rainer E., KOLUKISAOGLU, Uner, KUNZE, Reinhard, GRAAFF, Eric Van Der, SCHWACKE, Rainer, CATONI, Elisabetta, DESIMONE, Marcelo and FLÜGGE, Ulf-Ingo. "An *Arabidopsis thaliana* knock-out mutant of the chloroplast triose phosphate/phosphate translocator is severely compromised only when starch synthesis, but not starch mobilisation is abolished". *The Plant Journal*. 2002, vol. 32, p. 685–699.

SCHOENHEIMER, Rudolf. "The dynamic state of body constituents". *The dynamic state of body constituents*. 1946,

SEUNG, David, SOYK, Sebastian, COIRO, Mario, MAIER, Benjamin A., EICKE, Simona and ZEEMAN, Samuel C. "PROTEIN TARGETING TO STARCH is required for localising GRANULE-BOUND STARCH SYNTHASE to starch granules and for normal amylose synthesis in Arabidopsis". *PLoS Biol*. 2015, vol. 13, p. e1002080.

SEUNG, David, LU, Kuan-Jen, STETTLER, Michaela, STREB, Sebastian and ZEEMAN, Samuel C. "Degradation of glucan primers in the absence of starch synthase 4 disrupts starch granule initiation in Arabidopsis". *Journal of Biological Chemistry*. 2016, vol. 291, p. 20718–20728.

SEUNG, David, BOUDET, Julien, MONROE, Jonathan, SCHREIER, Tina B., DAVID, Laure C., ABT, Melanie, LU, Kuan-Jen, ZANELLA, Martina and ZEEMAN, Samuel C. "Homologs of PROTEIN TARGETING TO STARCH control starch granule initiation in Arabidopsis leaves". *The Plant Cell*. 2017, vol. 29, p. 1657–1677.

SEUNG, David, SCHREIER, Tina B., BURGY, Leo, EICKE, Simona and ZEEMAN, Samuel C. "Two plastidial coiled-coil proteins are essential for normal starch granule initiation in Arabidopsis". *The Plant Cell*. 2018, vol. 30, p. 1523–1542.

SEUNG, David and SMITH, Alison M. "Starch granule initiation and morphogenesis—progress in Arabidopsis and cereals". *Journal of Experimental Botany*. 2019, vol. 70, no. 3, p. 771–784.

SEUNG, David. "Amylose in starch: towards an understanding of biosynthesis, structure and function". *New Phytologist*. 2020, vol. 228, no. 5, p. 1490–1504.

SHEPPARD, C. J. R. and CHOUDHURY, A. "Image formation in the scanning microscope". *Optica Acta*. 1977, vol. 24, p. 1051–1073.

SINGH, David G., LOMAKO, Joseph, LOMAKO, Wieslawa M., WHELAN, William J., MEYER, Helmut E., SERWE, Maria and METZGER, Jörg W. "β-Glucosylarginine: a new glucose-protein bond in a self-glucosylating protein from sweet corn". *FEBS Letters*. 1995, vol. 376, p. 61–64.

SMITH, Alison M. and STITT, Mark. "Coordination of carbon supply and plant growth". *Plant, cell and environment*. 2007, vol. 30, p. 1126–1149.

SMITH, Alison M. and ZEEMAN, Samuel C. "Starch: a flexible, adaptable carbon store coupled to plant growth". *Annual Review of Plant Biology*. 2020, vol. 71, p. 217–245.

SONG, and JANE, Jay-Lane. "Characterization of barley starches of waxy, normal, and high amylose varieties". *Carbohydrate polymers*. 2000, vol. 41, no. 4, p. 365–377.

STAEHELIN, Andrew L. and PAOLILLO, Dominick J. "A brief history of how microscopic studies led to the elucidation of the 3D architecture and macromolecular organization of higher plant thylakoids". *Photosynthesis Research*. 2020, vol. 145, p. 237–258.

STEIN, Ofer and GRANOT, David. "An overview of sucrose synthases in plants". *Frontiers in Plant Science*. 2019, vol. 10, p. 95.

STERLING, Clarence. "A low angle spacing in starch". *Journal of Polymer Science*. 1962, vol. 56, p. S10-S12.

STITT, Mark and ZEEMAN, Samuel C. "Starch turnover: pathways, regulation and role in growth". *Current Opinion in Plant Biology*. 2012, vol. 15, p. 282–292.

STREB, Sebastian, DELATTE, Thierry, UMHANG, Martin, EICKE, Simona, SCHORDERET, Martine, REINHARDT, Didier and ZEEMAN, Samuel C. "Starch granule biosynthesis in Arabidopsis is abolished by removal of all debranching enzymes but restored by the subsequent removal of an endoamylase". *The Plant Cell*. 2008, vol. 20, p. 3448–3466.

STREB, Sebastian, EICKE, Simona and ZEEMAN, Samuel C. "The simultaneous abolition of three starch hydrolases blocks transient starch breakdown in Arabidopsis". *Journal of Biological Chemistry*. 2012, vol. 287, p. 41745–41756.

STREB, Sebastian and ZEEMAN, Samuel C. "Replacement of the endogenous starch debranching enzymes ISA1 and ISA2 of Arabidopsis with the rice orthologs reveals a degree of functional conservation during starch synthesis". *PLoS One*. 2014, vol. 9, p. e92174.

STUVE, J. and GALLE, P. "Role of mitochondria in the handling of gold by the kidney: A study by electron microscopy and electron probe microanalysis". *Journal of Cell Biology*. 1970, vol. 44, p. 667–676.

SUH, Dong Soon, VERHOEVEN, Tamara, DENYER, Kay and JANE, Jay Lin. "Characterization of *nubet* and *franubet* barley starches". *Carbohydrate Polymers*. 2004, vol. 56, p. 85–93.

SUNDBERG, Maria, PFISTER, Barbara, FULTON, Daniel, BISCHOF, Sylvain, DELATTE, Thierry, EICKE, Simona, STETTLER, Michaela, SMITH, Steven M., STREB, Sebastian and ZEEMAN, Samuel C. "The hetero-multimeric debranching enzyme involved in starch synthesis in Arabidopsis requires both isoamylase 1 and isoamylase 2 subunits for complex stability and activity". *PLoS One*. 2013, vol. 8, p. e75223.

SZYDLOWSKI, Nicolas, RAGEL, Paula, RAYNAUD, S, Y, LUCAS, M. Mercedes, ROLDÁN, Isaac, MONTERO, Manuel, MUÑOZ, Francisco José, OVECKA, Miroslav, BAHAJI, Abdellatif, PLANCHOT, Véronique, POZUETA-ROMERO, Javier, D'HULST, Christophe and MÉRIDA, Angel. "Starch granule initiation in Arabidopsis requires the presence of either class IV or class III starch synthases". *The Plant Cell*. 2009, vol. 21, p. 2443–2457.

SZYDLOWSKI, Nicolas, RAGEL, Paula, HENNEN-BIERWAGEN, Tracie A., PLANCHOT, Véronique, MYERS, Alan M., MÉRIDA, Angel, D'HULST, Christophe and WATTEBLED, Fabrice. "Integrated functions among multiple starch synthases determine both amylopectin chain length and branch linkage location in Arabidopsis leaf starch". *Journal of Experimental Botany*. 2011, vol. 62, p. 4547–4559.

TAKEDA, Yasuhito, SHIBAHARA, Shunpei and HANASHIRO, Isao. "Examination of the structure of amylopectin molecules by fluorescent labelling". *Carbohydrate Research*. 2003, vol. 338, p. 471–475.

TAO, Keyu, YU, Wenwen, PRAKASH, Sangeeta and GILBERT, Robert G. "High-amylose rice: Starch molecular structural features controlling cooked rice texture and preference". *Carbohydrate Polymers*. 2019, vol. 219, p. 251–260.

TATGE, H., MARSHALL, J., MARTIN, C., EDWARDS, E. A. and SMITH, A. M. "Evidence that amylose synthesis occurs within the matrix of the starch granule in potato tubers". *Plant, Cell and Environment*. 1999, vol. 22, p. 543–550.

TESTER, Richard F., YOUSUF, Rabiah, KARKALAS, John, KETTLITZ, Bernd and RÖPER, Harald. "Properties of protease-treated maize starches". *Food Chemistry*. 2008, vol. 109, no. 2, p. 257–263.

TETLOW, Ian J., WAIT, Robin, LU, Zhenxiao, AKKASAENG, Rut, BOWSHER, Caroline G., ESPOSITO, Sergio, KOSAR-HASHEMI, Behjat, MORELL, Matthew K. and EMES, Michael J. "Protein phosphorylation in amyloplasts regulates starch branching enzyme activity and protein–protein interactions". *The Plant Cell*. 2004, vol. 16, p. 694–708.

TETLOW, Ian J., BEISEL, Kim G., CAMERON, Scott, MAKHMOUDOVA, Amina, LIU, Fushan, BRESOLIN, Nicole S., WAIT, Robin, MORELL, Matthew K. and EMES, Michael J. "Analysis of protein complexes in wheat amyloplasts reveals functional interactions among starch biosynthetic enzymes". *Plant Physiology*. 2008, vol. 146, no. 4, p. 1878–1891.

THORMÄHLEN, Ina, RUBER, Joachim, ROEPENACK-LAHAYE, Edda Von, EHRLICH, Sven Matthias, MASSOT, Vincent, HÜMMER, Christine, TEZYCKA, Justyna, ISSAKIDIS-BOURGUET, Emmanuelle and GEIGENBERGER, Peter. "Inactivation of thioredoxin f1 leads to decreased light activation of ADP-glucose pyrophosphorylase and altered diurnal starch turnover in leaves of Arabidopsis plants". *Plant, Cell and Environment*. 2013, vol. 36, p. 16–29.

TIESSEN, Axel, HENDRIKS, Janneke H. M., STITT, Mark, BRANSCHEID, Anja, GIBON, Yves, FARRÉ, Eva M. and GEIGENBERGER, Peter. "Starch synthesis in potato tubers is regulated by post-translational redox modification of ADP-glucose pyrophosphorylase: a novel regulatory mechanism linking starch synthesis to the sucrose supply". *The Plant Cell*. 2002, vol. 14, p. 2191–2213.

TORIJA, Maria Jesъs, NOVO, Maite, LEMASSU, Anne, WILSON, Wayne, ROACH, Peter J., FRANCOIS, Jean and PARROU, Jean Luc. "Glycogen synthesis in the absence of glycogenin in the yeast *Saccharomyces cerevisiae*". *FEBS Letters*. 2005, vol. 579, p. 3999–4004.

TRINH, Le A. and FRASER, Scott E. "Imaging the cell and molecular dynamics of craniofacial development. challenges and new opportunities in imaging developmental tissue patterning". *Current Topics in Developmental Biology*. 2015, vol. 115, p. 599–629.

TRUERNIT, Elisabeth and HASELOFF, Jim. "A simple way to identify non-viable cells within living plant tissue using confocal microscopy". *Plant Methods*. 2008, vol. 4,

TSAI, Huang-Lung, LUE, Wei-Ling, LU, Kuan-Jen, HSIEH, Ming-Hsiun, WANG, Shue-Mei and CHEN, Jychian. "Starch synthesis in Arabidopsis is achieved by spatial co-transcription of core starch metabolism genes". *Plant physiology*. 2009, vol. 151, p. 1582–1595.

UGALDE, Juan E., PARODI, Arm, J., o and UGALDE, Rodolfo A. "*De novo* synthesis of bacterial glycogen: *Agrobacterium tumefaciens* glycogen synthase is involved in glucan initiation and elongation". *Proceedings of the National Academy of Sciences*. 2003, vol. 100, p. 10659–10663.

UWIZEYE, Clarisse, DECELLE, Johan, JOUNEAU, Pierre-Henri, FLORI, Serena, GALLET, Benoit, KECK, Jean-Baptiste, BO, Davide Dal, MORISCOT, Christine, SEYDOUX, Claire, CHEVALIER, Fabien, SCHIEBER, Nicole L., TEMPLIN, Rachel, ALLORENT, Guillaume, COURTOIS, Florence, CURIEN, Gilles, SCHWAB, Yannick, SCHOEHN, Guy, ZEEMAN, Samuel C., FALCONET, Denis and FINAZZI, Giovanni. "Morphological bases of phytoplankton energy management and physiological responses unveiled by 3D subcellular imaging". *Nature Communications*. 2021, vol. 12, p. 1049.

VANDROMME, Camille, SPRIET, Corentin, DAUVILLÉE, David, COURSEAUX, Adeline, PUTAUX, Jean Luc, WYCHOWSKI, Adeline, KRZEWINSKI, Frédéric, FACON, Maud, D'HULST, Christophe and WATTEBLED, Fabrice. "PII1: a protein involved in starch initiation that determines granule number and size in Arabidopsis chloroplast". *New Phytologist*. 2019, vol. 221, p. 356–370.

VANDROMME, Camille, KASPROWICZ, Angelina, COURSEAUX, Adeline, TRINEL, Dave, FACON, Maud, PUTAUX, Jean-Luc, D'HULST, Christophe, WATTEBLED, Fabrice and SPRIET, Corentin. "NegFluo, a fast and efficient method to determine starch granule size and morphology in situ in plant chloroplasts". *Frontiers in Plant Science*. 2019, vol. 10, p. 1075.

WANG, Kai, VILAPLANA, Francisco, WU, Alex, HASJIM, Jovin and GILBERT, Robert G. "The size dependence of the average number of branches in amylose". *Carbohydrate Polymers*. 2019, vol. 223, p. 115134.

WANNEMACHER, Reinhold. *Confocal laser scanning microscopy*. Dordrecht: Springer Netherlands. 2012.p. 500–516.

WATTEBLED, Fabrice, BULÉON, Alain, BOUCHET, Brigitte, RAL, Jean-Philippe, LIÉNARD, Luc, DELVALLÉ, David, BINDERUP, Kim, DAUVILLÉE, David, BALL, Steven and D'HULST, Christophe. "Granule-bound starch synthase I: A major enzyme involved in the biogenesis of B-crystallites in starch granules". *European Journal of Biochemistry*. 2002, vol. 269, no. 15, p. 3810–3820.

WATTEBLED, Fabrice, DONG, Ying, DUMEZ, Sylvain, DELVALLÉ, David, PLANCHOT, Véronique, BERBEZY, Pierre, VYAS, Darshna, COLONNA, Paul, CHATTERJEE, Manash, BALL, Steven and D'HULST, Christophe. "Mutants of Arabidopsis lacking a chloroplastic isoamylase accumulate phytoglycogen and an abnormal form of amylopectin". *Plant Physiology*. 2005, vol. 138, p. 184–195.

WILSON, Wayne A., ROACH, Peter J., MONTERO, Manuel, BAROJA-FERNÁNDEZ, Edurne, MUÑOZ, Francisco José, EYDALLIN, Gustavo, VIALE, Alej M. and POZUETA-ROMERO, Javier. "Regulation of glycogen metabolism in yeast and bacteria". *FEMS Microbiology Reviews*. 2010, vol. 34, p. 952–985.

XIE, Ying, BARB, Adam W., HENNEN-BIERWAGEN, Tracie A. and MYERS, Alan M. "Direct determination of the site of addition of glucosyl units to malto-oligosaccharide acceptors catalysed by maize starch synthase 1". *Frontiers in Plant Science*. 2018, vol. 9, p. 1252.

YAMAGUCHI, Mamoru, KAINUMA, Keiji and FRENCH, Dexter. "Electron microscopic observations of waxy maize starch". *Journal of Ultrasructure Research*. 1979,

YUN, Min-Soo and KAWAGOE, Yasushi. "Septum formation in amyloplasts produces compound granules in the rice endosperm and is regulated by plastid division proteins". *Plant and Cell Physiology*. 2010, vol. 51, p. 1469–1479.

ZEEMAN, Samuel C., UMEMOTO, Takayuki, LUE, Wei-Ling, AU-YEUNG, Pui, MARTIN, Cathie, SMITH, Alison M. and CHEN, Jychian. "A mutant of Arabidopsis lacking a chloroplastic isoamylase accumulates both starch and phytoglycogen". *The Plant Cell*. 1998, vol. 10, p. 1699–1711.

ZEEMAN, Samuel C., TIESSEN, Axel, PILLING, Emma, KATO, K. Lisa, DONALD, Athene M. and SMITH, Alison M. "Starch synthesis in Arabidopsis. Granule synthesis, composition, and structure". *Plant Physiology*. 2002, vol. 129, p. 516–529.

ZHANG, Xiaoli, MYERS, Alan M. and JAMES, Martha G. "Mutations affecting starch synthase III in Arabidopsis alter leaf starch structure and increase the rate of starch synthesis". *Plant Physiology*. 2005, vol. 138, p. 663–674.

ZHANG, Xiaoli, SZYDLOWSKI, Nicolas, DELVALLÉ, David, D'HULST, Christophe, JAMES, Martha G. and MYERS, Alan M. "Overlapping functions of the starch synthases SS2 and SS3 in amylopectin biosynthesis in Arabidopsis". *BMC Plant Biology*. 2008, vol. 8, p. 1–18.

ZHU, Fan, BERTOFT, Eric, SZYDLOWSKI, Nicolas, D'HULST, Christophe and SEETHARAMAN, Koushik. "Branching patterns in leaf starches from Arabidopsis mutants deficient in diverse starch synthases". *Carbohydrate Research*. 2015, vol. 401, p. 96–108.

ZIEGLER, Gregory R., CREEK, John A. and RUNT, James. "Spherulitic crystallization in starch as a model for starch granule initiation". *Biomacromolecules*. 2005, vol. 6, no. 3, p. 1547–1554.

Contact information

Leo Burgy

1993-01-05

Swiss nationality

leo.burgy@gmail.com

+41 76 308 48 07

Working experience

- Research assistant at ETH Zürich (2016–February 2021)

Education

- Ph.D. in Biochemistry at ETH Zürich (2016–February 2021); "Quantitative multi-dimensional imaging of starch granule development in leaves"
- Master's in bioinformatics and Computational Biology at Universität Bern (2014–2016); "Development of an automated supervised machine learning pipeline for clinical Omics datasets"
- Bachelor's in biology at Université de Neuchâtel (2011–2014)

Technical skills

Data processing pipelines (Python (NumPy, Pandas), R) and relational databases (SQL); version control (git); statistical analysis (Bayesian analysis, hierarchical models, Stan); technical writing (scientific communication); image analysis (FIJI, OpenCV) and convolutional neural networks (Pytorch).

Transferable skills

Analysis; creative problem solving; project and time management; teamwork and collaboration.

Languages

English and German: C1; French: native.

Interests

Photography; cycling; gastronomy; politics and economy.